January 2015

Design and Characterization of Biomimetic Adhesive Materials

Mary Jane Brennan
Purdue University

Graduate School Form 30
Updated 1/15/2015

PURDUE UNIVERSITY
GRADUATE SCHOOL
Thesis/Dissertation Acceptance

This is to certify that the thesis/dissertation prepared

By M. Jane Brennan

Entitled
Design and Characterization of Biomimetic Adhesive Materials

For the degree of Doctor of Philosophy

Is approved by the final examining committee:

Julie Liu
Chair

Jonathan Wilker

You-Yeon Won

Chongli Yuan

To the best of my knowledge and as understood by the student in the Thesis/Dissertation Agreement, Publication Delay, and Certification Disclaimer (Graduate School Form 32), this thesis/dissertation adheres to the provisions of Purdue University's "Policy of Integrity in Research" and the use of copyright material.

Approved by Major Professor(s): Julie Liu

Approved by: John A. Morgan 7/17/2015

Head of the Departmental Graduate Program Date

DESIGN AND CHARACTERIZATION OF BIOMIMETIC ADHESIVE MATERIALS

A Dissertation

Submitted to the Faculty

of

Purdue University

by

M. Jane Brennan

In Partial Fulfillment of the

Requirements for the Degree

of

Doctor of Philosophy

August 2015

Purdue University

West Lafayette, Indiana

This dissertation is dedicated to my husband (my favorite).

ACKNOWLEDGMENTS

First and foremost, I would like to convey my gratitude and respect for my advisor, Dr. Julie Liu. She has helped me grow as a scientist and as a person and has guided and supported me as I fumbled my way through to the end. She never settled for less than my best, and she taught me what my best could be. I am so happy that you were my mentor.

Thanks also to my committee, Dr. Jon Wilker, Dr. You-Yeon Won, and Dr. Chongli Yuan, for their support and discussions. They provided useful advice to narrow my research path, and at times helpfully pointed out those things that I did not yet understand. Thanks to Dr. Wilker in particular for sharing a laugh or two and for helping me understand the science of adhesion (or at least the idea that no one really understands it all that well).

I would also like to thank the current and former members of the Liu lab and various members of the Wilker lab for the supportive and welcoming community they've helped create, and for their friendship. Thanks to Dr. Julie Renner and Dr. Richard Galas for not being too annoyed at the new student who didn't know anything. To Dr. Yeji Kim, thanks for all of the help with cell culture and for being there when I needed a hug. To Dr. Heather Meredith, Dr. Cori Jenkins, and Jessica Román, thanks for helping me out so often and being wonderful people with whom to collaborate. To Renay Su, thanks for making me laugh so much and being fun to be around. To Claire Kilmer, thanks for always being so peppy and understanding of my near-graduation crankiness. To Charng-yu Lin, thanks for the fun and insightful conversations, and for helping me stay positive when I was stressed out. To Sydney Hollingshead, thanks for helping me to see my project from a new and different

perspective, and for helping me get that last-minute data. I couldn't have finished without all of your help!

I have also had the pleasure of mentoring numerous outstanding undergraduate students, including Teresa Lin, Peter Meléndez, MacKenzie Tweardy, Vicente García, Max Zubrenic, Christine Peercy, Victoria Messerschmidt, Haefa Mansour, and Bridget Kilbride. I would like to thank these students for helping me to discover my love of teaching and mentoring, for helping my project progress when I didn't have enough time to do it all myself, and for your friendship.

Outside of graduate research, I would also like to thank Dr. Jenna Rickus for being an all-around great mentor throughout my time at Purdue and for getting me in the door at iGEM. I would also like to thank Dr. Heidi Diefes-Dux and Dr. Phil Wankat for their insights into engineering education and their encouragement to pursue a career in teaching. Thanks also to my "Lafayette friends" (Dr. Tarun Madangopal, Jessamine and Craig Pilcher) and my "McDonald's study group" (Dr. John Austin, Myles Thomas, and Melissa Sweat) for helping to get me out of the building to relax and have fun.

Finally, thanks to my family, most especially my husband Kevin. Your endless love and faith in my success have meant the world to me and have kept me going even when I thought I couldn't. I am so lucky to have you all in my life. Thank you!

TABLE OF CONTENTS

LIST OF TABLES

LIST OF FIGURES

Figure Page

Figure Page

Figure Page

Figure Page

Figure Page

ABSTRACT

Brennan, M. Jane PhD, Purdue University, August 2015. Design and Characterization of Biomimetic Adhesive Materials. Major Professor: Julie C. Liu.

When we engineer new materials, nature provides us with a wealth of inspiration, often in the form of proteins. The blue mussel *Mytilus edulis* and sandcastle worm *Phragmatopoma californica* produce adhesive proteins that help them to adhere in wet, turbulent environments [1]. The frog *Notaden bennetti* secretes a sticky, proteinaceous emulsion that helps it defend against predators; the velvet worm bombards a similar protein onto its prey to prevent its escape [2]. Mammals and insects produce remarkably elastic proteins to support highly repetitive motions [3, 4]. This work describes the design, production, and characterization of several biomimetic materials inspired by natural adhesive proteins.

First, we evaluated the cytotoxicity of a mussel-mimetic polymer, poly[(3,4-dihydroxystyrene)-*co*-styrene]. This polymer was previously shown to be strongly adhesive with strengths similar to a variety of commercial glues. To investigate the versatility of the polymer for biomedical applications, we evaluated the polymer cytotoxicity by assessing the viability, proliferation rate, and morphology of fibroblasts cultured with polymer. We demonstrated that the polymer is highly cytocompatible and is therefore a promising material for applications in which biological contact is necessary.

Next, we investigated the adhesive capabilities of a system of recombinant elastin-like polypeptides (ELPs) as well as the extrinsic and intrinsic factors influencing their adhesion strengths. We found that pH, concentration, and crosslinking did not affect the adhesion strength, whereas moisture was a critical factor. When comparing protein designs, amino acid composition did not affect the strength as significantly

as protein structure and length. Finally, our adhesive proteins exhibited comparable strengths to commercially available protein-based glues. These results have strong implications for the general understanding and future design of proteinaceous adhesives.

Finally, we developed an elastin-based mussel-mimetic adhesive. The ELP is easily over-expressed and purified from *E. coli*. Following enzymatic conversion to produce adhesive DOPA residues, the protein demonstrated strong cytocompatibility, enhanced adsorption to glass, significant dry adhesion, and moderate adhesion in a humid environment. Additionally, the protein possesses a reversible phase transition behavior that can be tuned to physiological conditions. Upon transitioning, the protein forms a protein-rich coacervate phase that can provide measurable adhesion strength after being applied underwater. This novel material has potential applications as a surgical adhesive or a scaffold for tissue engineering.

1. INTRODUCTION

1.1 Protein-based Adhesion

Adhesive materials can be found throughout nature. Numerous organisms produce adhesive compounds for a variety of purposes, including attachment, defense, predation, and others. Many of these adhesives come in the form of proteins [1, 5, 6]. In the pursuit of better glues and a better understanding of adhesive bonding, scientists have studied or mimicked many of these adhesive proteins. In other cases, natural proteins with native functions unrelated to adhesion have been formulated to act as novel adhesives [7, 8]. The following section will describe some of the major types of protein-based adhesives.

1.1.1 Mussel Adhesion

Mussels produce several proteins that allow them to adhere to nearly any solid surface, even under the duress of crashing waves. Mussels attach to their rocky tidepools by secreting a byssus from their foot. The byssus consists of a bundle of fibers, each with a sticky plaque at the tip [6, 9–11]. The byssus threads and plaques are made up of six distinct foot proteins which are numbered in the order of discovery [9, 10].

One unifying characteristic of mussel adhesive proteins (MAPs) is the high concentration (up to 30 mol%) of 3,4-dihydroxyphenyl-L-alanine (DOPA) residues, which are formed by post-translational hydroxylation of tyrosines [9, 10]. It has been shown that DOPA alone can furnish adhesive properties [12], and indeed that the presence of DOPA in MAPs is essential for strong adhesion [13].

DOPA contributes to adhesion via several different mechanisms. When DOPA is oxidized to its reactive quinone form, it is able to crosslink with itself through radical

chemistry to form a hardened, sclerotized material [14, 15]. In the lab, crosslinking can be performed by enzymatic oxidation with tyrosinase [16], chemical oxidation with periodate or hydrogen peroxide [12], or by metal chelation followed by radical generation [17, 18]. In nature, the mussel secretory gland is acidic (pH $\approx$ 5); the sudden exposure to seawater (pH $\approx$ 8) induces crosslinking [19]. Optimal adhesion requires an intermediate level of DOPA crosslinking since both adhesive and cohesive forces are necessary for a strong bond [20].

DOPA may also provide adhesive interactions by reacting with its substrate directly. Like most adhesive materials, DOPA forms very strong interactions with high energy (highly polar) surfaces such as glass and steel but interacts very poorly with low energy (non-polar) surfaces such as plastic [12, 21]. Atomic force microscopy (AFM) measurements of the interactions of a single DOPA residue revealed that DOPA formed a reversible bond with inorganic TiO_2 with the highest strength ever reported for a small biomolecule [22]. This bond was weakened significantly by oxidation to the quinone form. However, with an organic amine-modified surface, DOPA could form an irreversible covalent bond [22]. Furthermore, these experiments were performed underwater, where the high dielectric constant of water normally inhibits strong interactions between an adhesive and substrate [10].

Although MAPs possess strong underwater adhesive properties, the use of natural MAPs is limited; the production of 1 g of MAP requires $\sim$10,000 mussels [9]. Commercially, MAPs are sold as Cell-Tak (BD Biosciences) for approximately $1500 per 10 mg. As a result, many scientists have mimicked mussel adhesion by incorporating catechol groups into synthetic polymers [23, 24] or recombinant proteins [25–33].

1.1.2 Adhesives from Soy and Other Crops

In 1923, Otis Johnson patented an adhesive material formulated from soy protein isolate [34]. Shortly thereafter, soy protein became popular as a commercial wood glue and lost popularity only when petroleum products became inexpensive [7]. More

recently, soy and other plant-based adhesives have shown a resurgence in popularity because of the modern focus on environmental sustainability [8, 35].

Soy proteins are primarily globulins whose solubility shows a strong dependence on pH, with maximum insolubility occurring at the isoelectric point (pH 4.2-4.6) [36]. Methods for the production of soy protein concentrate (64% protein content) or soy protein isolate (92% protein content) [36] often utilize the isoelectric point; the pH of soy flour solution is lowered to the isoelectric point, at which point the proteins become insoluble (but not denatured) and are easily separated from contaminating carbohydrates and lipids [37]

Adhesive bonding of soy proteins occurs largely as a result of mechanical interlocking with the substrate combined with molecular attractive forces (e.g., hydrogen bonds, van der Waals forces) [7]. Because of this mechanism, adhesion strength is highly dependent on numerous factors, including particle size, viscosity, protein structure, substrate surface roughness, and processing conditions [38]. For example, the substrate surface should be porous but not too rough since excessive roughness will cause cohesive failure [39]. In addition, significant adhesion strength can only be achieved upon protein denaturation, which exposes the proteins' internal residues to the wood surface [7]. Denaturation is commonly achieved through alkali treatment at pH 10 or higher [38]. This treatment also results in increased water resistance; however, too high of a pH can reduce the useful life of the adhesive to only a few hours [38] as well as cause alkali stain in the wood substrate [40].

Numerous studies have investigated various protein modifications to improve adhesive properties such as viscosity, water resistance, economics, or worker safety [7]. Many modifications explore alternate methods of reducing protein structure, including chemical denaturation with organic solvents, urea, guanidine hydrochloride, or sodium dodecyl sulfate [38, 41, 42]; physical denaturation with heat or grinding [38]; or the addition of salts or reducing agents to weaken interactions among proteins [36, 43, 44]. Other types of modifications include crosslinking [38, 45], treatment with enzymes such as trypsin [46], or various chemical reactions (acylation, oxidation, etc.) [7].

Inspiration has even come from mussels; soy proteins have been modified via the addition of catechol groups to improve water resistance [47, 48].

1.1.3 Other Natural Protein-based Adhesives

A variety of other organisms produce protein-based glues, including barnacles, sandcastle worms, frogs, and various insects [5, 49, 50]. Adult barnacles permanently attach to their chosen substrate by producing a cement in a layer ∼5 μm thick [51,52]. The cement layer is composed of ten proteins, several of which are highly insoluble, and none of which have any significant homologs in current databases [51, 53]. The fully cured cement is composed of a laminated array of matrix proteins surrounded by a layer of calcium carbonate [54]. The mechanism for barnacle cement adhesion remains unclear but could involve the formation of disulfide bonds [55] or amyloid plaques [52].

Like barnacles, sandcastle worms also adhere to their environment by forming a protein-based cement [1,56]. Unlike barnacles, however, DOPA contributes to the adhesion of sandcastle worm cement [57]. Phosphoserine, another non-canonical amino acid, is also present in sandcastle cement proteins at up to 30 mol% and is thought to participate in adhesive bonding [57]. Other sandcastle glue proteins belong to one of three classifications: glycine/tyrosine-rich, serine/tyrosine-rich, and histidine-repeats [58]. The adhesive mechanism of sandcastle worm cement is thought to involve complex coacervation triggered by a pH change upon secretion into seawater [57, 59], although more recent findings suggest a mechanism based on electrostatic interactions between soluble macromolecules [57].

Biomimetic approaches to sandcastle worm cement have yielded success. One approach utilized a coacervate network formed from two different methacrylamide-based molecules to mimic DOPA- and lysine-rich proteins; upon addition of divalent cations, wet adhesion increased to a maximum of ∼100 kPa [60]. Recently, the bond strength of this system was improved by the addition of polymerizing polyethylene glycol (PEG)-diacrylate (PEGDA) monomers as a second network within the first

coacervate network [61]; adhesion strength after a 24 h cure underwater reached up to 1.2 MPa and was directly related to the concentration of PEGDA.

An entirely different type of proteinaceous adhesive is produced by the *Notaden bennetti* frog, various types of insects, and the velvet worm [2, 5]. These adhesives are secreted as protein-rich hydrogels and are used for many purposes, including for defense (in the case of *Notaden bennetti*) [62], for egg attachment (in the case of insects such as the sheep blowfly, gum moth, ladybird, etc.) [5], or for predation (in the case of the velvet worm) [2,5]. The protein adhesives are often secreted as viscous solutions or emulsions that quickly dehydrate into a glassy state and thus immobilize the target object [2]. Unlike the adhesive proteins of mussels or sandcastle worms, however, the proteins in these adhesives do not contain DOPA, and do not often contain other non-canonical amino acids such as hydroxyproline [2, 5]. Instead, the unifying characteristic of these adhesives is an amino acid composition rich in glycine and/or proline or serine; because of the over-abundance of glycine, these proteins are also largely unstructured [2, 5, 62]. Notably, the glycine/proline-rich amino acid composition and disordered structure are quite similar to those of elastomeric proteins such as elastin [5, 62], the details of which will be in the next section.

1.2 Elastin

Elastin is a natural protein found in vertebrates and provides reversible elasticity to connective tissues, including skin and elastic cartilage. Elastin is also found in arterial walls where its role is to store elastic strain energy; it facilitates the pulsing flow of blood which lowers blood pressure and maintains a steady flow of blood to tissues [3, 63]. In humans, the elastin gene product is known as tropoelastin and is characterized by repetitive hydrophobic domains and crosslinking domains. The hydrophobic domains are dominated by repeated motifs of amino acids consisting of valine (V), proline (P), glycine (G), alanine (A), leucine (L), and isoleucine (I) residues. The crosslinking domains contain numerous lysine (K) residues within P-

and A-rich regions [3]. Mature elastin consists of numerous crosslinked tropoelastin molecules, which form an insoluble polymer [3].

Mature elastin demonstrates low stiffness (E_{init} = 1.1 MPa), high extensibility (σ_{max} = 2 MPa), and high resilience (90%) [64]. These properties are strongly affected by hydration level [63,65]. In the body, elastin turnover is incredibly low, and as such, elastin possesses a long lifetime of 60-80 years in humans [63]. However, elastin is not found in situations with high-frequency loading such as that found in insect wings. At these frequencies, the resilience of elastin drops significantly [63]. A similar effect is seen with low hydration.

Elastin is also characterized by an inverse transition temperature, which is also known as the lower critical solution temperature (LCST). At low temperatures, elastin is soluble in water. Upon raising the temperature past the LCST, phase separation occurs via coacervation; in this process, elastin fibers first align and then aggregate [66]. The mechanical properties of elastin change with the coacervation process. At low temperatures or high strain rates, elastin exhibits high stiffness and low extensibility, which are properties of a rigid polymeric glass [63]. At high temperatures or low strain rates, elastin exhibits low stiffness and high extensibility, which are properties of a typical rubber [63].

Structurally, elastin has been studied extensively with circular dichroism (CD), Fourier transform infrared (FTIR) spectroscopy, Raman spectroscopy, nuclear magnetic resonance (NMR) spectroscopy, and X-ray diffraction (XRD) [67]. Unfortunately, detailed structural information is limited due to the insolubility of mature elastin and the significant mobility of the elastin backbone [67]. However, it is known that elastin's structure is dynamic and composed largely of β-II turns as well as some disordered β-sheets [68, 69]. Originally, this dynamic structure was thought to be the source of the entropic driving force for elasticity [70–72]. However, molecular dynamics simulations have found that the interaction between elastin and surrounding water molecules is more likely responsible for its elasticity as well as its transition behavior [69]. In its soluble state, elastin's main-chain polar atoms hydrogen bond

with surrounding water and form a low-entropy hydration shell. Upon heating, elastin collapses to a compact, higher-structure, lower-entropy state and expels the waters of hydration. However, the total change in entropy is positive due to a large increase in entropy of the surrounding water [69]. This entropic driving force is responsible for elastin's elastic behavior.

Because native elastin is characterized by repetitive amino acid motifs, many research groups have studied elastin-like polypeptides (ELPs) constructed from those motifs. These ELPs possess physical and mechanical properties similar to native elastin, including the properties self-assembly and an inverse transition temperature [73,74]. One of the most common ELPs is the repeating pentapeptide poly(VPGXG), where X indicates any amino acid except proline [73,74]. This repeated motif is based on VPGVG, the most common repeat in native elastin [75]. The LCST of these ELPs can be tuned by adjusting the protein molecular weight or the hydrophobicity of residue X [76, 77]. In addition, poly(VPGXG) has been shown to be highly biocompatible [78] and easily over-expressed and purified from *Escherichia coli* [79, 80]; thus, poly(VPGXG) is an attractive choice for protein engineering.

1.3 Tissue Adhesives

Each year, more than 230 million major surgical procedures are performed worldwide; many of these surgeries utilize sutures or staples for wound closure [81]. Although sutures and staples provide advantages such as accurate closure with high tensile strength and low dehiscence rate [82], they inherently cause damage to the surrounding healthy tissue, require the use of local anesthetics [83], are infection-prone [84, 85], and cause patient discomfort [86]. As such, surgical adhesives are an attractive alternative for wound closure. Adhesives have several advantages, including ease of application [85], low infection risk [85], and no need for anesthetics [83]. To be an effective surgical adhesive, however, a material should, at a minimum, possess four characteristics: biocompatibility, adhesion in wet environments, appropriate adhesive and cohesive properties [25], and mechanical properties to match the surrounding

tissue to ensure normal tissue function during healing. Unfortunately, there is no adhesive currently available that fulfills all four criteria for the case of soft tissues.

Current FDA-approved surgical adhesives and sealants include cyanoacrylate-based glues such as SurgiSeal [87] and Dermabond [88]; fibrin-based sealants such as Tisseel and Artiss; albumin/glutaraldehyde adhesives such as BioGlue [89]; PEG-based adhesives [90, 91]; and TissuGlu, a urethane-based adhesive [92–94]. However, each of these adhesives possesses specific drawbacks. Although cyanoacrylates cure in the presence of moisture, they are stiff [95] and their degradation products are toxic [96]. Consequently, cyanoacrylates are approved only for external wound closure [97].

Fibrin-based adhesives are biocompatible and biodegradable, but their bond strength is weak; thus, fibrin adhesives are only sufficient for use as hemostatic agents or sealants and are insufficient for wound closure [98–100]. In addition, fibrin is derived from blood, and thus there is an additional risk of bloodborne pathogen transmission [101, 102].

Albumin/glutaraldehyde adhesives have similar advantages to fibrin adhesives, but due to similarly low adhesion strengths, they are approved only for hemostasis and not wound closure [89].

PEG adhesives, on the other hand, are non-toxic, biocompatible, and exhibit strong bonding and rapid curing [91]. They are currently approved for internal use as a sealant for sutures and vascular grafts [90]. However, PEG adhesives must cure in a dry environment [90], and when in a wet environment, they swell up to 400% by volume and have the potential to cause moderate inflammatory responses [103].

The most recently approved tissue adhesive, TissuGlu, is a urethane-based adhesive composed of isocyanate groups that form a high-affinity bond with nucleophiles such as water [92]. Like cyanoacrylates, urethane-based adhesives therefore polymerize upon contact with moisture while bonding with tissue through a urea bond. However, due to low overall bond strength, TissuGlu is not approved for wound closure; instead, it is used to hold planes of tissue together to eliminate dead space for fluid

accumulation following abdominoplasty [104]. In addition, in biocompatibility tests, TissuGlu showed an increased risk of irritation following subcutaneous implantation, and in clinical trials, seroma formation occurred in 22% of patients [104].

In conclusion, although there have been many recent advances in tissue adhesive technology, the challenge of a strong, underwater bond with appropriate mechanical properties has yet to be met. However, biomimetic approaches such as mussel-inspired adhesion are promising solutions, and are currently under investigation by many researchers [50, 105].

1.4 Thesis Outline and Contributions

The goal of this thesis was to explore various characteristics of engineered biomimetic adhesive materials. We show in Chapter 2 that a synthetic mussel-mimetic adhesive polymer is highly cytocompatible and therefore has potential use for biomedical applications. In Chapter 3, we assess the effect of extrinsic and intrinsic factors on the adhesion strength of elastomeric proteins and demonstrate their potential as adhesive materials. In Chapter 4, we describe the development of a novel elastomeric adhesive protein that can be applied underwater. For this dissertation, I designed and produced all proteins, planned and carried out all experiments, and wrote all of the chapters unless stated otherwise.

Chapter 2 describes the evaluation of the cytocompatibility of a mussel-mimetic adhesive polymer, poly[(3,4-dihydroxystyrene)-*co*-styrene]. Following ISO standards for *in vitro* evaluation of cytotoxicity, we examined the effect of the polymer alone and polymer with crosslinker on fibroblast viability, proliferation rate, and morphology. Cell viability was assessed with cells grown with polymer extracts, leached polymer, and unleached polymer. Proliferation and morphology were assessed with cells on unleached polymer only. Our data show that cell viability, proliferation rate, and morphology are similar to cells cultured on a positive control which indicates that the polymer is highly cytocompatible. Dr. Heather J. Meredith and Dr. Courtney L. Jenkins (Department of Chemistry, Purdue University) prepared the polymer solu-

tion and polymer-coated coverslips and wrote the corresponding methods and results sections. Dr. Courtney L. Jenkins also created the schematic shown in Figure 2.1A.

Chapter 3 describes the investigation of critical factors for the bulk adhesion strength of ELPs. Using a single ELP, the effects of pH, concentration, crosslinker, humidity, cure time, and temperature were examined. Of these extrinsic factors, only humidity, cure time, and cure temperature had a significant effect on protein adhesion. Generally, moisture was detrimental to adhesion since longer cure times and higher temperatures caused the protein solutions to dry out and resulted in increased adhesion strength. The effect of intrinsic factors such as protein amino acid composition, structure, and molecular weight were also probed. Amino acid composition did not have a strong effect on adhesion strength, but higher molecular weights resulted in increased adhesion strength. Protein structure was also found to be important as the addition of a denaturant to a structured control protein improved its adhesion strength, whereas it had no effect on a naturally unstructured elastomeric protein. Adhesion strength of the elastomeric proteins was also found to be equivalent or greater than two commercially available protein-based adhesives. Haefa Mansour and Victoria Messerschmidt assisted with cloning. Sydney E. Hollingshead developed the temperature cycling purification protocol for ELP[KEY_4-48]. Michael Laird Johnston (Department of Chemistry, Purdue University) performed the thermogravimetric analysis. Dr. Connie Bonham (Campus-Wide Mass Spectrometry Center, Purdue University) performed matrix-assisted laser desorption/ionization-time of flight (MALDI-TOF) spectrometry. Dr. John Schulze (Molecular Structure Facility, University of California, Davis) performed amino acid analysis.

Chapter 4 describes the development of a novel elastin-based adhesive for underwater application. An ELP was designed to be rich in lysine and tyrosine residues. Upon treatment with mushroom tyrosinase enzyme, the tyrosines were converted to adhesive DOPA residues to provide wet adhesion strength reminiscent of MAPs. The converted ELP displayed high cytocompatibility, strong adsorption to glass, and significant dry adhesion strength (>2 MPa). In a humid environment, the converted

ELP exhibited significantly higher adhesion strength than either the unconverted ELP, BSA, or the fibrin sealant Tisseel. In addition, the ELP formed a coacervate in physiological conditions; the coacervate could be dispensed underwater and provided measureable underwater adhesion strength. Bridget Kilbride developed the protocol for purification and performed the purification of the protein. Sydney E. Hollingshead obtained turbidity measurements. Melissa L. Sweat (School of Chemical Engineering, Purdue University) captured videos of underwater adhesion testing. Dr. Connie Bonham (Campus-Wide Mass Spectrometry Center, Purdue University) performed MALDI-TOF spectrometry. Dr. John Schulze (Molecular Structure Facility, University of California, Davis) performed amino acid analysis.

Chapter 5 contains a summary with the major conclusions of this research. Future directions are also outlined.

2. CYTOCOMPATIBILITY STUDIES OF A BIOMIMETIC POLYMER WITH SIMPLIFIED STRUCTURE AND HIGH-STRENGTH ADHESION

This chapter consists of a manuscript by Brennan MJ, Meredith HJ, Jenkins CL, Wilker JJ, and Liu JC, prepared for submission in 2015.

2.1 Abstract

The development of wet-setting adhesives suitable for biomedical applications has been challenging given that these materials must exhibit sufficient adhesion strengths, clinically-relevant cure times, and biocompatibility. Biomimetic materials inspired by mussel adhesive proteins appear to contain many of the necessary characteristics for wet-setting adhesives. In particular, poly[(3,4-dihydroxystyrene)-*co*-styrene] has been shown to be a high strength adhesive material with bonding comparable to or even greater than several commercial glues. Herein, a thorough study on the cytocompatibility of this copolymer provides insights on the suitability of a mussel-mimicking adhesive for applications development. The cytotoxicity of poly[(3,4-dihydroxystyrene)-*co*-styrene] was evaluated through assessment of the viability, proliferation rate, and morphology of NIH/3T3 fibroblasts when cultured with copolymer extracts or directly in contact with the copolymer adhesive. After 1 and 3 days of culture, both the copolymer alone and copolymer cross-linked with periodate exhibited minimal effects on cell viability. Likewise, cells cultured on the copolymer displayed proliferation rates and morphologies similar to cells on poly-L-lysine. These results indicate that poly[(3,4-dihydroxystyrene)-*co*-styrene] is highly cytocompatible and therefore a promising material for use where biological contact is important.

2.2 Introduction

The development of materials exhibiting strong adhesive bonds in wet environments has posed challenges for decades. In the context of biomedical applications, wet adhesion is especially difficult. In addition to maintaining a strong bond, such a biomedical material needs to comply with numerous other requirements including durability, [106] degradability, [96] surgically-relevant cure times, [107] and biocompatibility [25, 106]. Current adhesives and sealants fall short of some, if not most, of these requirements. For example, fibrin-based sealants (e.g., Tisseel) possess high biocompatibility and degradability but are difficult to use, require precise mixing ratios, and fail to create bonds with relevant strengths [108, 109]. Poly(ethylene glycol) (PEG) sealants (e.g., SurgiSeal) demonstrate similarly low adhesion strengths and also elicit inflammatory reactions upon swelling of the material [91]. As a result of their low adhesion strengths, these two types of materials are often used only as sealants and hemostatic agents because they are ineffective for wound closure. Conversely, cyanoacrylate-based adhesives (e.g., Dermabond) possess high adhesion strengths on moist tissue, but the degradation products are highly toxic and therefore cannot be used for internal applications [96, 110].

Animals such as mussels [23, 24], geckos [111, 112], and sandcastle worms [60, 61] have inspired the development of non-toxic adhesives for wet environments. In particular, mussels have received significant attention due to their ability to adhere in turbulent tidal environments. The mechanism by which mussel adhesives function is largely related to the non-canonical amino acid 3,4-dihydroxyphenylalanine (DOPA) present at 3-30 mol % in the adhesive proteins that form the mussel plaques [9, 10]. Marine mussels are able to sequester metals such as iron from seawater and thus enable DOPA in the plaques to undergo chelation, oxidation, and radical formation, which creates a cross-linked, cured adhesive [113, 114]. The catechol functionality of DOPA provides both adhesive bonding at the surface and cohesive interactions in the bulk through cross-linking, which forms a durable adhesive even in the presence

of water [114, 115]. Taking advantage of the material design used by these animals has allowed biomimetic materials to be developed in the form of both recombinant proteins [25–33, 116] and synthetic polymers [23, 24].

One of the simplest mussel-mimetic polymers is poly[(3,4-dihydroxystyrene)-*co*-styrene]. This copolymer is constructed from a polystyrene backbone with randomly distributed pendant catechol groups and is reminiscent of mussel adhesive proteins' polypeptide backbone with periodic DOPA groups [117]. Past studies of this copolymer system have provided essential information on bulk adhesion. It is now known that ∼33 mol % of 3,4-dihydroxystyrene incorporated into poly[(3,4-dihydroxystyrene)-*co*-styrene] achieves a suitable balance of adhesive and cohesive bonds [118]. A detailed look at molecular weight, copolymer concentration, different cross-linkers, addition of fillers, and cure time and temperature provided a formulation that gave strengths greater than that of commercial adhesives (i.e., Elmer's Glue-All, SuperGlue, and Loctite Epoxy) on a variety of surfaces (i.e., aluminum, polytetrafluoroethylene, polyvinylchloride, steel, and red oak) [117–120]. Even when glued underwater, poly[(3,4-dihydroxystyrene)-*co*-styrene] has been shown to bond aluminum [121].

Although much is known about the adhesive properties of poly[(3,4-dihydroxystyrene)-*co*-styrene], little is known of the ways in which a biological environment would respond to this copolymer. To determine if this material is relevant for biomedical applications such as a surgical adhesive or tissue engineering scaffold, cytocompatibility studies with poly[(3,4-dihydroxystyrene)-*co*-styrene] are presented in this paper. Following ISO standard 10993-5 for the *in vitro* cytotoxicity evaluation of medical devices, NIH/3T3 mouse fibroblasts were cultured with leached copolymer, leached extracts, and in direct contact with copolymer-coated coverslips (Figure 2.1A). After 1 and 3 d of culture, cell viability, proliferation rate, and morphology were evaluated with a LIVE/DEAD assay, a bromodeoxyuridine (BrdU) assay, and actin staining, respectively. Copolymer groups were compared to culture on a positive control substrate, poly-L-lysine. Because the biomimetic copolymer

group demonstrated equivalent cytocompatibility to the positive control group in all tests, it can be considered non-cytotoxic.

2.3 Materials and Methods

Materials

All materials used in this study were purchased from Sigma-Aldrich, unless indicated otherwise.

Copolymer Synthesis and Characterization

A detailed procedure for the synthesis of poly[(3,4-dihydroxystyrene)-*co*-styrene] has been described in previous work [117, 118]. In short, the protected copolymer, poly[(3,4-dimethoxystyrene)-*co*-styrene], was synthesized by anionic polymerization using n-BuLi with purified styrene and 3,4-dimethoxystyrene monomers. For the deprotection, BBr_3 was used to remove the methoxy groups to give poly[(3,4-dihydroxystyrene)-*co*-styrene]. The composition and purity of the copolymer was determined by ^{1}H NMR spectroscopy recorded on a Varian Inova-300 MHz spectrometer. Molecular weights were determined by gel permeation chromatography (GPC) using a Polymer Laboratories PL-GPC20 system. The composition of the copolymer used in this study was 27 mol % 3,4-dihydroxystyrene and 73 mol % styrene with a number average molecular weight (M_n) = 49,000 g/mol, weight average molecular weight (M_w) = 73,000 g/mol, and polydispersity index (PDI) = 1.5.

Spin Coating

A spin coater (Laurell Technologies Corporation, Model WS-650MZ-23NPP) was used to deposit a layer of poly[(3,4-dihydroxystyrene)-*co*-styrene] onto glass coverslips (12-mm diameter, VWR). The copolymer was dissolved in acetone at a concentration of 0.10 g/mL . The copolymer solution (45 μL) was statically dispensed onto the entire area of the coverslip before spinning. For the cross-linked system, tetra-

butylammonium periodate $[N(C_4H_9)_4](IO_4)$ was prepared according to a published procedure [122] and characterized by ultraviolet-visible absorption spectroscopy, ^1H NMR spectroscopy and melting point determination. To coat the coverslips, tetrabutylammonium periodate solution (15 μL of 0.104 g/mL in acetone) was immediately added to the copolymer solution on the coverslip prior to spinning. These volumes maintained a 1:3 molar ratio of cross-linker to 3,4-dihydroxystyrene. The coated coverslips were then spun for 15 s at 3500 rpm followed by 30 s at 3000 rpm. The coverslips were cured for 2 h at 55 °C. Thickness and roughness measurements were determined by profilometry (Tencor Instruments, Alpha-Step 200).

Cell Culture

NIH/3T3 mouse fibroblasts (courtesy of Dr. Alyssa Panitch) were cultured at 37 °C and 5% CO_2 in high-glucose Dulbecco's Modified Eagle's Medium (DMEM) supplemented with 100 U/mL penicillin-streptomycin (Gibco) and 10% fetal bovine serum (Lonza, 14-501F). Cells were subcultured upon reaching 60-80% confluency. For experiments, cells were seeded onto coverslips in a 24-well plate (BD Falcon) at 2500 cells per cm^2. As a positive control, base-washed coverslips were coated for 5 min in 0.01% poly-L-lysine (Trevigen) then washed three times with phosphate-buffered saline (PBS, 4.2 mM $NaHPO_4$, 0.8 mM KH_2PO_4, 50 mM NaCl, Avantor Performance Materials). Copolymer-coated coverslips were sterilized for 30 min in 70% ethanol at 37 °C and then washed three times with PBS. All images were taken with a Nikon Ti-E C-1 Plus microscope. All groups were tested in triplicate.

LIVE/DEAD Viability Assay

The effect of the copolymer on fibroblast viability was assessed with the LIVE/DEAD Viability/Cytotoxicity Kit (Molecular Probes). After culturing cells for either 1 or 3 d, cells were rinsed with PBS and incubated for 45 min at 37 °C with a solution of 1.5 μM ethidium homodimer-1 and 0.5 μM calcein AM (calcein acetoxymethyl ester)

in PBS. Once staining was complete, cells were rinsed three times with PBS and imaged. All PBS contained 0.01% $CaCl_2$ and 0.01% $MgCl_2$ to prevent cell detachment. To ensure that the protocol was able to detect dead cells, a negative control was created by incubating cells in filtered 70% ethanol for 30 min at 37 °C prior to staining. For experiments with leached coverslips or copolymer extracts, leaching was performed in accordance with the International Organization for Standardization (ISO) standard 10993-5 for *in vitro* cytotoxicity evaluation of medical devices. Briefly, coverslips were leached by incubating copolymer-coated or uncoated base-washed coverslips with culture medium for 24 h at 37 °C before sterilization with ethanol. Culture medium containing leached extracts was sterile-filtered before use. Cells were imaged with a 10x objective. A minimum of 40 cells were imaged per replicate. Cells were counted with NIS-Elements software (Nikon), and viability for each replicate was calculated as the number of living cells divided by the total number of cells counted.

BrdU Proliferation Assay

The effect of the copolymer on the proliferation rate of fibroblasts was determined with a bromodeoxyuridine (BrdU) assay (Calbiochem). After culturing cells for either 1 or 3 d, BrdU label was added to all wells at a final dilution of 1:12000 and incubated at 37 °C for 2 h. Cells were then fixed with ice-cold, filtered 70% ethanol for 5 min and washed twice with filtered PBS. DNA denaturation was achieved by incubating coverslips in 2 N HCl for 30 min. Cells were once again washed twice in filtered PBS before being blocked in PBS with 1% bovine serum albumin (BSA, EMD Chemicals 2930) and 0.1% Triton X-100 for 1 h at room temperature. Coverslips were then incubated with anti-BrdU primary antibody at 1:100 dilution for 1 h and washed three times with PBS. Secondary antibody (Alexa Fluor 488 Goat Anti-Mouse IgG, Molecular Probes) was applied at a 1:1000 dilution in PBS with 1% BSA for 1 h followed by three washes with PBS. To check for non-specific labeling, control groups either without primary or without secondary antibody were performed. All cell nuclei

were stained with DRAQ5 (Biostatus Limited) diluted 1:500 in PBS for 30 min. Coverslips were rinsed twice in PBS, mounted with 50% glycerol in PBS, sealed with clear nail polish, and stored at 4 °C. Confocal imaging was performed with EZ-C1 software (Nikon) using a 20x objective. Nuclei were counted with NIS-Elements software with a minimum of 60 cells counted per replicate. Results were expressed as the percentage of cells stained with BrdU relative to the total number of cells.

Actin Staining

The effect of the copolymer on fibroblast morphology was assessed via actin staining. After culture on the copolymer for 1 or 3 d, cells were fixed in ice-cold acetone for 1 min and then washed three times with filtered PBS. Coverslips were then incubated for 20 min with Alexa Fluor 488 phalloidin (Molecular Probes) at a 1:40 dilution in PBS. Following three 10 min washes with PBS, cells were then counterstained with 1.5 μM ethidium homodimer-1 (Molecular Probes L-3224) for 45 min. Finally, coverslips were rinsed twice in PBS, mounted with Vectashield (Vector Laboratories), and sealed with nail polish. Confocal imaging was performed with EZ-C1 software using a 40x objective.

Statistical Analysis

The percent viability and percent BrdU-positive are represented as the mean $\pm$ the standard deviation. Assumptions of normality and homogeneous variance were first checked using the Shapiro-Wilk test and Levene's test, respectively. Data for direct contact LIVE/DEAD testing at 3 d did not comply with these assumptions, so they were transformed according to the Box-Cox method. Statistically significant groupings within a single time point were calculated using one-way analysis of variance (ANOVA) followed by Tukey's Honestly Significant Difference (HSD) *post hoc* test. All statistical analyses were performed using Statistical Analysis Software (SAS), version 9.4. A p-value less than or equal to $\alpha = 0.05$ was considered significant.

2.4 Results

Copolymer Synthesis and Coating

Spin coating was a simple way to prepare a thin layer of poly[(3,4-dihydroxystyrene)-*co*-styrene] onto coverslips. The resulting film was uniform (average roughness of ~0.1 μm) with an average thickness of ~20 μm. Coverslips with poly[(3,4-dihydroxystyrene)-*co*-styrene] alone and with the same copolymer cross-linked with tetrabutylammonium periodate were evaluated. Although both samples were translucent, the copolymer alone samples were colorless and the cross-linked samples had a yellowish-brown hue (Figure 2.1B). After sterilization with a 70% ethanol solution, the coverslips coated with copolymer alone became slightly opaque.

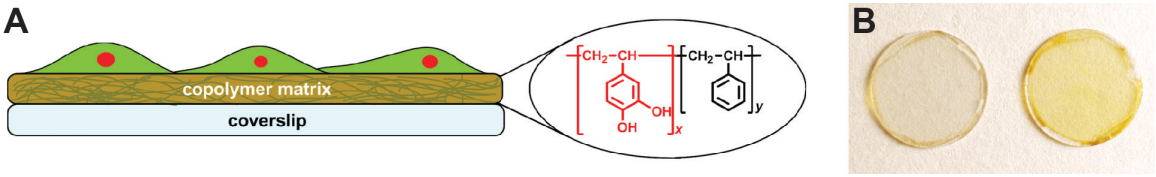

Figure 2.1. (A) Schematic of fibroblast cells cultured directly on poly[(3,4-dihydroxystyrene)-*co*-styrene]-coated coverslips for evaluation of cytotoxicity. (B) Photo of glass coverslips coated with copolymer alone (left) and copolymer with tetrabutylammonium periodate as the cross-linker (right).

LIVE/DEAD Viability Assay

The viability of NIH/3T3 mouse fibroblasts was tested on leached biomimetic copolymer or a positive control (poly-L-lysine, PLL) after culturing for 1 and 3 d (Figure 2.2A). Leaching was performed in culture medium for 24 h at 37 °C in accordance with ISO standard 10993-5 for *in vitro* cytotoxicity evaluation of medical devices. After 1 d of culture, cell viabilities on PLL, copolymer alone, and cross-linked copolymer were 99 ± 1%, 89 ± 4%, and 95 ± 2%, respectively. After 3 d, cell viabilities were 93 ± 4%, 99 ± 1%, and 97 ± 1%, respectively. Although the viability

on copolymer alone was lower than those on PLL and cross-linked copolymer after 1 d, viability on copolymer alone was significantly higher than that on PLL and was similar to that on cross-linked copolymer after 3 d. Overall, cell viability on all surfaces was high, which demonstrates that the leached biomimetic copolymer did not have a strong effect on cell viability.

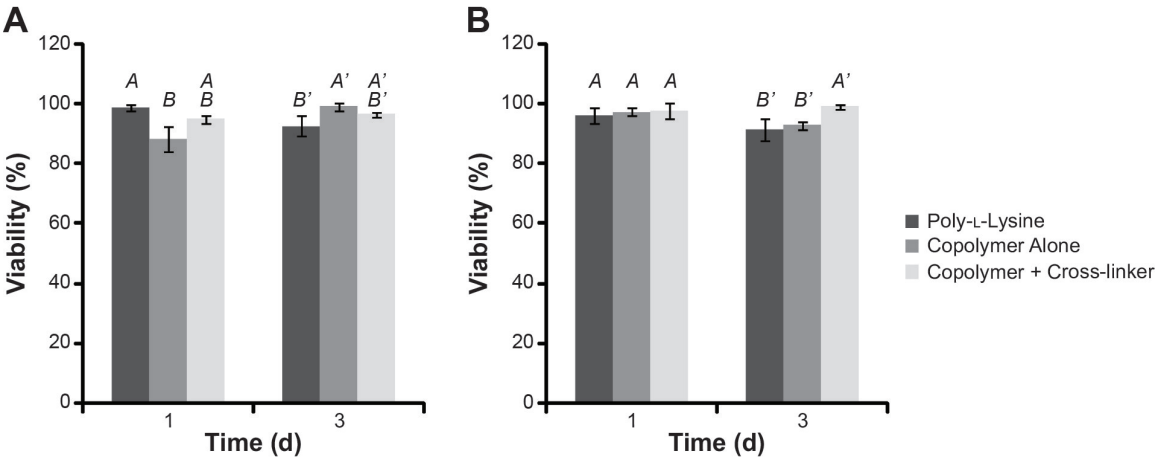

Figure 2.2. LIVE/DEAD viability data for cells cultured on (A) leached coverslips and (B) with leached copolymer extracts. After both 1 and 3 d, viability in all groups is above 85%, and the copolymer demonstrated minimal toxicity. Groups with identical letters within a single time point are statistically similar ($p > 0.05$) as determined by Tukey's HSD *post hoc* test.

Because toxic agents may have been leached out of the copolymer prior to cell seeding, the effect of leached copolymer extracts on fibroblast viability was also tested (Figure 2.2B). After 1 d of culture, all groups had similar viabilities of 96 ± 3%, 97 ± 1%, and 98 ± 3% for PLL, copolymer alone, and cross-linked copolymer, respectively. After 3 d, cells on PLL and copolymer alone had similar viabilities of 92 ± 4% and 93 ± 1%, which were significantly lower than the viability on cross-linked copolymer, 99 ± 1%. Once again, however, the viability of fibroblasts in all conditions was high, which indicates that the biomimetic copolymer has low cytotoxicity.

As a more stringent test of copolymer toxicity, a third set of viability tests was performed with fibroblasts cultured in direct contact with unleached copolymer (Figure 2.3). Similar to previous tests, there was no difference in viability in any group after 1 d of culture. Cell viabilities on PLL, copolymer alone, and cross-linked copolymer were 99 ± 1%, 99 ± 2%, and 95 ± 1%. After 3 d, cells cultured on copolymer demonstrated higher viability (98 ± 0.3% and 98 ± 0.4% for copolymer alone and cross-linked copolymer, respectively) than those cultured on PLL (93 ± 3% viability). In general, treatments with viabilities exceeding 90% are considered non-toxic, and thus no group demonstrated any significant level of toxicity after either 1 or 3 d of culture.

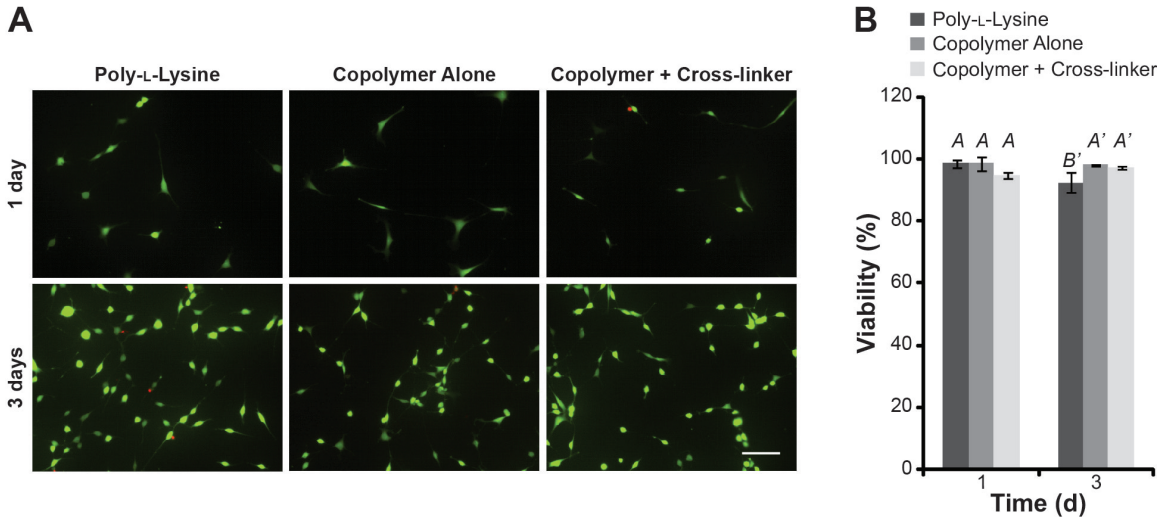

Figure 2.3. (A) Representative images and (B) quantified results for LIVE/DEAD viability assay for cells in direct contact with unleached copolymer. Viable cells are shown in green, whereas non-viable cell nuclei are colored red. Scale bar represents 100 μm. After 1 d of culture, there is no difference in viability between the copolymer groups and the positive control (PLL). After 3 d, the biomimetic copolymer shows higher viability than PLL. Cells in all groups exhibit high viability (>90%) at all time points. Groups with identical letters within a single time point are statistically similar ($p > 0.05$) as determined by Tukey's HSD *post hoc* test. Poly-L-lysine data are the same as shown in Figure 2.2A.

BrdU Proliferation Assay

To assess the effect of the copolymer on cell proliferation rates, a BrdU assay was performed after 1 and 3 d of culture (Figure 2.4). As seen in the representative images in Figure 2.4A, all groups showed a similar percentage of BrdU-positive cells at both time points, and therefore, all groups were proliferating at similar rates. The quantified data (Figure 2.4B) show that after 1 d, 54 ± 7% of cells on PLL were BrdU-positive compared to 51 ± 9% on copolymer alone and 40 ± 12% on cross-linked copolymer. After 3 d, 66 ± 15% of cells on PLL were BrdU-positive. On copolymer alone and on cross-linked copolymer, 49 ± 8% and 58 ± 2% were BrdU-positive, respectively. No statistical differences were found between the proliferation rates of fibroblasts on either copolymer alone or cross-linked copolymer compared to a positive control at any time point.

Actin Staining

The overall morphology of fibroblasts cultured on the copolymer was compared to a positive control by staining the cytoskeletal actin filaments with fluorescently labeled phalloidin (Figure 2.5). After both 1 and 3 d of culture, cells in all groups had similar morphology and exhibited well-organized actin fibers and long, leading lamellae. Whether cross-linked or not, the biomimetic copolymer had no discernable effect on fibroblast morphology compared to the positive control, PLL.

2.5 Discussion

The cytotoxicity of poly[(3,4-dihydroxystyrene)-*co*-styrene] was assessed by examining the viability, proliferation rate, and morphology of fibroblasts cultured in contact with the copolymer. The copolymer consists of a polystyrene backbone with periodic pendant catechol groups that mimic the DOPA groups of natural mussel adhesive proteins. Previous studies with polystyrene have demonstrated strong biocompatibility [123–125]. An FDA-approved tri-block copolymer containing 30% polystyrene

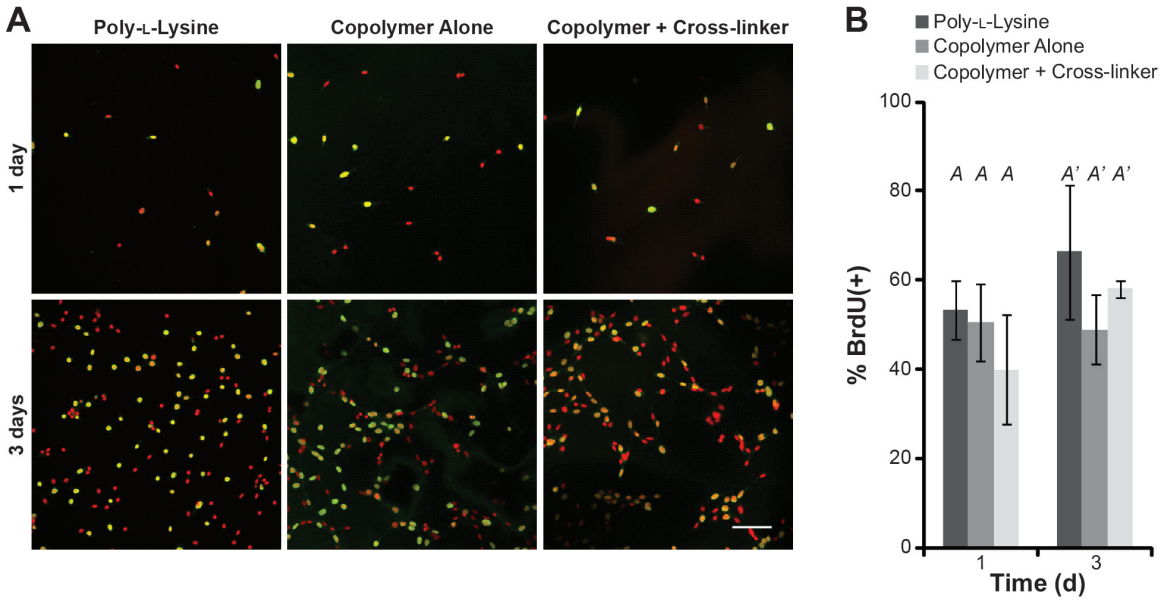

Figure 2.4. (A) Representative images for BrdU proliferation assay. All cell nuclei are shown in red, and BrdU-positive nuclei are shown in green. Scale bar represents 100 μm. (B) Quantified results for BrdU proliferation assay. All groups show similar percentages of BrdU-positive cells at all time points, and therefore neither copolymer group has any effect on the proliferation rate of NIH/3T3 fibroblasts grown in direct contact with the copolymer. Groups with identical letters within a single time point are statistically similar ($p > 0.05$) as determined by Tukey's HSD *post hoc* test.

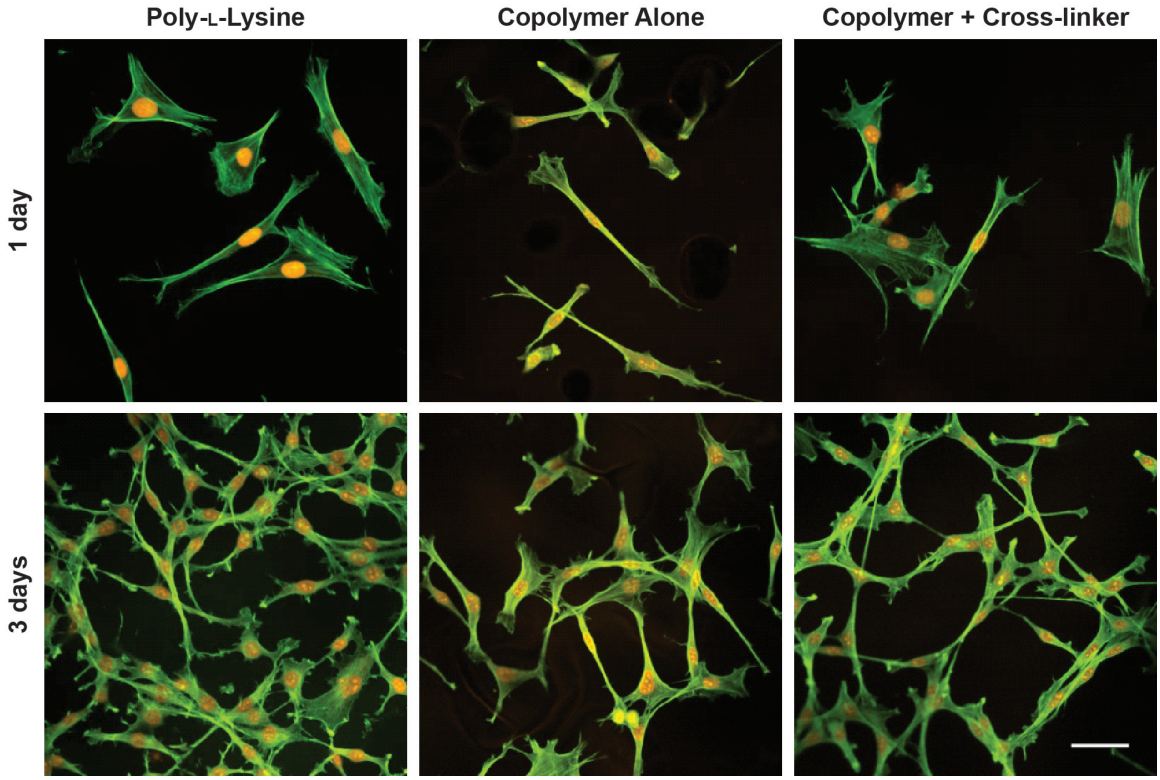

Figure 2.5. Representative images from actin staining of fibroblasts cultured on PLL, copolymer alone, and copolymer with cross-linker. Actin fibers are shown in green, whereas cell nuclei are shown in red. At both 1 and 3 d, there is no obvious difference in overall cell morphology among the groups. Fibroblasts demonstrate normal spread morphology on all substrates. Scale bar represents 50 μm.

(SIBS30) elicited normal capsule formation and inflammatory cell counts corresponding to the lowest categorical level of toxicity after 30 and 180 d of implantation in mice [123]. More data are available regarding the safety of polystyrene when used for food packaging [124, 125]. In a report to the FDA, the Styrene Information and Research Center estimates that up to 90 g of polystyrene can be consumed each day without any adverse health risks [124]. When used in contact with food, the U.S. Code of Federal Regulations mandates that polystyrene should contain less than 1% of unpolymerized styrene monomer [125]. Our previous NMR results suggest that poly[(3,4-dihydroxystyrene)-*co*-styrene] conforms to this specification [117, 118]. Taken together, the previous research on polystyrene suggests that our polystyrene-based material should not be toxic. However, it was still critical to test our material to ensure that the pendant catechol groups did not elicit a toxic response.

When cultured with NIH/3T3 fibroblasts, poly[(3,4-dihydroxystyrene)-*co*-styrene] showed a minimal effect on the cells' viability, proliferation rate, and morphology. These three aspects were assessed in accordance with the recommendation of ISO standard 10993-5 to evaluate cytotoxicity with respect to cell damage (either quantitatively or qualitatively via morphology), cell growth, and aspects of cell metabolism. Specifically, our experimental design followed the ISO guidelines of testing at time points of >24 h with subconfluent cells cultured with sample extracts and on the sample itself.

In the first set of experiments, an initial assessment of cytotoxicity was made by determining cell viability when cultured on leached copolymer or with the corresponding leached extracts. The LIVE/DEAD assay was chosen to provide a quantitative assessment of cell survival by directly counting the number of viable and non-viable cells. After 1 d, the leached copolymer alone group showed a slight decrease in viability compared to the PLL or cross-linked copolymer, but by day three, all biomimetic copolymer groups had statistically similar or higher viability than PLL. When culturing cells with the extracts, both biomimetic copolymer groups displayed equal or

greater viability than the PLL group at all time points. These results indicated high cytocompatibility of the copolymer and its extracts.

From this point on, all experiments were conducted with cells cultured directly on the copolymer (with no leaching of the copolymer), which is a more stringent assay. The unleached direct contact LIVE/DEAD results showed equal or greater viability on both biomimetic copolymer groups compared to the positive control, PLL; therefore, the copolymer again demonstrates high cytocompatibility. In all of our viability assays, the positive control group (PLL) exhibits very mild cytotoxicity on day three of culture. Although PLL is a common cell attachment reagent, it is also known to induce a toxic response in mammalian systems [26, 126].

To ensure that poly[(3,4-dihydroxystyrene)-*co*-styrene] did not affect the rate of cell proliferation or overall cell morphology, additional testing was conducted. Quantitative assessment of proliferation rate was determined using the BrdU assay. In this assay, newly-synthesized DNA is labeled via incorporation of a thymidine analog (BrdU) that can be detected with a specific antibody [127, 128]. For cells cultured on both copolymer alone and cross-linked copolymer, no difference in the percentage of BrdU incorporated was seen compared to cells cultured on PLL at any time point. To assess cell morphology, actin cytoskeletons were stained with fluorescently labeled phalloidin. After both 1 and 3 d, there were no obvious qualitative differences among the three groups, and cells showed normal elongated fibroblast morphology. Interestingly, cells attached and spread on the polystyrene-based copolymer even though fibroblasts do not normally attach well to untreated polystyrene [129]. This observed improvement in cell attachment can most likely be attributed to the adhesive quality of the catechol groups shown in previous studies [130–132].

Some mussel-inspired catechol-rich materials have demonstrated low levels of toxicity. A citrate-based adhesive with a poly(ethylene glycol) (PEG) backbone showed minor to moderate cytotoxicity *in vitro* compared to unmodified PEG diacrylate solutions [108]. The citrate-based polymer was presented in a concentrated pre-polymer form and as a leached extract from the polymerized material. Mild to moderate tox-

icity was observed and found to be directly correlated to both the soluble fraction of the adhesive and the concentration of the sodium periodate cross-linker. At its highest value, the concentration of periodate ion used to cross-link the citrate adhesive reached over twice the concentration used in the present study, which might account for some of the disparity in observed toxicity. A catechol-modified PEG hydrogel was similarly tested for toxicity both *in vitro* and *in vivo* [133]. *In vitro* testing with leached extracts and in direct contact with the hydrogel showed very slight toxicity compared to the control. A mussel-inspired hyperbranched poly(amino ester) polymer also demonstrated mild toxicity *in vitro*; when polymer was added to the cell culture medium, metabolic activity was reduced by ∼25% compared to a positive control after 4 and 7 d of culture [87]. These results are in contrast to the polystyrene-based copolymer in the present study, which showed almost no toxicity. A minimal cytotoxic response was also found with another PEG-DOPA hydrogel [130]. L-929 mouse fibroblasts cultured with the leached extracts and in direct contact with the hydrogel displayed similar metabolic activity to a control group after 1 d but significantly lower metabolic activity after 2 and 3 d. These results contrast with our polystyrene-based copolymer, which showed very slight toxicity after 1 d when leached, but showed no toxicity after 3 d for all conditions. Much like our copolymer, however, morphology of cells cultured on the PEG-DOPA hydrogel was comparable to the control after 2 d of culture directly on the gel.

Numerous mussel-inspired materials, however, show little or no cytotoxicity, much like poly[(3,4-dihydroxystyrene)-*co*-styrene]. A recombinant DOPA-containing protein derived from natural mussel protein sequences has been shown to have no effect on *in vitro* metabolic activity and proliferation rate over 24 h compared to a PLL control [27]. For another set of PEG-DOPA polymers, the toxicity has been thoroughly investigated both *in vitro* with human fetal membranes45 and *in vivo* with islet transplantation [134]. Fetal membranes displayed a similar percentage of apoptotic cells compared to control groups when cultured either with leached extracts or in direct contact with the PEG-DOPA polymer, which indicates its low cytotoxicity. When

used as an adhesive for extrahepatic islet transplantation in mice, the PEG-DOPA polymer elicited a minimal inflammatory response. Both of these studies utilized a sodium periodate cross-linker but, similar to the present study, saw no adverse effects from the cross-linker. Thus, similar to many mussel-inspired materials in the literature, the addition of catechol groups to polystyrene and the use of periodate for a cross-linker still resulted in high cytocompatibility of this biomimetic copolymer.

2.6 Conclusions

The mussel-mimetic material, poly[(3,4-dihydroxystyrene)-*co*-styrene], is an adhesive that provides strong bonds, sets in a wet environment, and exhibits cytocompatibility. In this study, the copolymer was tested for *in vitro* cytotoxicity following the guidelines of ISO standard 10993-5. NIH/3T3 fibroblasts were cultured both directly and indirectly with copolymer alone and copolymer cross-linked with tetrabutylammonium periodate. After 1 and 3 d of culture, cell viability in response to leached copolymer extracts, leached copolymer, and unleached copolymer was fairly similar to that on a positive control, PLL. Also, no effect was seen on cell proliferation rate or morphology when cells were cultured directly on the copolymer. These results establish the high cytocompatibility of poly[(3,4-dihydroxystyrene)-*co*-styrene]. From these promising results, future studies of this copolymer could investigate use in applications requiring biological contact such as tissue engineering scaffolds, bone cements, or tissue adhesives.

2.7 Acknowledgments

This work was supported by the Purdue School of Chemical Engineering and the College of Engineering, the National Science Foundation (Awards DMR-1309787, CHE-0952928, and a Graduate Fellowship to M.J.B.), a 3M Nontenured Faculty Award, a Steven C. Beering Fellowship to M.J.B., and the Office of Naval Research

(Award N00014-13-1-0327). We thank Dr. Alyssa Panitch (Purdue University) for her kind gift of NIH/3T3 mouse fibroblasts.

3. CRITICAL FACTORS FOR THE BULK ADHESION OF ELASTOMERIC PROTEINS

This chapter consists of a manuscript by Brennan MJ, Hollingshead SE, Wilker JJ, and Liu JC, prepared for submission in 2015.

3.1 Abstract

Many natural protein-based adhesives, such as soy protein and mussel adhesive proteins, have been the subject of scientific and commercial interest. Recently, a variety of protein adhesives have been isolated from diverse sources such as insects, frogs, and even squid ring teeth. Many of these protein adhesives have similar amino acid compositions to well-studied elastomeric proteins such as elastin. Although elastin is widely investigated as a structural biomaterial, little work has been done to assess its potential as an adhesive. In this study, a recombinant system of elastin-like polypeptides (ELPs) was created to probe the factors affecting adhesion strength. Lap shear adhesion was used to examine the effects of extrinsic factors (pH, concentration, crosslinker, humidity, cure time, and cure temperature) and intrinsic factors (protein sequence, structure, and molecular weight). Of the extrinsic factors tested, only humidity, cure time, and cure temperature had a significant effect on adhesion strength. Generally, as water content was reduced, adhesion strength increased. Of the intrinsic factors tested, protein amino acid sequence did not significantly affect adhesion strength, but less protein structure and higher molecular weights directly increased adhesion strength. The adhesion strengths of the proteins in this study (>2 MPa) were comparable to or higher than the strengths of commercially available protein-based adhesives (hide glue and fibrin sealant). These results indicate general rules for the design of adhesives from elastomeric proteins.

3.2 Introduction

Protein-based adhesion has been the subject of recent and historical scientific interest. Soy protein was originally patented in 1923 and has been used commercially as a renewable, low-cost wood glue for nearly a century [7, 34]. Similar adhesives can be created from other crops, including sorghum, camelina, and canola [135]. For these glues, adhesive performance derives primarily from the mechanical interlocking between protein chains and the porous wood structure with contributions from hydrogen bonding and van der Waals forces [7]. As such, adhesion strength is directly related to a variety of factors, including protein denaturation, glue viscosity, particle size, and substrate physical properties [7, 136].

Mussel adhesive proteins (MAPs) have also received significant interest from the scientific community for their ability to form adhesive bonds in wet environments [23, 24]. The wet adhesion strength of MAPs is largely due to the presence of the non-canonical amino acid 3,4-dihydroxyphenylalanine (DOPA) [9,10,137]. DOPA provides bulk adhesive strength through the combination of adhesive interactions with the substrate and cohesive interactions from crosslinking [114,115]. The presence of many charged lysine residues in MAPs has also been cited as a potential contributor to MAP adhesion strength [12, 121, 138, 139].

More recently, other natural protein-based adhesives have been isolated and characterized. For example, the frog species *Notaden bennetti* secretes a sticky protein solution as a defense mechanism [62], and the velvet worm captures its prey with a similar protein solution [2]. A wide variety of insects also produce protein-based glues for a number of purposes. Gum moths, blowflies, and ladybirds utilize protein glues for egg attachment, and spittle bugs, froghoppers, and lerps produce protein-based materials for protection [5]. If raised above their glass transition temperature, the structural proteins from squid ring teeth also form a strong underwater adhesive [140]. Interestingly, the reported shear adhesion strengths (1 - 2 MPa) for these protein adhesives are all quite similar [5, 62, 140]. Furthermore, many of these protein adhesives

have similar amino acid compositions: glycine is nearly always over-represented, and proline and serine are often present at unusually high mole percentages [2, 5, 62, 140].

The amino acid compositions of these natural adhesive proteins are also similar to that of elastin, an elastomeric protein renowned for its structural properties of low stiffness, high extensibility, and high resilience [3,66,73,74]. In addition, elastin can be produced recombinantly with high yields in *Escherichia coli* [73]. Recombinant design provides for precise control over protein molecular weight and amino acid sequence; this control allows for investigation into the effect of small protein sequence changes on protein function [77, 141, 142]. Despite the fact that elastomeric proteins have been widely studied as biomaterials, only a few studies have examined the adhesive properties of elastomeric proteins [32, 143].

Because of their similarities to natural protein-based adhesives, we hypothesized that elastin-like polypeptides (ELPs) would have significant bulk adhesion strength. Furthermore, we wanted to assess the potential of ELPs as adhesive materials and understand the important factors contributing to the adhesive qualities of these and other natural protein-based glues. In this study, we used a set of recombinant ELPs with varied guest residue compositions to systematically investigate the effect of various extrinsic and intrinsic factors on the lap shear strength of protein adhesives.

3.3 Materials and Methods

Reagents

All chemicals were purchased from Sigma-Aldrich (St. Louis, MO) or Avantor Performance Materials (Center Valley, PA) unless stated otherwise. Water was ultrapurified with a Milli-Q ultrapurification system (Millipore, Billerica, MA).

Protein Design and Cloning

DNA sequences were designed using Geneious software (Biomatters Inc., San Francisco, CA). Complete amino acid sequences for the final protein constructs are shown

in Figure 3.1. Predicted protein isoelectric points (pI) were estimated with Geneious software. The grand average of hydropathicity (GRAVY), based on the scale by Kyte and Doolitte [144], was calculated for each protein using the ExPASy ProtParam tool (http://web.expasy.org/protparam).

The elastin-based proteins ELP[KEY_4-24], ELP[KEY_4-48], ELP[KEY_4-96], ELP[$K_2Y_2V_2$-48], and ELP[K_3Y_3-48] were constructed with a cloning scheme modified from one previously developed by our lab [145]. The new scheme utilized AgeI and AvaI restriction enzymes (New England Biolabs, Ipswich, MA) to achieve seamless repeats of the elastin-like sequence. Standard molecular cloning techniques were used throughout [146].

Protein Expression

For each protein, the following bacterial expression strains were screened to identify the strain with the highest expression: Rosetta2(DE3)pLysS (EMD Chemicals, Gibbstown, NJ), BL21(DE3)pLysS (courtesy of Dr. Chongli Yuan, Purdue University), BL21(DE3), and BL21-CodonPlus-(DE3)-RIPL (both courtesy of Dr. Jo Davisson, Purdue University). The strains chosen for expression of each protein are shown in Table 3.1. Cells were grown overnight at 37 °C in 2xYT medium containing appropriate antibiotics.

For ELP[KEY_4-48] and ELP[K_3Y_3-48], overnight cultures were diluted at a 1:250 ratio into a fermentor (BioFlo 110, 14 L capacity, New Brunswick Scientific, Enfield, CT) with 10 L of Terrific Broth (TB) containing appropriate antibiotics. At an optical density (OD) of 4-6, protein expression was induced by 2.5 mM isopropyl β-D-1-thiogalactopyranoside (IPTG, EMD Chemicals). After culturing for an additional 1-3 h, cells were harvested by centrifugation at 8000g for 15 min at 4 °C.

For ELP[KEY_4-24], ELP[KEY_4-96], and ELP[$K_2Y_2V_2$-48], overnight cultures were diluted at a 1:140 ratio into 4 L baffled flasks containing 1 L of 2xYT medium with appropriate antibiotics. Cells were cultured at 37 °C and 300 rpm. Once cell growth had reached an OD of $\sim$1, protein expression was induced by 1 mM IPTG. Cells were

then cultured for an additional 3 h and harvested by centrifugation at 3220g for 20 min at 4 °C.

Protein Purification

ELP[KEY_4-48] was purified by a temperature cycling method similar to those previously described [80]. The cell pellet was resuspended in 0.01 M sodium carbonate with ∼0.1 mg each of deoxyribonuclease I, ribonuclease A, and phenylmethanesulfonylfluoride (PMSF). The pellet was then subjected to at least two freeze-thaw cycles and followed by sonication with a Misonix XL-2000 (Qsonica, Newtown, CT) for at least 90 cycles of 1 min sonication followed by 1 min cooling on ice. Next, a hot cycle was performed to induce the protein into a coacervate state: the pH of the cell lysate was adjusted to 8.6, heated at ∼60 °C for 45 min, and centrifuged at 11000g for 45 min at 40 °C. The pellet from the hot cycle was then subjected to a cold cycle to resolubilize the target protein: the pellet was resuspended in 0.01 M sodium carbonate at 3 mL per gram of pellet, adjusted to pH ∼11, cooled on ice, and then centrifuged at 11000g for 45 min at 4 °C. Beginning with the supernatant from this cold step, an additional hot cycle and cold cycle were performed, but the second heated pellet was resuspended at 20 mL per gram of pellet.

ELP[K_3Y_3-48] was purified similarly to ELP[KEY_4-48], but with both hot and cold cycles at pH 7.4 and the addition of sodium chloride to a final concentration of 1 M during the hot cycles.

ELP[KEY_4-24], ELP[KEY_4-96], and ELP[$K_2Y_2V_2$-48] were purified using denaturing nickel affinity chromatography. Cell pellets were resuspended in Buffer B (8 M urea, 100 mM NaH_2PO_4, 100 mM Tris-Cl, pH 8.0), subjected to at least two freeze-thaw cycles, and sonicated as above. The cell lysate was centrifuged at 10000g for 45 min at 4 °C to remove cell debris. The supernatant was mixed with nickel-nitrilotriacetic acid (Ni-NTA) agarose (QIAGEN, Valencia, CA) at a concentration of 2 mL of lysate per mL of Ni-NTA and loaded onto a chromatography column (Flex-Column, Kimble Chase, Vineland, NJ). The column was incubated at 37 °C

and 100 rpm for 1 h to allow the desired protein to bind to the Ni-NTA. Next, undesired proteins were allowed to drip out of the column by gravity flow, and the column was washed with 3 bed volumes of Buffer C (8 M urea, 100 mM NaH_2PO_4, 100 mM Tris-Cl, 10 mM imidazole, pH 6.3). Purified protein was eluted with 5 bed volumes of Buffer D/E (8 M urea, 100 mM NaH_2PO_4, 100 mM Tris-Cl, pH 5.5).

Purified proteins were dialyzed extensively against 5% acetic acid at 4 °C to remove salts and were then lyophilized. Protein expression and purification were confirmed by analysis with sodium dodecyl sulfate-polyacrylamide gel electrophoresis (SDS-PAGE) and Western blot using standard techniques [147]. Proteins were detected using an anti-T7 tag antibody conjugated to horseradish peroxidase (EMD Chemicals, Gibbstown, NJ) with a colorimetric substrate (3,3',5,5'-tetramethylbenzidine, Kirkegaard & Perry Laboratories, Gaithersburg, MD). SDS-PAGE gels were stained with Coomassie Brilliant Blue R-250. Protein purity was assessed through densitometry analysis with ImageJ software (NIH, Bethesda, MD) [148]. Purified protein molecular weights were verified by matrix-assisted laser desorption/ionization-time of flight (MALDI-TOF) mass spectrometry (Dr. Connie Bonham, Campus-Wide Mass Spectrometry Center, Purdue University). Briefly, the MALDI mass spectra were obtained on a Voyager DE-Pro TOF mass spectrometer (Applied Biosystems, Framingham, MA) in the linear mode with delayed extraction. The matrix was sinapinic acid. Positive-ion spectra were obtained with an acceleration voltage of 25000 V. Additionally, purified protein amino acid compositions were verified by the Molecular Structure Facility at the University of California, Davis.

Lap Shear Adhesion

Bulk lap shear adhesion bonding was performed following a modified version of the ASTM D1002 standard, as previously described [119, 149]. Briefly, adherends were prepared using ASTM standard D2651-01 for adherend cleaning [150]. Protein was resuspended at 150 mg/mL in water (unless otherwise specified), and 5 μL of this solution was spread onto each aluminum adherend. Tris(hydroxymethyl) phos-

phine (THP, Strem Chemicals, Newburyport, MA) was used to crosslink primary amine groups. For all crosslinked protein samples, protein was resuspended at 167 mg/mL, and crosslinker solution was added to make a final protein concentration of 150 mg/mL. The concentration of crosslinker solution was calculated based on the ratio of hydroxyl groups to the number of primary amines in the protein. Titebond Liquid Hide Wood Glue was tested by applying an equivalent weight of glue solids (1.5 mg per test) based on a 41.3 wt% water content (previously determined by C. L. Jenkins, personal communication). Tisseel (donated by Baxter Biosurgery, Deerfield, IL) was prepared according to the manufacturer's directions and tested by applying an equivalent protein content (1.5 mg per test).

Adherends were overlapped with an area of 1.2 cm x 1.2 cm and were cured for 6 h at 37 °C (unless otherwise specified). Humid curing conditions were created by covering the adherends with a layer of damp paper towels followed by a layer of plastic wrap to prevent drying. Lap shear bond strengths were measured using an Instron 5544 Materials Testing System (Norwood, MA) with a loading rate of 2 mm/min and a 2000 N load cell. Maximum force was divided by overlap area to determine the adhesion strength. When investigating the effects of pH, concentration, crosslinker, moisture, cure time, and cure temperature, 5 samples were tested for each condition. For all other conditions, 10 samples were tested.

Circular Dichroism (CD)

The secondary structure of proteins in solution (0.1-0.2 mg/mL in water or 3 M urea) was determined using a Jasco-815 circular dichroism spectrometer (Halifax, Nova Scotia, Canada) with the following parameters: 1 mm path length, 1 nm data pitch, 2 nm bandwidth, 100 nm/min scanning speed. Each spectrum, including the baseline spectra of water and 3 M urea, was averaged from five scans.

Thermogravimetric Analysis (TGA)

The residual water content during curing at 37 °C was determined via thermogravimetric analysis. For each cure time tested, 20 μL of ELP[KEY$_4$-48] at 150 mg/mL in water was pipetted into a 6.7 mm x 2.7 mm aluminum pan (Thermal Support, Hayesville, NC). The sample was then heated in a TGA Q50 (TA Instruments, New Castle, DE) to 37 °C at a rate of 5 °C/min and held at 37 °C for the duration of the cure. Finally, the sample underwent a temperature ramp to 200 °C at a rate of 20 °C/min. Water content was calculated from the weight loss that occurred near 100 °C. Throughout the experiment, the sample was purged with nitrogen gas at a rate of 40 mL/min.

Statistical Analysis

Adhesion data are represented as the mean ± the standard deviation. First, outliers were removed from the data after assessment with Grubbs' test. Next, equality of variance was evaluated with Levene's test. Statistically significant differences were determined by one-way ANOVA followed by Tukey's Honestly Significant Difference (HSD) or the Games-Howell (for unequal variances) *post hoc* test. The normality of ANOVA residuals was assessed with the Komogorov-Smirnov test. In the case of non-normally distributed residuals, the original data were transformed according to the Box-Cox or Johnson method before repeating the above analysis. Statistical difference between two groups was determined with an unpaired t-test. Statistical analyses were performed with Minitab 17 (State College, PA) or GraphPad online software (La Jolla, CA). A p-value ≤ 0.05 was considered significant.

3.4 Results

Protein Design, Expression, and Purification

In this study, we designed and produced a system of ELPs that would allow us to probe the effects of protein design on protein adhesion (see Figure 3.1 and Table 3.1

for details). Three ELPs were designed with varying charged residue content, and hydrophobic tyrosine and valine residues were used to maintain a similar average hydrophobicity based on the scale developed by Urry [77, 151]. ELPs are named following the method previously described by the Chilkoti lab [76, 152]. Briefly, each ELP is designated as ELP[$A_iB_jC_k$-n], in which A, B, and C refer to guest residues (X) of the VPGXG pentapeptide. Subscripts i, j, and k describe the numbers of each guest residue used within a group of six pentapeptides, and n refers to the total number of pentapeptides in the protein. For example, ELP[KEY_4-96] contains 96 total VPGXG pentapeptides in which 1/6 of the guest residues are K, 1/6 are E, and 4/6 are Y. One of the ELPs, ELP[KEY_4-n], was produced with 24, 48, and 96 total pentapeptides to probe the effect of protein molecular weight.

Figure 3.1. Complete amino acid sequences of the ELPs used in this study. (A) At their N-terminus, all proteins contain a T7 tag for Western blot identification, a 7xHis tag for nickel column purification, and an enterokinase cleavage site. (B) Within the elastomeric domains, ELP guest residues are bolded, and charged residues are underlined.

Each of the proteins was cloned and then over-expressed using the T7 expression system. ELP[KEY_4-48] and ELP[K_3Y_3-48] were purified using a temperature cycling protocol similar to others used to purify ELPs [80]. The remaining ELPs were purified using nickel affinity chromatography. Final purified yields are shown in Table 3.1. Expression and purification were confirmed by SDS-PAGE and Western blot (Supporting Information, Figure 3.10). Protein molecular weight was confirmed

Table 3.1.
Detailed information on recombinant proteins.

Protein	Predicted pI	Molecular Weight (kDa)	Hydropathicity (GRAVY)	Expression Strain	Yield (mg/L)[a]
ELP[KEY$_4$-n]					
$n = 24$	6.38	15.5	-0.321	BL21(DE3)pLysS	62
$n = 48$	6.39	26.6	-0.209	Rosetta2(DE3)pLysS	358
$n = 96$	6.40	48.8	-0.140	BL21(DE3)	47
ELP[K$_2$Y$_2$V$_2$-48]	10.11	25.5	0.095	BL21-CodonPlus-(DE3)-RIPL	71
ELP[K$_3$Y$_3$-48]	10.23	26.3	-0.295	BL21(DE3)pLysS	17

[a]Yield was calculated per liter of bacterial culture.

by MALDI-TOF (Supporting Information, Figure 3.11), and protein composition was confirmed by amino acid analysis (Supporting Information, Tables 3.4 - 3.8).

Effect of Extrinsic Factors on Bulk Adhesion

To examine the effect of pH, concentration, crosslinker, humidity, and cure time and temperature, lap shear adhesion testing was performed on a single protein, ELP[KEY_4-48]. Unless stated otherwise, all extrinsic factors were tested with the protein at 150 mg/mL, pH 3, and cured at 37 °C for 6 h with 5 replicates.

pH can affect protein charge, solubility, and secondary structure and in doing so, could affect protein adhesive and cohesive interactions. The overall charge as a function of pH was estimated for ELP[KEY_4-48] (see Supporting Information, Figure 3.12), and the secondary structure was examined with circular dichroism (Figure 3.2A). At a pH below 4 or above 10, the protein is highly charged, is soluble in aqueous solution, and although largely unstructured (negative peak at 198 nm), it exhibits β-II turn structure (negative peak at 220 nm) characteristic of ELPs [153]. At intermediate pH values ($\sim$4.5 and $\sim$9), ELP[KEY_4-48] again displays β-II turn structure and is moderately charged. At a relatively neutral pH, the protein is near its isoelectric point and is completely insoluble and aggregated in aqueous solution. As a result, we were unable to obtain spectra near neutral pH. In addition, spectra could not be recorded at pH 12 due to the interference of high concentrations of acid and base required.

The bulk adhesive strength of ELP[KEY_4-48] was tested at pH 3, 4.5, 7, 9, 10.5, and 12 (Figure 3.2B). Average strengths ranged from 0.65 MPa at pH 10.5 to 1.2 MPa at pH 4.5 and 7. Despite the strong effect that pH has on protein charge, solubility, and structure, there were no statistically significant differences in adhesion strengths across the range of pH values tested.

The next extrinsic factor tested was protein concentration (Figure 3.3). Concentration can affect the solution viscosity and bond thickness, and therefore could have an effect on adhesion strength [154]. Although the concentration of ELP[KEY_4-48]

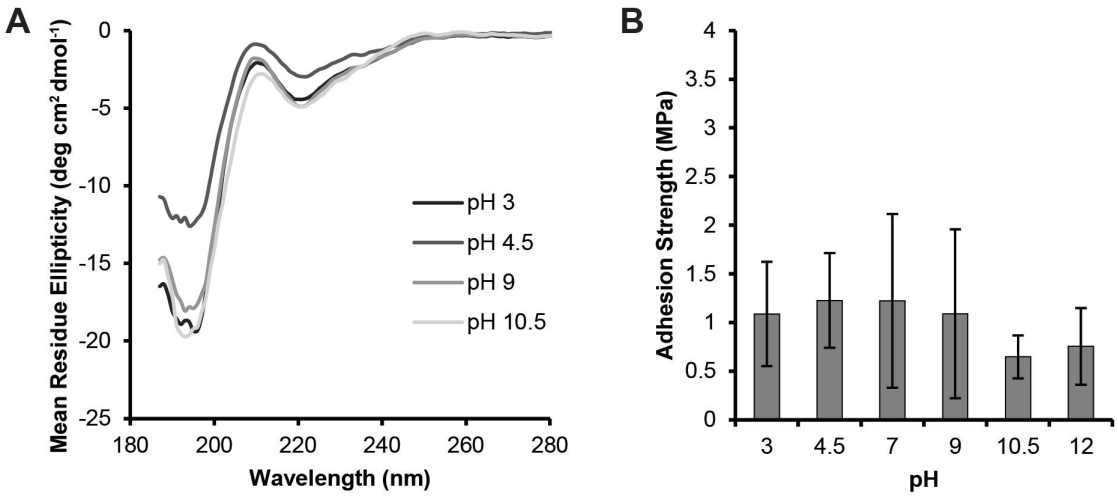

Figure 3.2. Effect of pH on (A) secondary structure and (B) bulk adhesion strength of ELP[KEY_4-48]. (A) CD spectrometry was performed on protein solutions at pH 3, 4.5, 9, and 10.5. Secondary structure did not vary significantly with pH. (B) Bulk adhesion testing was performed with protein at pH 3, 4.5, 7, 9, 10.5, and 12. Adhesion strengths did not demonstrate significant variation with pH, as assessed by one-way ANOVA followed by Tukey's HSD *post hoc* analysis.

was varied from 50 to 500 mg/mL, adhesion strengths at all concentrations were not significantly different from each other.

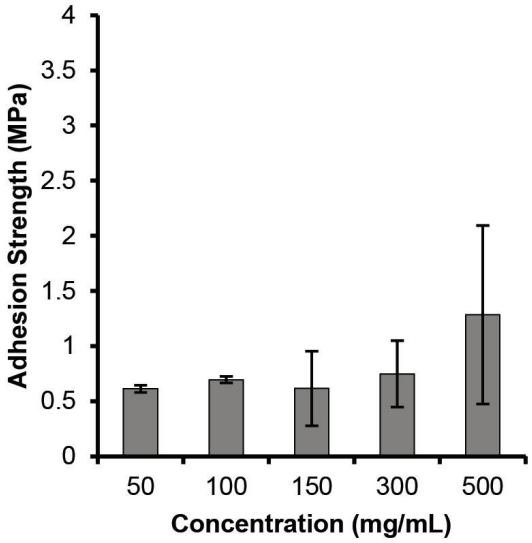

Figure 3.3. Effect of ELP[KEY_4-48] protein concentration on bulk adhesion strength. Varying the concentration of protein from 50 to 500 mg/mL resulted in no change in the adhesion strength as assessed by one-way ANOVA followed by Tukey's HSD *post hoc* analysis.

Bulk adhesion is a balance of adhesive and cohesive interactions between the glue and the substrate [11]. The addition of a crosslinking agent could change this balance and thus affect the adhesion strength. THP, the crosslinker used in this study, crosslinks primary amine groups on the protein via condensation reactions in relatively mild reaction conditions with water as a byproduct. When testing the effects of crosslinker on adhesion strength, the stoichiometric ratio of reactive THP hydroxyl groups to primary amines on ELP[KEY_4-48] was varied between 0x and 100x (Figure 3.4). However, there were no significant differences in bulk adhesion strengths across the crosslinker ratios tested.

Historically, adhesion in the presence of moisture has been one of the key challenges for glue development. To determine the effect moisture might have on the adhesion of elastomeric proteins, ELP[KEY_4-48] was cured in a highly humid environment (Fig-

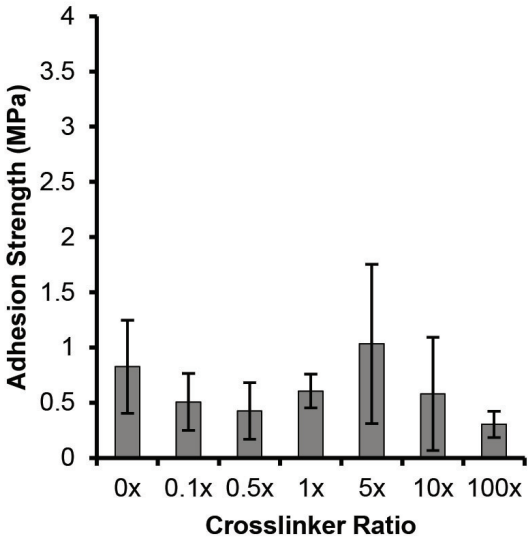

Figure 3.4. Effect of THP crosslinker on the bulk adhesion strength of ELP[KEY_4-48]. Stoichiometric crosslinker ratio (THP reactive hydroxyl groups to protein primary amines) was varied between 0x and 100x, but no significant changes in the adhesion strength were detected as assessed by one-way ANOVA followed by Tukey's HSD *post hoc* analysis.

ure 3.5). As might be expected, samples cured in humid conditions demonstrated significantly reduced adhesion strength (0.19 MPa) compared with previous tests in a dry environment (1.31 MPa). In addition, it was observed that samples cured in a humid environment retained visible moisture, whereas those cured in a dry environment had visibly dried out upon testing.

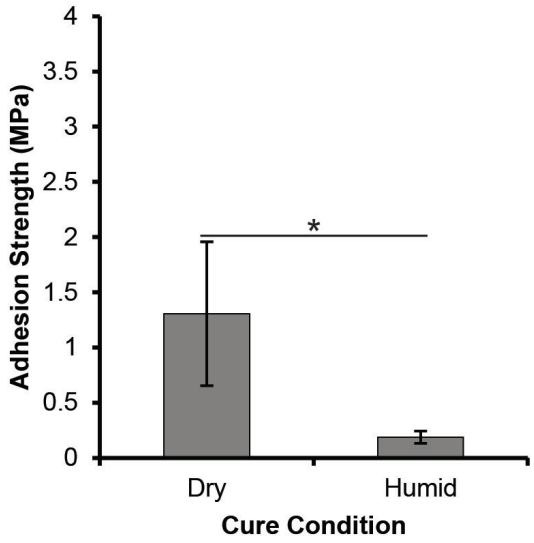

Figure 3.5. Effect of a humid cure environment on bulk adhesion strength. ELP[KEY_4-48] was cured at 37 °C in both dry and highly humid environments. Humid curing conditions significantly decreased the bulk adhesion strength of the protein. The dry cure data is the same as that shown in Figure 3.2B at pH 3. A statistically significant difference (unpaired t-test, $p < 0.05$) is indicated by the asterisk.

Other curing factors such as time and temperature can also be critical to the final adhesion strength. In this study, samples were cured in a dry environment for eight different times (1 min, 5 min, 1 h, 3 h, 6 h, 12 h, 24 h, 7 d) at each of three different temperatures (22 °C, 37 °C, 55 °C). Results are shown in Figure 3.6. When a two-way ANOVA was used, both cure time and temperature were significant factors for adhesion strength. With regards to temperature, 22 °C resulted in significantly lower strengths than either 37 or 55 °C. With regards to time, 1 min and 5 min cure times

were statistically equivalent, as were 12 h, 24 h, and 7d. Samples cured for 1 h, 3 h, and 6 h were significantly different from each other and from samples cured for very short (< 1 h) or very long (> 6 h) cure times. One-way ANOVA allows us to more closely examine the trends identified by two-way ANOVA. Similar to what was identified in two-way ANOVA, higher temperatures increased adhesion strengths, but this effect was only found at short cure times ($\leq$6 h). At long cure times ($\geq$12 h), this phenomenon was no longer observed.

We believed that the increase in adhesion strength with cure time was most likely related to the remaining water content in the samples. To test this hypothesis, TGA was performed on a protein solution at the same concentration and pH (Table 3.2). The protein solution was cured at 37 °C for 2, 5, 30, 60, and 100 min. As the cure time at 37 °C was increased from 2 min to 100 min, the water content remaining in the sample decreased from 75.3% to 1.3%. TGA results show that significant water loss occurs over time at 37 °C; however, the time scale of water loss does not match that seen in lap shear adhesion, and this discrepancy is most likely due to the differences in exposed surface area. Combined with the adhesion results from a humid cure, the TGA results demonstrate that water loss is likely responsible for the increase in adhesion strength with cure time and temperature.

Table 3.2.
Thermogravimetric analysis results.

Cure Time (min)	Remaining Water Content (%)
2	75.3
5	71.4
30	19.5
60	2.8
100	1.3

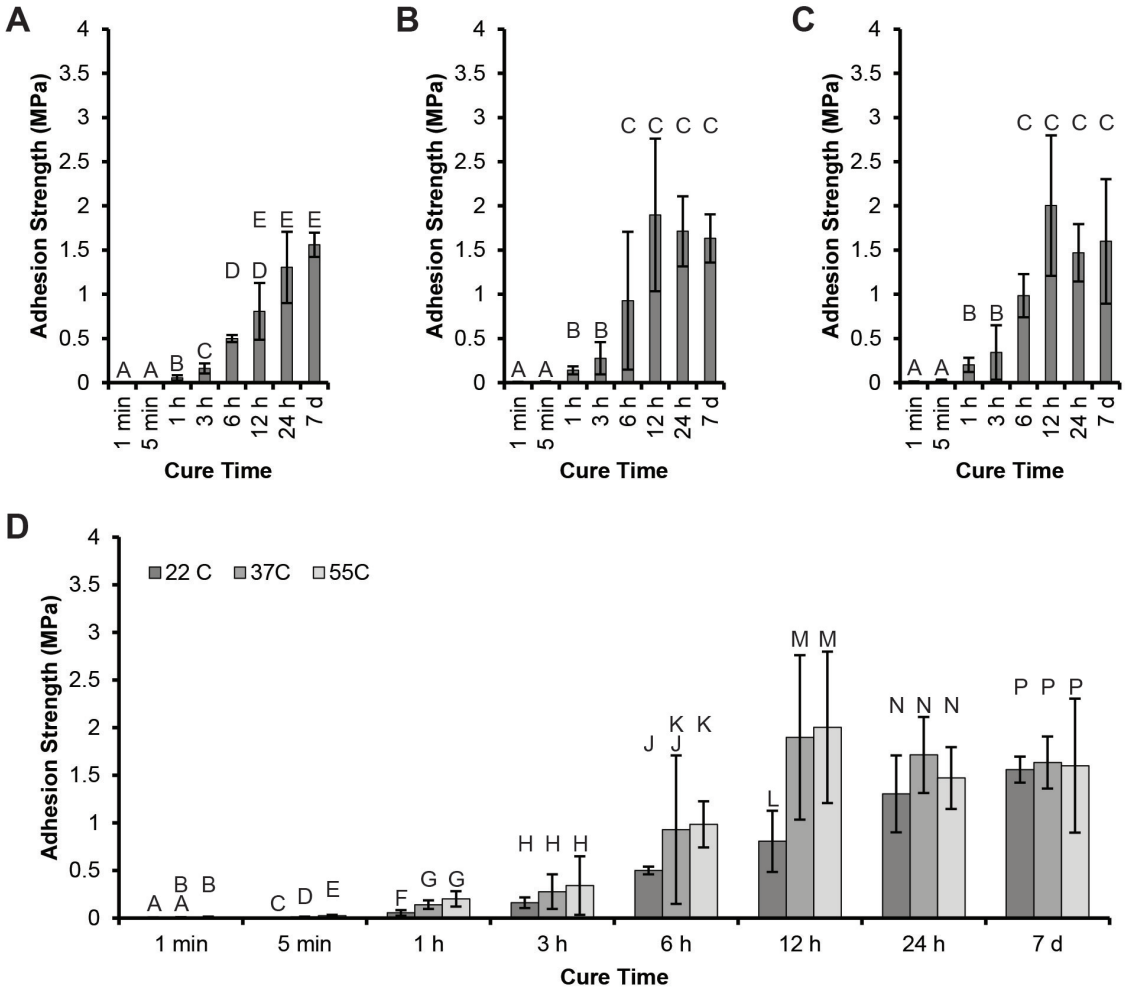

Figure 3.6. Effect of cure time and temperature on the bulk adhesion of ELP[KEY$_4$-48]. Adhesion strengths vs. cure times are shown at (A) 22, (B) 37, and (C) 55 °C. Groups with identical letters are statistically similar ($p > 0.05$) as determined by one-way ANOVA followed by Tukey's HSD *post hoc* analysis. (D) The same data are grouped by cure time. Groups that share a letter are statistically similar ($p > 0.05$) as determined by a one-way ANOVA (performed within a single time point) followed by either Tukey's HSD or the Games-Howell *post hoc* test. Adhesion strength increases with cure time and temperature up to 6-12 h, after which adhesion strength remains constant at all temperatures. Two-way ANOVA results indicate that the relative adhesion strengths vary according to 22 °C < 37, 55 °C and 1 min, 5 min < 1 h < 3 h < 6 h < 12 h, 24 h, 7 d.

Effect of Intrinsic Factors on Bulk Adhesion

To examine the effect of amino acid composition, structure, and molecular weight, lap shear adhesion testing was performed using different recombinant proteins. Unless stated otherwise, all intrinsic factors were tested with 10 replicates of 150 mg/mL of protein cured at 37 °C for 24 h. These cure conditions were based on the optimum found from the extrinsic factor tests.

Three ELPs were used to elucidate the effect of amino acid composition on bulk adhesion strength: ELP[KEY$_4$-48], ELP[K$_3$Y$_3$-48], and ELP[K$_2$Y$_2$V$_2$-48]. The three ELPs have similar hydrophobicities based on the scale by Urry [77,151], but they have different numbers of charged residues (i.e., lysine and glutamic acid), which results in an overall sequence difference of ∼10%. To control for the factor of size, all of these proteins have approximately the same molecular weight (∼26 kDa). Bulk adhesion strengths of these proteins are shown in Figure 3.7. All of the ELPs have statistically similar adhesion strengths.

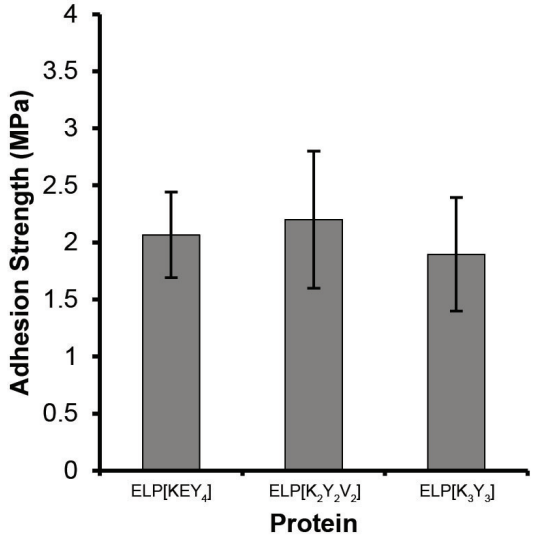

Figure 3.7. Effect of protein amino acid sequence on the bulk adhesion strength. Despite a ∼10% variation in protein sequence, all of the ELPs possessed similar adhesion strengths as assessed by one-way ANOVA followed by Tukey's HSD *post hoc* analysis.

Based on previous work with soy protein adhesives, the addition of a denaturant could increase adhesion strength due to disruption of protein structure [41]. The effect of protein structure on bulk adhesion was examined by the addition of a denaturant (3 M urea) to ELP[KEY$_4$-48] and BSA, a folded protein control. Because a denaturant could have more impact on a structured protein than an unstructured one, BSA was used as a control. As seen in Figure 3.8, the presence of 3 M urea significantly increased the adhesion strength of BSA; however, even with the enhancement, BSA was still significantly weaker than ELP[KEY$_4$-48] alone. Urea did not have an effect on the strength of ELP[KEY$_4$-48].

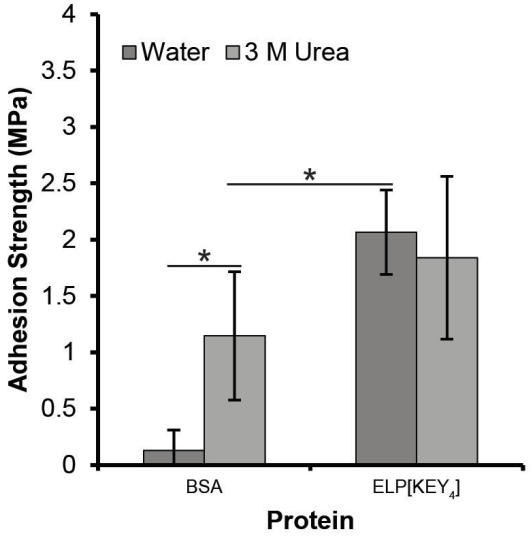

Figure 3.8. Effect of a denaturant (3 M urea) on bulk adhesion strength. The adhesion strength of the highly structured BSA protein was compared with the relatively unstructured ELP[KEY$_4$-48] protein. The addition of denaturant had a highly positive effect on the adhesion strength of BSA, whereas it had no effect on the ELP. Statistically significant differences (unpaired t-test, $p < 0.05$) are indicated by an asterisk.

The final factor investigated in this study was the effect of protein molecular weight, or length, on bulk adhesion strength (Figure 3.9). The protein ELP[KEY$_4$-n] was produced with 24, 48, and 96 repeats (15.5, 26.6, and 48.8 kDa, respectively)

to directly assess the effect of molecular weight on adhesion strength. Adhesion strength of ELPs improved with increasing molecular weight. Furthermore, a 1:1:1 molar ratio (keeping the total mass constant) of the three protein sizes was also tested to determine the effect of a mixture of molecular weights since this strategy improved adhesion strength in a previous study with a mussel-mimetic polymer [119]. The mixture of molecular weights exhibited similar adhesion strength to the proteins with 48 and 96 pentapeptides.

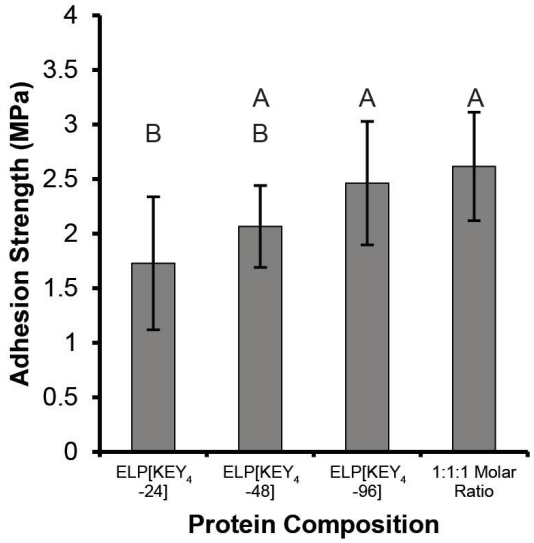

Figure 3.9. Effect of protein molecular weight on bulk adhesion strength. The adhesion strength of ELP[KEY_4-n] with 24, 48, and 96 pentapeptides was tested. To see the effect of a mixture of molecular weights, a 1:1:1 molar ratio of the three weights was also tested. Generally, adhesion strength increased with molecular weight. The mixture of molecular weights resulted in a similar adhesion strength to that of either of the two longest proteins tested alone. Groups with identical letters are statistically similar ($p > 0.05$) as determined by one-way ANOVA followed by Tukey's HSD *post hoc* analysis.

Comparison to Commercial Adhesives

To put these results in broader context, the adhesion strength of commercial protein-based adhesives was compared with that of our proteins. Two commercial adhesives were chosen for comparison: Titebond Liquid Hide Wood Glue and Tisseel fibrin sealant. For each adhesive, total protein mass was kept consistent with our testing (i.e., ∼1.5 mg total protein per test). Results are shown in Table 3.3. The adhesion strength of Hide Glue was ∼2 MPa, which is similar to the highest strength measured in this study using the ELP[KEY_4] 1:1:1 molar ratio (2.6 MPa). The adhesion strength of Tisseel was significantly lower, however, at an average strength of 0.7 MPa.

Table 3.3.
Lap shear adhesion of recombinant elastomeric proteins compared with commercial adhesives.

Adhesive	Strength ± Standard Deviation (MPa)[a]
Hide Glue	1.9 ± 1.1^{A}
Tisseel	0.7 ± 0.3^{B}
ELP[KEY_4] 1:1:1 Ratio[b]	2.6 ± 0.8^{A}

[a]Groups with identical superscript capital letters are statistically similar ($p > 0.05$) as determined by one-way ANOVA followed by the Games-Howell *post hoc* analysis.
[b]ELP data is the same as in Figure 3.9.

3.5 Discussion

Nature has created numerous protein-based glues for a wide variety of purposes. Interestingly, many of these protein adhesives have similar adhesion strengths and amino acid contents [2, 5, 62, 140]. In this study, we systematically probed potential factors critical to protein-based adhesion strength to: 1) better understand the function of these adhesives in nature and 2) aid in the design of future protein-based

adhesives. We approached this problem by designing a system of recombinant ELPs since these proteins have similar amino acid compositions to natural protein glues and have been widely studied as structural biomaterials [2,5,62,73,140]. In addition, the use of recombinant proteins allows us to have precise control over sequence and molecular weight. Using these proteins, we examined the effect of various extrinsic and intrinsic factors on lap shear adhesion strength.

We first investigated the effect of extrinsic factors on the adhesion of a single protein, ELP[KEY_4-48]. Our results suggest that neither pH nor concentration contributes to adhesion strength in any significant fashion despite the fact that variations in pH affect protein surface charge, structure, and solubility (see Figures 3.2A and 3.12) and variations in concentration affect solution viscosity and bond thickness [154]. In the literature, concentration is often a factor in adhesion strength, whereas the contribution of pH to protein-based adhesion is mixed.

pH is highly critical to soy protein adhesives [36,38,40]. When formulating the adhesive, the processing pH affects protein solubility and therefore the product formed. When applying the glue, a moderately high pH leads to protein hydrolysis and increased adhesion strength [7]. An excessively high pH negatively affects the adhesive properties of soy, however [38, 40].

The changes in protein properties resulting from pH can also affect the interactions between protein and substrate and thereby affect the adhesive bond. For example, the adsorption of a DOPA-less mussel adhesive protein varied greatly between pH 3 and 5.5 [155]. In general, adsorption of other proteins is highly dependent on pH [156]. On the other hand, adjusting the pH from 4 to 11 did not have an effect on the single molecule adhesion of a silk-based protein [157].

Other adhesive systems suggest that protein concentration should affect adhesion strength. For a synthetic mussel-mimetic polymer, increasing the concentration from 75 mg/mL to 1.2 g/mL led to a significant increase in adhesion strength [120]. The increase in strength was attributed to an increase in viscosity, which can affect bond thickness and resulting strength [154]. Viscosity and concentration are also central

to soy protein adhesion. Strength increases up to an optimal concentration of ∼100 mg/mL before decreasing at a concentration of ∼140 mg/mL [158], and viscosity affects adhesion strength by altering the interaction between soy protein and its substrate [36, 38, 158].

The use of a crosslinker was also thought to be potentially important because bulk adhesion strength is dependent on a balance between adhesive and cohesive forces [20]. A crosslinking agent can induce greater protein-protein interactions and thus theoretically reduce the possible protein-substrate interactions. In our recombinant protein system, however, varying the crosslinker ratio from 0x to 100x did not affect the adhesion strength of ELP[KEY_4-48]. In contrast, the addition of a crosslinker has a strong effect on adhesion strength in systems that utilize DOPA [116, 120, 159, 160]. Crosslinking agents have also been used to improve the adhesive properties of soy protein adhesives [7, 38, 45]. Notably, however, the adhesive proteins derived from the frog *Notaden bennetti* display no evidence of crosslinking as part of the curing process [62].

The single most important extrinsic factor for our protein adhesives was moisture. When cured in a humid environment, the adhesion strength of ELP[KEY_4-48] decreased by a factor greater than 4. When cure time and temperature were varied, adhesion strength increased with time and temperature until it reached a stable optimum around ∼2 MPa; thermogravimetric analysis suggests that the increase in strength is directly related to residual water content. These results are not unexpected; with few exceptions [140], adhesion in wet environments is nearly always weaker than in a dry environment and remains one of the greatest challenges for adhesive engineering. For example, proteinaceous glue from *Notaden bennetti* also produced optimum strengths of ∼1.7 MPa when completely dried [62]. It should be noted, however, that final adhesion strength of our protein was not related to the cure temperature. This result is similar to that with a mussel-mimetic recombinant protein [116] but quite distinct from that with a mussel-mimetic polymer [120]. Soy protein adhesives demonstrate varying responses to cure temperature; in one study,

increasing the cure temperature from 25 °C to 100 °C increased the strength from ∼1.5 to ∼2 MPa [158], whereas another study found that varying the temperature between 120 °C and 160 °C had no effect on strength [161].

Our recombinant protein system also allowed us to examine the effect of factors intrinsic to the proteins themselves, including amino acid composition, structure, and molecular weight. To probe the effect of small changes in protein sequence, we compared the bulk adhesion of several ELPs whose guest residues varied in their content of charged (lysine, glutamic acid) and hydrophobic (tyrosine, valine) residues while maintaining similar overall hydrophobicity. The ELP sequences differed by ∼10% and varied in their isoelectric points from 6.38 to 10.23. However, there was little difference in adhesion strength. A similar effect was seen with silk-elastin-like polypeptides [143]. Cysteine, glutamic acid, and tyrosine were each over-represented in different constructs, but there was no difference in protein surface adhesion as measured by a tape peel test. Likewise, other natural adhesive proteins demonstrate strong adhesion despite large variations in amino acid composition and overall hydrophobicity [2, 5, 62, 140].

However, other types of protein adhesives have noted a strong influence of amino acid composition. For example, numerous studies of mussel-mimetic systems have noted the potential importance of lysine residues in MAP adhesion [12, 121, 138, 139]. In one study, increasing the cation content of a synthetic mussel-mimetic polymer from 0% to 7% increased the dry adhesion strength from 2.4 MPa to 2.8 MPa and doubled the underwater adhesion strength to a maximum value of 0.4 MPa [121]. Although hydrophilic lysine residues are thought to improve adhesion in MAPs, the adhesion strength of soy and sorghum adhesives has been correlated with increased hydrophobicity and hydrophobic amino acid content; it is thought that these residues aid in repelling water from the adhesive bond [41, 162].

Although amino acid composition varies among many natural adhesive proteins, many of these adhesives are unified by the over-representation of glycine, proline, and/or serine [2, 5, 62, 140]. Because glycine is over-represented in many of these natu-

ral adhesive proteins, many of them also lack significant secondary structure [2,62,163] and are thus similar to ELPs [153]. To determine the effect that protein structure might have on adhesion strength, we compared the adhesion strength of BSA and an ELP dissolved in either water or 3 M urea. As shown by CD (Figure 3.2A), ELP[KEY$_4$-48] is largely unstructured (negative peak at 198 nm) but possesses slight secondary structure in the form of β-II turns (negative peak at 220 nm). In contrast, BSA is a highly structured globular protein. The addition of 3 M urea to BSA resulted in a significant improvement in adhesion strength, whereas it had no effect on the adhesion strength of ELP[KEY$_4$-48]. The BSA results match studies performed with soy adhesives. In general, denaturation of soy proteins is required to produce significant adhesion strength [7, 36]. One of the most effective methods of soy protein denaturation is alkali treatment [40], although other methods have been used, including sodium dodecyl sulfate, sodium dodecylbenezene sulfonate, urea, and guanidine hydrochloride [41, 42, 164]. In one study, the adhesion strength of soy protein increased with denaturant concentration up to an optimum concentration of 3 M urea or 1 M guanidine hydrochloride; very high concentrations of either denaturant (8 M and 3 M, respectively) resulted in reduced adhesion strength [41]. Similar results were observed in another study: partial denaturation of soy protein with 1 M urea increased adhesion strength, whereas further denaturation with 3 M urea reduced adhesion strength [164]. Altogether, these results indicate that unstructured proteins may be beneficial to protein-based adhesion.

The final factor examined in this study was the effect of protein molecular weight. We produced one of our ELPs, ELP[KEY$_4$-n], with n = 24, 48, or 96 elastin-like pentapeptides, which resulted in proteins of three different molecular weights: 15.5 kDa, 26.6 kDa, and 48.8 kDa, respectively. The adhesion strength of these proteins increased with protein molecular weight. This result is similar to numerous other adhesive systems: poly(dimethylsiloxanes) (tested up to 68,000 g/mol) [165, 166], a mussel-mimetic polymer (tested up to 100,000 g/mol) [119], silk-elastin-like polypeptides (tested up to 130 kDa) [143], and trypsinized soy protein isolate (mixtures of

proteins with molecular weights $\leq$ 200 kDa) [136]. The bond strength enhancement is thought to be related to increased chain entanglement and elongation prior to breaking [119, 166, 167]. On the other hand, another study with soy protein adhesives showed increased adhesion strength after treatment with the protease trypsin, which should have reduced the average molecular weight of the soy proteins [46]. In addition, epoxidized natural rubber [168, 169] and poly(vinyl alcohol) [170, 171] demonstrated optimum adhesion at intermediate molecular weights (50,000 g/mol and 100,000 g/mol, respectively), but this result may be due to increased surface wetting [166, 169].

Because bonding derives from a balance between wettability and strength [168, 169], optimum conditions could result from a blend of molecular weights [119]. In nature, protein adhesives from insects and amphibians are often a mixture of molecular weights [2, 5, 62]. Additionally, mussels are known to adhere through a spatially organized combination of six adhesive proteins of varying molecular weights, and proteins with lower molecular weights are found closer to the adhesive interface [6]. When this idea was applied to a synthetic mussel-mimetic polymer, a blend of molecular weights possessed an adhesion strength similar to the average strength of the individual components [119]. We investigated how a similar approach would affect the adhesion strength of our protein adhesives. We mixed the three molecular weights of ELP[KEY$_4$-n] in a 1:1:1 molar ratio. Unlike the mussel-mimetic polymer, however, we did not see a strength corresponding to the strength of the average molecular weight; instead, the blended protein mixture demonstrated equivalent strength to that of the two largest molecular weight proteins alone.

To bring greater context to our results, we also compared the adhesion strength of our proteins with those of two commercial protein adhesives: a wood glue derived from animal hide and Tisseel, a fibrin-based surgical sealant. When tested in identical conditions with an equivalent mass of protein per test, our elastomeric proteins demonstrated equivalent adhesion strength to that of hide glue and superior adhesion strength to that of Tisseel. From this work, it can be said that unstructured

ELPs are able to produce significant adhesion strength that rivals commercial glues and that these protein adhesives are not affected by variations in pH, concentration, crosslinking, or sequence.

3.6 Conclusions

In this work, we examined the potential for elastomeric proteins to be used as adhesive materials. By using a system of ELPs, we were able to probe the critical factors related to adhesion strength. We found that for a single protein, moisture content was a more significant factor than pH, concentration, or crosslinking. In terms of protein design, protein length and structure had the most significant effect on adhesion strength. Finally, our proteins demonstrated significant adhesion strengths equivalent to or greater than two commercially available protein-based adhesives. These results have strong implications for the general understanding of natural and recombinant protein-based adhesion and for the design of future protein-based adhesives.

3.7 Acknowledgments

This work was supported by the Purdue School of Chemical Engineering and the College of Engineering (J.C.L.), the National Science Foundation (Awards DMR-1309787 to J.C.L. and J.J.W., CHE-0952928 to J.J.W., and a Graduate Fellowship to M.J.B.), a 3M Nontenured Faculty Award to J.C.L., a Purdue Research Foundation Summer Faculty Grant to J.C.L., a Steven C. Beering Fellowship to M.J.B., and the Office of Naval Research (Awards N00014-13-1-0327 and N00014-13-1-0245 to J.J.W.). We thank Dr. Alyssa Panitch, Dr. Jo Davisson, and Dr. Chongli Yuan for bacterial expression hosts and Baxter Biosurgery for the generous donation of Tisseel. We also thank Haefa Mansour and Victoria Messerschmidt for their assistance with cloning; Michael Laird Johnston for his assistance with thermogravimetric analysis; Dr. Elizabeth Topp for the use of the CD spectrometer; Dr. Connie Bonham (Campus-Wide Mass Spectrometry Center, Purdue University) for her assistance with MALDI-TOF;

Dr. John Schulze (Molecular Structure Facility, University of California, Davis) for his assistance with amino acid analysis; and Dr. Courtney L. Jenkins, Dr. Heather J. Meredith, and Jessica K. Román for their insightful discussions about adhesion.

3.8 Supporting Information

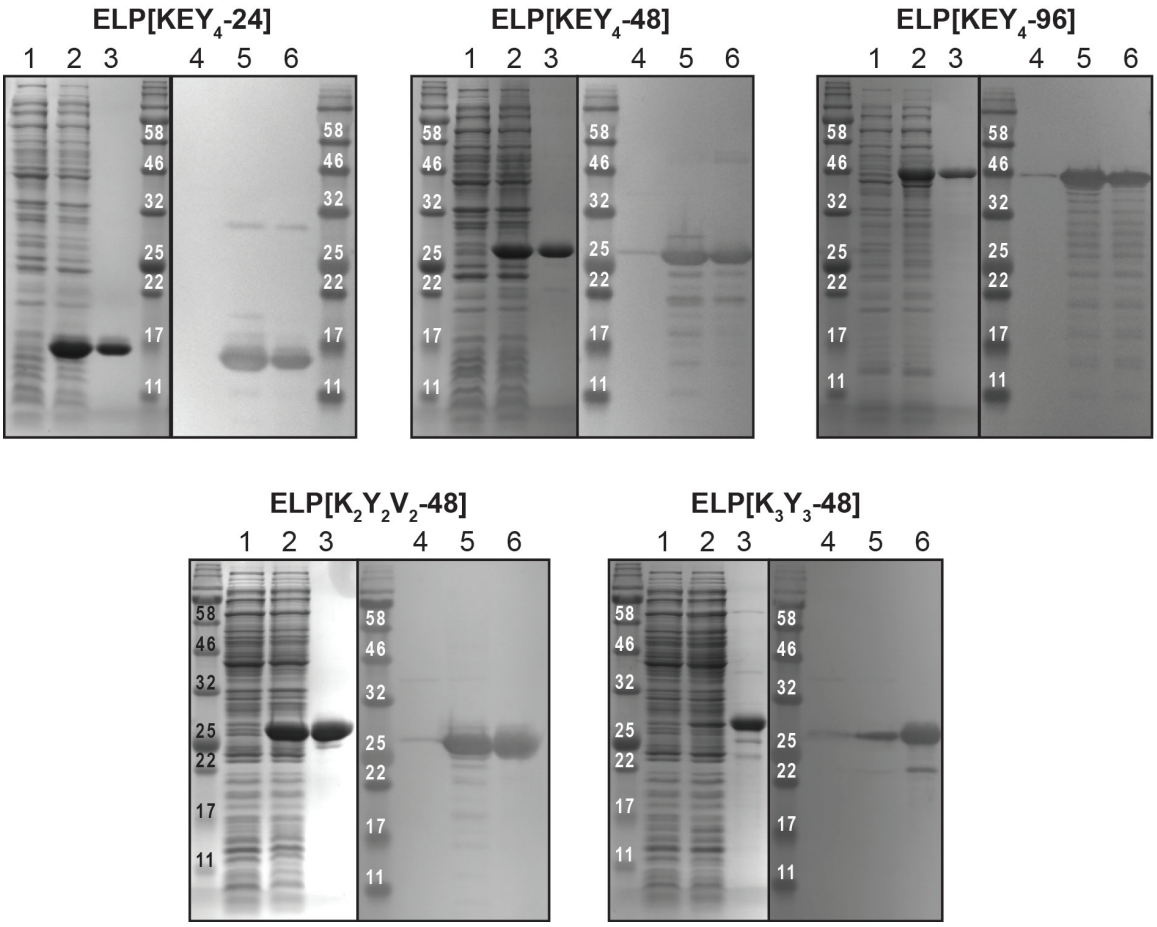

Figure 3.10. SDS-PAGE gels and Western blots showing expression and purified protein samples for each protein in this study. Lanes 1-3 correspond to SDS-PAGE gels, whereas lanes 4-6 correspond to Western blots. Lanes 1 and 4 show culture samples prior to induction of expression with IPTG. Lanes 2 and 5 show culture samples at harvest with over-expressed proteins. Lanes 3 and 6 show purified protein at ∼1 mg/mL. Protein standard bands are labeled with their weight in kDa. The expected molecular weights of the proteins are shown in Table 3.1.

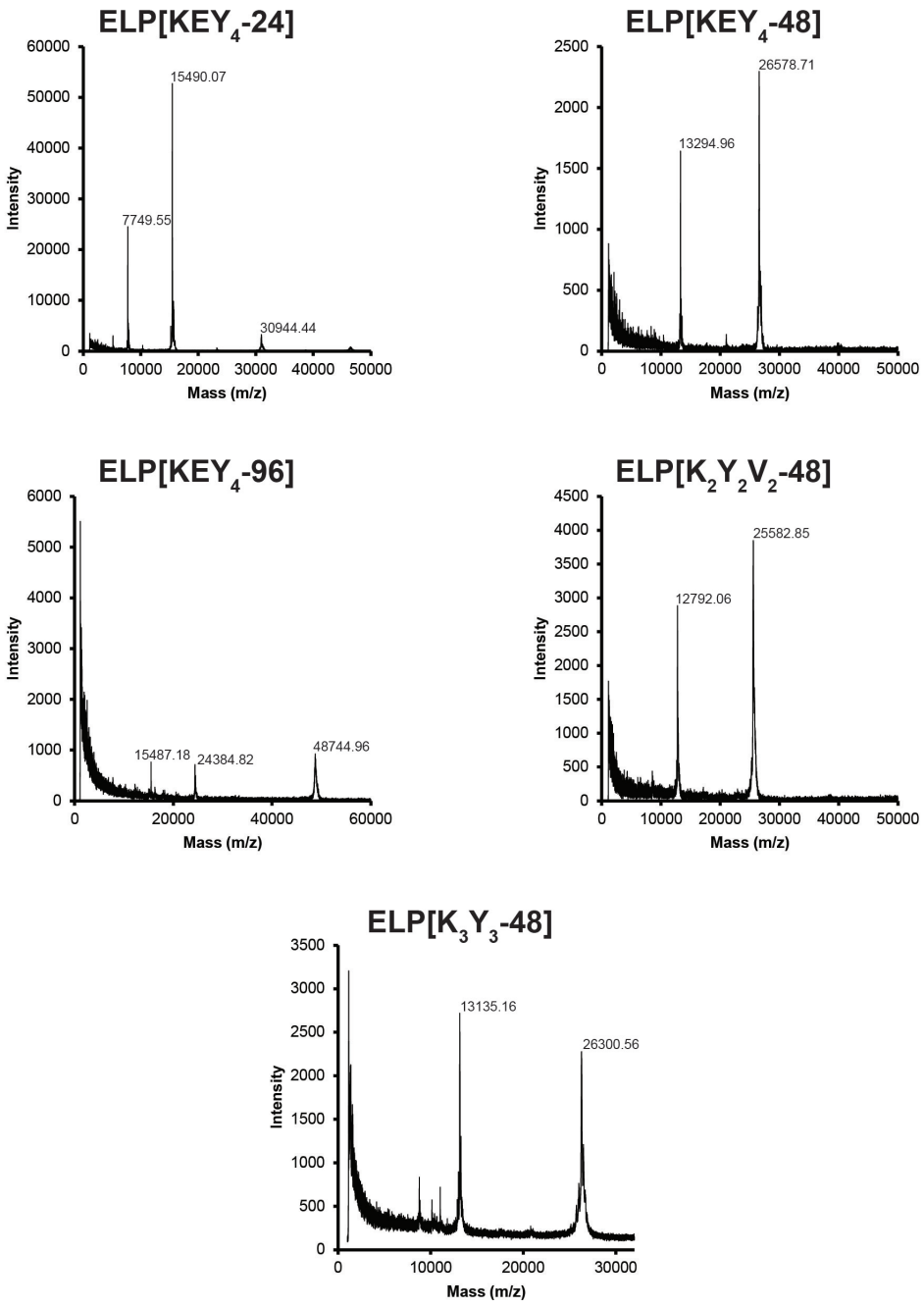

Figure 3.11. MALDI-TOF spectra of the proteins used in this study. Spectra for all proteins exhibited peaks within 0.13% of the expected protein molecular weights. Many spectra also contained the doubly charged ion peak, which appears at ∼50% of the protein expected molecular weight. In addition, the spectrum for ELP[KEY_4-24] exhibits a peak at twice the expected molecular weight corresponding to a protein dimer.

Table 3.4.
Amino acid analysis of ELP[KEY_4-24].

Amino Acid	**Observed mol %**	**Expected mol %**
ASX	4.00	3.90
THR	1.33	1.30
SER	0.65	0.65
GLX	4.42	4.55
PRO	15.83	16.23
GLY	34.57	34.42
ALA	1.40	1.30
VAL	15.72	16.23
ILE	0.04	0.00
LEU	2.01	1.95
TYR	10.40	10.39
PHE	0.00	0.00
HIS	4.56	4.55
LYS	3.59	3.25
ARG	1.47	1.30

Table 3.5.
Amino acid analysis of ELP[KEY_4-48].

Amino Acid	**Observed mol %**	**Expected mol %**
ASX	3.41	2.17
THR	1.42	0.73
SER	1.64	0.36
GLX	5.49	4.01
PRO	16.27	17.88
GLY	32.91	36.86
ALA	2.02	0.73
VAL	15.26	17.88
ILE	0.44	0.00
LEU	2.14	1.09
TYR	10.20	11.68
PHE	0.53	0.00
HIS	2.68	2.55
LYS	3.83	3.28
ARG	1.67	0.73

Table 3.6.
Amino acid analysis of ELP[KEY_4-96].

Amino Acid	**Observed mol %**	**Expected mol %**
ASX	1.77	1.17
THR	0.75	0.39
SER	0.46	0.19
GLX	3.90	3.70
PRO	17.93	18.87
GLY	37.44	38.33
ALA	0.89	0.39
VAL	17.70	18.87
ILE	0.19	0.00
LEU	0.99	0.58
TYR	11.68	12.45
PHE	0.06	0.00
HIS	1.72	1.36
LYS	3.72	3.31
ARG	0.82	0.39

Table 3.7.
Amino acid analysis of ELP[$K_2Y_2V_2$-48].

Amino Acid	**Observed mol %**	**Expected mol %**
ASX	2.45	2.19
THR	0.84	0.73
SER	0.41	0.36
GLX	1.15	1.09
PRO	17.53	17.88
GLY	37.13	36.86
ALA	0.84	0.73
VAL	22.74	23.72
ILE	0.05	0.00
LEU	1.17	1.09
TYR	5.72	5.84
PHE	0.00	0.00
HIS	2.70	2.55
LYS	6.45	6.20
ARG	0.80	0.73

Table 3.8.
Amino acid analysis of ELP[K_3Y_3-48].

Amino Acid	Observed mol %	Expected mol %
ASX	2.48	2.19
THR	0.93	0.73
SER	0.48	0.36
GLX	1.44	1.09
PRO	17.20	17.88
GLY	36.48	36.86
ALA	1.13	0.73
VAL	17.18	17.88
ILE	0.24	0.00
LEU	1.26	1.09
TYR	8.39	8.76
PHE	0.17	0.00
HIS	2.17	2.55
LYS	9.65	9.12
ARG	0.80	0.73

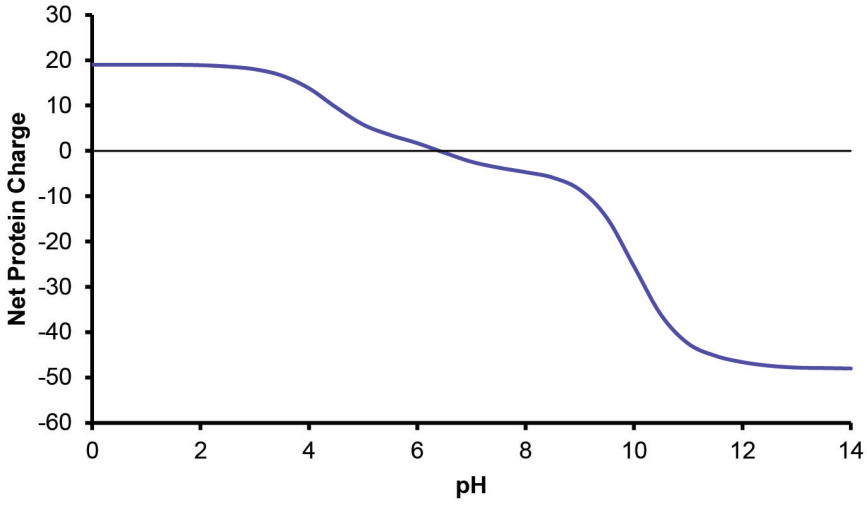

Figure 3.12. Estimated net charge vs. pH for ELP[KEY_4-48]. An online calculator (available at http://protcalc.sourceforge.net/) was used to estimate charge based on the pKa values of the amino acids.

4. A BIOINSPIRED ELASTIN-BASED PROTEIN AS A CYTOCOMPATIBLE UNDERWATER ADHESIVE

This chapter consists of a manuscript by Brennan MJ, Kilbride BF, Wilker JJ, and Liu JC, prepared for submission in 2015.

4.1 Abstract

The development of adhesives that can be applied and bond underwater is a significant challenge for materials engineering. When the adhesive is intended for biomedical applications, further criteria, such as biocompatibility, must be met. Current biomedical adhesive technologies do not meet these needs. In response, we designed a bioinspired adhesive material that shows promise to achieve biocompatible underwater adhesion with environmentally responsive, or "smart", behavior. The material, ELY_{16}, is constructed from an elastin-like polypeptide (ELP) that can be produced in high yields from *Escherichia coli* and coacervate in response to environmental factors such as temperature, pH, and salinity. To confer wet adhesion, we utilized design principles from marine organisms such as mussels and sandcastle worms. When expressed, ELY_{16} is rich in tyrosine; upon modification with tyrosinase to form $mELY_{16}$, the tyrosine residues are converted to 3,4-dihydroxyphenylalanine (DOPA). Both ELY_{16} and $mELY_{16}$ exhibit cytocompatibility and significant dry adhesion strength (>2 MPa). Modification with DOPA increases protein adsorption to glass and provides adhesion strength in a highly humid environment (∼250 kPa). Furthermore, our ELP exhibits a tunable phase transition behavior that can be formulated to coacervate in physiological conditions and provides a convenient mechanism for application underwater. Finally, $mELY_{16}$ possessed significantly higher adhesion strength in dry, humid, and

underwater environments compared with a commercially available fibrin sealant. In conclusion, our ELP shows great potential as a new "smart" underwater adhesive.

4.2 Introduction

There has been a wealth of recent interest in the development of adhesive materials that function in wet or underwater environments. In particular, much of this focus has been placed on adhesive development for biomedical applications, as a suitable biomedical adhesive could have an immense impact on health and the economy. Each year, over 230 million major surgeries are performed worldwide [81], and over 12 million traumatic wounds are treated in the U.S. alone [172]. Approximately 60% of these wounds are closed using mechanical methods such as sutures and staples [50]. Sutures and staples have several disadvantages relative to adhesives, including patient discomfort [86], higher risk of infection [84,85], and the inherent damage to surrounding healthy tissue. With the aid of developments in adhesive technology, it has been estimated that by 2017, hemostats, sealants, and adhesives could comprise a market share of $38 billion [50].

Current FDA-approved adhesives and sealants face several challenges. First, numerous adhesives exhibit toxic characteristics. For example, cyanoacrylate-based adhesives like Dermabond and SurgiSeal can only be applied topically due to carcinogenic degradation products [96,97]. Fibrin sealants like Tisseel and Artiss are derived from blood sources and therefore carry the potential for bloodborne pathogen transmission [101, 102]. Poly(ethylene glycol) (PEG) adhesives are approved as a suture sealant but, due to intense swelling when wet, have the potential to cause moderate inflammatory responses [103]. TissuGlu, a recently approved urethane-based adhesive, showed increased risk of irritation following subcutaneous implantation, and, in clinical trials, seroma formation occurred in 22% of patients [104]. More important, however, is that most of these adhesives do not possess strong adhesion in an excessively wet environment and are not approved for application in wound clo-

sure [90, 98–100, 104]. In fact, many of these materials specifically advise to dry the application area as much as possible [90, 173].

In approaching the challenge of developing a strong adhesive for wet applications, many researchers have been inspired by natural glues. Specifically, underwater application and bonding has been demonstrated with materials based on organisms such as sandcastle worms [60,61] and mussels [121]. Both of these organisms produce proteins containing the non-canonical amino acid 3,4-dihydroxyphenylalanine (DOPA), which has been shown to provide adhesion strength, even in wet environments [11, 12]. In the case of a mussel-mimetic polymer, underwater application was achieved by dissolving the polymer in a chloroform/methanol solution to maintain phase separation from the aqueous environment [121]. The use of toxic organic solvents, however, is not appropriate for biomedical applications.

An alternative method for underwater application uses the phenomenon of coacervation, a form of aqueous liquid-liquid phase separation that is implicated in the adhesion mechanism of sandcastle worms, caddisfly larvae, and mussels [57]. Adhesive coacervate materials mimicking both mussels [174] and sandcastle worms [60, 61] have been developed. To form these coacervates, multiple components needed to be mixed in specific conditions and thus limited their overall applicability.

On the other hand, elastin-like polypeptides (ELPs) possess the innate ability to coacervate without the need for additional components [66]. Instead of relying on the condensation of oppositely charged polyelectrolytes (as in the sandcastle worm) [57], the phase transition behavior of elastin derives from the entropically favored rearrangement of water that occurs when elastin is heated above its lower critical solution temperature (LCST) [69]. Additionally, ELPs are "smart" materials; their LCST is highly tunable and can be designed to respond to specific environmental factors such as temperature, pH, and salt concentration [73]. Furthermore, ELPs can be produced recombinantly and in high yields in *E. coli* [73, 74] and exhibit outstanding biocompatibility [78] due to sequence homology with native human elastin. Finally, crosslinked ELPs exhibit mechanical properties similar to native elastin: low stiffness,

high extensibility, and high resilience [3, 66, 73, 74]. These mechanical properties are attractive due to their similarities to the properties of soft tissues [73]. Furthermore, the properties can be modulated over a broad range (0.1 - 1 MPa) to match specific tissue types by varying the molecular weight between crosslinks and the extent of crosslinking [74].

In this study, we report the development of a mussel-inspired adhesive ELP (Figure 4.1A). To confer wet adhesion strength on the expressed protein, tyrosine residues are enzymatically converted to DOPA. The DOPA-rich material exhibits cytocompatibility, strong adsorption to glass, significant dry adhesion strength, and moderate adhesion strength in a humid environment. Furthermore, the ELP can tunably and reversibly coacervate near physiological conditions and is thus a convenient adhesive material for underwater applications.

4.3 Materials and Methods

Reagents

All chemicals were purchased from Sigma-Aldrich (St. Louis, MO) or Avantor Performance Materials (Center Valley, PA) unless stated otherwise. Water was ultrapurified with a Milli-Q ultrapurification system (Millipore, Billerica, MA). NIH/3T3 fibroblasts were a generous gift from Dr. Alyssa Panitch (Purdue University). Tisseel was generously donated by Baxter BioSurgery (Deerfield, IL).

Protein Design and Cloning

The ELP called ELY_{16} was designed with Geneious software (Biomatters Inc., San Francisco, CA) using the repeated amino acid sequence Val-Pro-Gly-Xaa-Gly; the guest residues Xaa were evenly divided among Tyr, Lys, and Val. The complete amino acid sequence for full-length ELY_{16} is shown in Figure 4.1B. Cloning was performed using standard techniques [146] and a scheme modified from one previously developed by our lab [145]. The new scheme utilized AgeI and AvaI restriction

enzymes (New England Biolabs, Ipswich, MA) to achieve seamless repeats of the elastin-like sequence.

Protein Expression and Purification

The recombinant plasmid encoding ELY_{16} was transformed into the Rosetta2(DE3)pLysS *E. coli* expression host(EMD Chemicals, Gibbstown, NJ). Bacterial colonies were inoculated into 2xYT medium containing appropriate antibiotics and grown overnight. The overnight culture was diluted 1:250 for expression in a 14 L-capacity fermentor (BioFlo 100, New Brunswick Scientific, Enfield, CT) with 10 L of Terrific Broth (TB). When the optical density (OD) at 600 nm reached 5-6, protein expression was induced by the addition of isopropyl β-D-1-thiogalactopyranoside (IPTG, EMD Chemicals) at a final concentration of 2.5 mM. Upon reaching stationary phase, cells were harvested at by centrifugation and immediately resuspended in Buffer B (8 M urea, 100 mM NaH_2PO_4, 100 mM Tris-Cl, pH 8.0) before being frozen at -80 °C.

Purification was performed by a salting and heating method that was modified from a previously described protocol [175, 176]. Cells were lysed by multiple freeze-thaw cycles in combination with sonication (Misonix XL-2000, Qsonica, Newtown, CT) for 1 min followed by a 1 min incubation on ice. Total sonication time was at least 2 h. The cell lysate was then centrifuged at 10000g for 45 min and 4 °C to remove cell debris. To salt out undesired proteins, 10 (w/v)% ammonium sulfate was added to the cleared supernatant. The mixture was incubated on ice for $\geq$10 min followed by centrifugation for 45 min at 10000g and 4 °C. The supernatant was decanted from the pellet, and an additional 10 (w/v)% ammonium sulfate was added to precipitate ELY_{16}. The solution was incubated on ice and centrifuged as before. The pellet was then resuspended in water at 500 mg/mL based on pellet wet weight, heated to 80 °C, vortexed, and heated again to 80 °C. The heated solution was centrifuged for 45 min at 10000g and 25 °C, and the supernatant was dialyzed extensively against reverse osmosis water at 10 °C before lyophilization.

Expression and purification of ELY_{16} were confirmed by sodium dodecyl sulfate-polyacrylamide gel electrophoresis (SDS-PAGE) and Western blot using standard techniques [147]. SDS-PAGE gels were stained with Coomassie Brilliant Blue R-250. The protein was detected in the Western blot using an anti-T7 tag antibody conjugated to horseradish peroxidase (EMD Chemicals, Gibbstown, NJ) in combination with a 1-component 3,3',5,5'-tetramethylbenzidine (TMB) colorimetric substrate (Kirkegaard & Perry Laboratories, Gaithersburg, MD). Purity was assessed using densitometry analysis with ImageJ software (NIH, Bethesda, MD) [148].

The molecular weight was confirmed using matrix-assisted laser desorption/ ionization-time of flight (MALDI-TOF) (Dr. Connie Bonham, Campus-Wide Mass Spectrometry Center, Purdue University) with sinapinic acid as the matrix. Briefly, the MALDI mass spectra were obtained on a Voyager DE-Pro TOF mass spectrometer (Applied Biosystems, Framingham, MA) in the linear mode with delayed extraction. Positive-ion spectra were obtained with an acceleration voltage of 25000 V.

The amino acid composition was verified with amino acid analysis (John Schulze, Molecular Structure Facility, University of California, Davis). Briefly, the sample underwent liquid phase hydrolysis in 2 N HCl/1% phenol at 110 °C for 24 h before being dried. The sample was then dissolved in norleucine dilution buffer to a final volume of 1 mL, vortexed, and spun down. Injection volume was 50 μL at a 2.0 nmol scale.

Tyrosinase Conversion

To convert tyrosine residues to DOPA, ELY_{16} was dissolved at 2 mg/mL in 0.1 M sodium acetate buffer with 0.1 M ascorbic acid, pH 5.5. Mushroom tyrosinase was added to a final concentration of 150 U/mL, and the mixture was incubated at 37 °C and 200 rpm for 8 h. Enzyme activity was halted with 0.2 mL of 6 N HCl per mL of reaction as described previously [16]. The tyrosinase-modified ELY_{16} ($mELY_{16}$) solution was dialyzed extensively in 5% acetic acid at 4 °C and lyophilized.

The extent of conversion was measured with difference spectrophotometry [177] and comparison to standard solutions of L-DOPA. The increase in molecular weight due to conversion was confirmed by MALDI-TOF and SDS-PAGE. DOPA content was also assessed with amino acid analysis using a procedure similar to that described above with the modifications of using a 5.0 nmol scale and S-2-aminoethyl-L-cysteine as a diluent. The DOPA elution peak was compared with that of an L-DOPA control solution.

Protein Adsorption to Coverslips

Acid-washed coverslips (12 mm diameter, VWR, Radnor, PA) were incubated overnight at 4 °C with ELY_{16}, $mELY_{16}$, or bovine serum albumin (BSA, Fraction V, EMD Chemicals, Gibbstown, NJ) dissolved at 1 mg/mL in water. Protein surface density was measured by washing coverslips three times with MilliQ water and performing a bicinchoninic acid (BCA) colorimetric assay. Separate standard solutions for ELY_{16} and BSA were used to determine adsorbed protein concentration. Four replicates were tested for each sample.

Cell Culture

NIH/3T3 fibroblasts were generously donated by Dr. Alyssa Panitch (Purdue University). Fibroblasts were cultured at 37 °C and 5% CO_2 in high-glucose Dulbecco's Modified Eagle's Medium (DMEM) supplemented with 100 U/mL penicillin-streptomycin (Gibco, Carlsbad, CA) and 10% bovine calf serum. Cells were subcultured at 60-80% confluency.

Cytocompatibility Testing

Coverslips coated in adsorbed protein were sterilized by incubation in 70% ethanol for 5 min, blocked in sterile-filtered BSA (1 mg/mL in water) for 30 min, and rinsed with phosphate-buffered saline (PBS, 4.2 mM $NaHPO_4$, 0.8 mM KH_2PO_4, 50 mM

NaCl, pH 7.4). Fibroblasts were seeded onto coverslips at 2500 cells per cm^2 in a 24-well plate (BD Falcon, Durham, NC). For a positive control, acid-washed coverslips were incubated for 5 min in 0.01% poly-L-lysine (PLL, Trevigen, Gaithersburg, MD) then rinsed three times in PBS. Images were taken with a Nikon Ti-E C-1 Plus microscope. All groups were tested in triplicate.

To assess cell viability, cells were cultured for 2 days and tested with a LIVE/DEAD viability/cytotoxicity kit (Molecular Probes, Carlsbad, CA). Cells were incubated in staining solution (1.5 μM ethidium homodimer-1 and 0.5 μM calcein acetoxymethyl ester (calcein AM) in PBS), rinsed three times with PBS, and imaged with a 10x objective. All PBS was supplemented with 0.01% $CaCl_2$ and 0.01% $MgCl_2$ to prevent cell detachment. As a negative control, cells on PLL were incubated in 70% ethanol for 30 min at 37 °C prior to staining. Cells were counted using NIS-Elements software (Nikon, Tokyo, Japan), and at least 90 cells were counted per replicate. Viability was calculated as the number of living cells divided by the total number of cells in each replicate.

Cell morphology was assessed via actin staining. After culturing for 2 days, cells were fixed in ice-cold acetone for 1 min and then washed three times with filtered PBS. Coverslips were then incubated for 20 min with Alexa Fluor 488 phalloidin (Molecular Probes, Carlsbad, CA) at a 1:40 dilution in PBS. Following three 10 min washes with PBS, cells were then counterstained for 30 min with DRAQ5 (Biostatus Limited, Leicestershire, UK) diluted 1:500 in PBS. Finally, coverslips were rinsed twice in PBS, mounted with Vectashield (Vector Laboratories), and sealed with nail polish. Confocal imaging was performed with EZ-C1 software using a 40x objective.

Turbidity Testing

Lower critical solution temperatures (LCSTs) of ELY_{16} and $mELY_{16}$ were assessed using turbidity readings from a Crystal16 (Technobis Group, Alkmaar, the Netherlands). Protein samples were held at 10 °C for 15 min, ramped at 1 °C/min to 50 °C, then held at 50 °C for 2 min. Light transmission data was recorded and normalized

to the maximum transmission for each sample. The LCST was calculated as the inflection point of the transmission vs. temperature curve.

Lap Shear Adhesion

Aluminum adherends were prepared and cleaned using ASTM standard D2651-01 [150]. Bulk lap shear adhesion bonding was tested with a modified version of the ASTM D1002 standard, as previously described [119, 149]. Briefly, protein was resuspended at 150 mg/mL in water, and 5 μL of this solution was spread onto each aluminum adherend. Tisseel (generously donated by Baxter Biosurgery, Deerfield, IL) was prepared according to the manufacturer's instructions and tested by applying an equivalent total mass of protein (1.5 mg per test), based on the stated protein content of Tisseel. Adherends were overlapped with an area of 1.2 cm x 1.2 cm and were cured for 24 h at 37 °C. Bond strengths were quantified using an Instron 5544 Materials Testing System (Norwood, MA) with a 2000 N load cell and a loading rate of 2 mm/min. Maximum force was divided by overlap area to determine the adhesion strength. Each condition was tested with at least 5 samples.

For humid curing, adherends were covered with a layer of damp paper towels followed by a layer of plastic wrap to prevent them from drying out. For underwater curing, protein solution (either ELY_{16} or $mELY_{16}$) was adjusted to pH 7.5. Aluminum adherends were placed in a PBS bath at 37 °C. Protein coacervate (10 μL) was applied to one adherend, and the other adherend was overlapped as before. For underwater testing, at least 7 samples were tested for each group.

Statistical Analysis

Data are represented as the mean $\pm$ the standard deviation. All data were first examined for outliers using Grubbs' test; any outliers were discarded from further analysis. Next, Levene's test was used to assess equality of variances, and data were analyzed with one-way analysis of variance (ANOVA) followed by Tukey's Hon-

estly Significant Difference (HSD) or the Games-Howell (for unequal variances) *post hoc* test. Finally, the normality of the ANOVA residuals was assessed with the Kolmogorov-Smirnov test. If the residuals were not normally distributed, the original data were transformed with the Box-Cox method, and the analysis was repeated on the transformed data. If only two groups were being compared, an unpaired t-test was used instead of ANOVA to assess statistical difference. All statistical analyses were performed with GraphPad online software (La Jolla, CA) or Minitab 17 (State College, PA). A p-value ≤ 0.05 was considered significant.

4.4 Results

Adhesive Protein Design and Production

The goal of this study was to create a cytocompatible adhesive with underwater functionality (Figure 4.1A). To achieve this goal, we designed an ELP with a mixture of three guest residues (tyrosine, lysine, and valine) and an overall LCST near body temperature; the LCST was calculated based on the hydrophobicity scale developed by Urry [77, 151]. Tyrosine was chosen as a precursor to DOPA. Lysine was chosen because numerous studies have suggested that it also contributes to wet adhesion strength in mussel adhesive proteins (MAPs) [6,12,121,138,178]. Valine was included as a third guest residue to balance out hydrophobicity. The final amino acid sequence is shown in Figure 4.1B. The ELP was named ELY_{16} to indicate that it contains 16 tyrosine (Y) residues available for conversion to DOPA.

ELY_{16} was highly over-expressed in a 14 L fermentor and then purified using a salting and heating method common to resilin-like polypeptides [4] (Figure 4.1C). Although the salting and heating method is not traditionally used for ELPs, it produced pure protein very efficiently with a final yield of 220 mg per liter of culture and >98% purity. MALDI-TOF and amino acid analysis confirmed protein identity (Supporting Information, Figure 4.6A and Table 4.1).

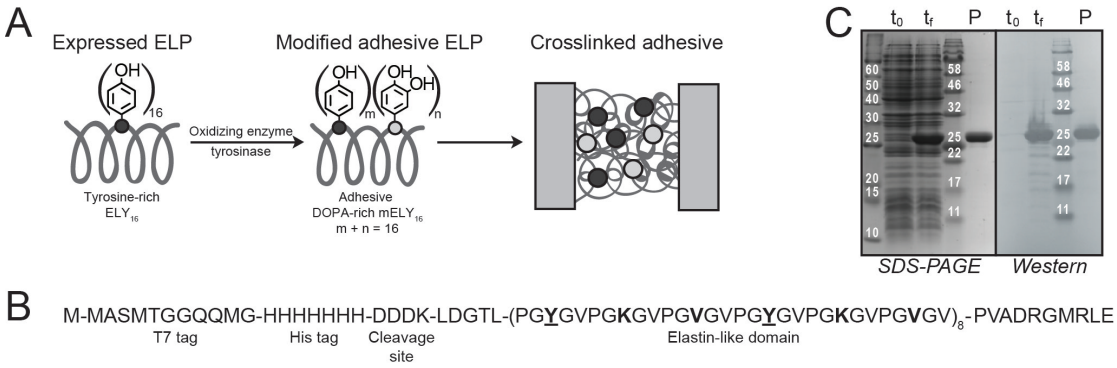

Figure 4.1. Design and production of underwater protein adhesive. (A) Schematic of material design. A tyrosine-rich ELP referred to as ELY_{16} is expresssed in *E. coli*. Using mushroom tyrosinase, tyrosines are then converted to DOPA to create our adhesive protein, $mELY_{16}$, which can form a crosslinked adhesive material. (B) Complete amino acid sequence of ELY_{16}. The final protein contains an N-terminal T7 tag, a 7xHis tag, and an enterokinase cleavage site followed by an elastin-like domain based on the repeated pentapeptide VPGXG. Guest residues (X) of the pentapeptides are shown in bold. Tyrosine residues available for conversion to DOPA are underlined. (C) Expression and purification of ELY_{16}. SDS-PAGE gel and Western blot showing pre-induction (t_0) and harvest (t_f) expression samples, as well as purified protein (P). ELY_{16} runs near its expected molecular weight of 25.548 kDa, as indicated by the standard protein ladders (band weights labeled in kDa).

Tyrosinase Conversion

Mushroom tyrosinase was used to convert tyrosines to adhesive DOPA residues. Several methods were used to confirm a successful reaction with tyrosinase, including amino acid analysis, difference spectrophotometry [177], SDS-PAGE, and MALDI-TOF. Amino acid analysis can be used to assess the loss of tyrosine residues, from which a conversion percent can be calculated. As seen in Supplementary Table 4.1, the molarity of tyrosine was reduced from 5.7% in ELY_{16} to 0.7% in $mELY_{16}$, a conversion of 88%.

Difference spectrophotometry, on the other hand, measures the difference in absorbance that results from the chelation of borate by DOPA [177]. Using this method, we measured a conversion of 54%. There are several reasons that difference spectrophotometry might estimate a lower conversion. First, because difference spectrophotometry relies on the presence of the reduced form of DOPA to chelate borate, it will underestimate DOPA concentration when DOPA has been oxidized [177]. Furthermore, although this method has been validated for use with DOPA, its effectiveness has not been assessed in the presence of reaction side products such as 3,4,5-trihydroxyphenylalanine (TOPA).

Finally, we assessed the change in molecular weight from tyrosinase conversion. On an SDS-PAGE gel (Supporting Information, Figure 4.7), $mELY_{16}$ ran distinctly higher than ELY_{16}, indicating that the molecular weight increased significantly with tyrosinase conversion. The change in molecular weight was quantitatively assessed with MALDI-TOF (Supporting Information, Figure 4.6B). The spectrum for $mELY_{16}$ shows a peak with a broad distribution centered around 25925 Da. This value is greater than the molecular weight one would expect if all of the tyrosines were converted to DOPA. However, tyrosinase is able to further oxidize DOPA to higher-molecular-weight TOPA [179,180]; thus, $mELY_{16}$ could contain a mixture of tyrosine, DOPA, and TOPA.

Cytocompatibility Testing

To assess the potential for use in biomedical applications, we tested the cytocompatibility of ELY_{16} and $mELY_{16}$. Testing was performed in compliance with ISO 10993-5 standards for *in vitro* evaluation of cytotoxicity by growing cells for >24 h in direct contact with the material. Using a LIVE/DEAD cytotoxicity kit, we first measured the viability of NIH/3T3 fibroblasts cultured for 48 h directly on an adsorbed layer of ELY_{16}, $mELY_{16}$, or PLL (positive control). Quantified results are shown in Figure 4.2A. In all groups, viability was >95%. Additionally, the viability in both ELP groups was statistically similar to the positive control group. Therefore, neither ELY_{16} nor $mELY_{16}$ has an effect on cellular viability.

To assess the effect of ELY_{16} and $mELY_{16}$ on cellular morphology, we also performed actin staining. As shown in Figure 4.2B, cells grown on PLL display normal spread fibroblast morphology. Cells grown on ELY_{16} or $mELY_{16}$ exhibit less spreading, which is likely due to the observation that cells grown on ELY_{16} and $mELY_{16}$ did not attach as firmly to the surfaces. However, cells on ELY_{16} and $mELY_{16}$ still appear healthy with relatively normal morphology.

Adsorption

To assess the surface coating abilities of ELY_{16} and $mELY_{16}$, we measured the amount of protein adsorbed to glass coverslips. Additionally, this allowed us to quantify the amount of protein on each surface during cytocompatibility testing. Using BSA as a control protein, we quantified protein adsorption with a BCA assay. Figure 4.3 shows that BSA and unmodified ELY_{16} adsorb to glass at similar densities ($\sim$0.3 $\mu g/cm^2$) whereas $mELY_{16}$ adsorbs significantly more strongly at more than twice the surface density (0.66 $\mu g/cm^2$).

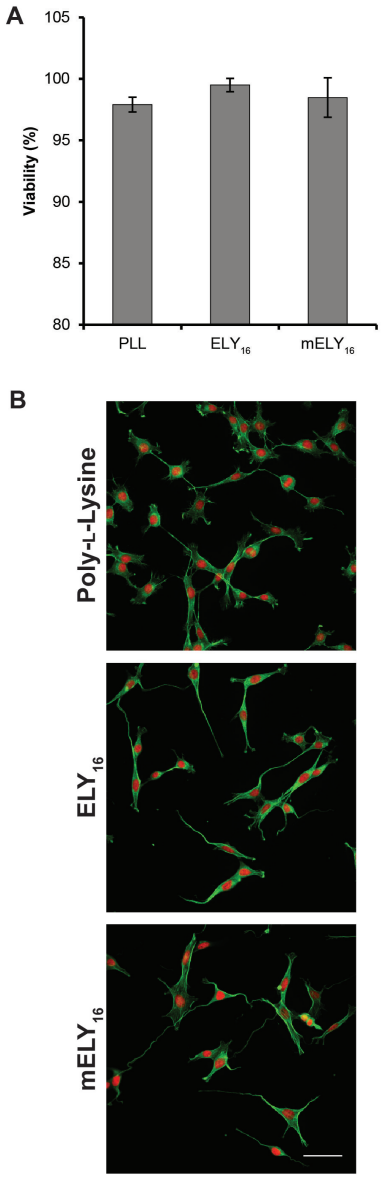

Figure 4.2. Cytocompatibility of ELY_{16} and $mELY_{16}$. NIH/3T3 fibroblasts were cultured directly on an adsorbed layer of ELY_{16} or $mELY_{16}$ for 48 h, after which they were tested with a (A) LIVE/DEAD assay to assess viability or (B) actin staining to assess morphology. (A) Cell viabilities on ELY_{16} and $mELY_{16}$ are statistically similar ($p > 0.05$) to cell viability on the positive control surface, PLL, as determined by Tukey's HSD *post hoc* test. All groups demonstrate >95% viability. (B) Cells grown on PLL show normal spread morphology. Cells grown on ELY_{16} and $mELY_{16}$ are slightly less spread but still relatively healthy. Scale bar represents 50 μm.

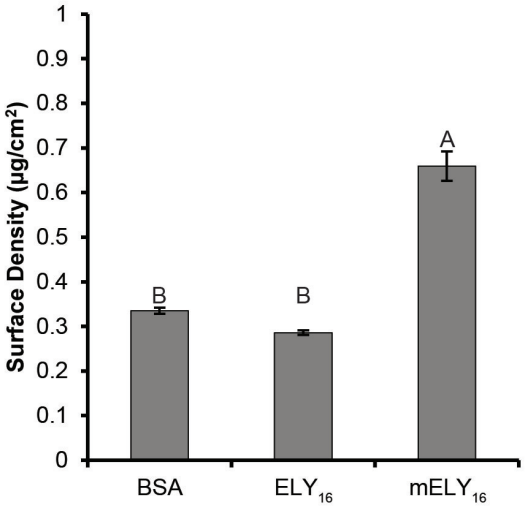

Figure 4.3. Addition of DOPA to ELY_{16} significantly increases its adsorption to glass. Protein solutions of BSA (control protein), ELY_{16}, and $mELY_{16}$ were adsorbed to acid-washed glass coverslips overnight at 4 °C then washed several times before quantification with a BCA assay. Groups with identical letters are statistically similar ($p > 0.05$) as determined by Tukey's HSD *post hoc* test.

Lap Shear Adhesion

Lap shear adhesion testing of ELY_{16} and $mELY_{16}$ was performed in both dry and humid environments to investigate their potential as bulk adhesives (Figure 4.4). BSA was used as a negative control protein, and the fibrin sealant Tisseel was used as a commercial adhesive comparison. After a 24 h dry cure at 37 °C, ELY_{16} and $mELY_{16}$ exhibited statistically similar strengths of 2.6 and 2.1 MPa, respectively; these strengths were significantly higher than either BSA (0.1 MPa) or Tisseel (0.7 MPa). When cured in a 100% humid environment, however, the adhesion strength of $mELY_{16}$ (0.24 MPa) was significantly higher than that of ELY_{16} alone (0.05 MPa), BSA (0.07 MPa), or Tisseel (0.07 MPa). These results indicate that addition of DOPA contributed wet adhesive strength to $mELY_{16}$ and that its strength in a humid environment exceeds that of a commercial tissue sealant.

Coacervation and Underwater Adhesion

One of the attractive properties of ELPs is their ability to form a phase-separated coacervate at a tunable LCST. To assess its tunability, we measured the LCSTs of both ELY_{16} and $mELY_{16}$ in conditions relevant to adhesion testing and biomedical applications (Figure 4.5A). In water at 150 mg/mL and pH 7, the LCST of ELY_{16} was 55 °C. Raising the pH to 7.5 lowered the LCST to 38 °C. The addition of salt via PBS or higher protein concentrations also resulted in lower LCSTs; at 150 mg/mL in PBS, the LCST was lowered to 26 °C, whereas at 75 mg/mL in PBS, the LCST was 28 °C. Finally, the LCST of $mELY_{16}$ at 150 mg/mL in water was 23 °C, a value much lower than that of ELY_{16} alone.

When raised above its LCST, a solution of ELP forms a separate protein-rich liquid phase, and this ability can be exploited for underwater adhesive application. As a proof of concept for this technique, we prepared solutions of ELY_{16} and $mELY_{16}$ that would be soluble in water at room temperature but would form a coacervate in PBS at 37 °C. We then applied these solutions underwater in a PBS bath to test their adhesion

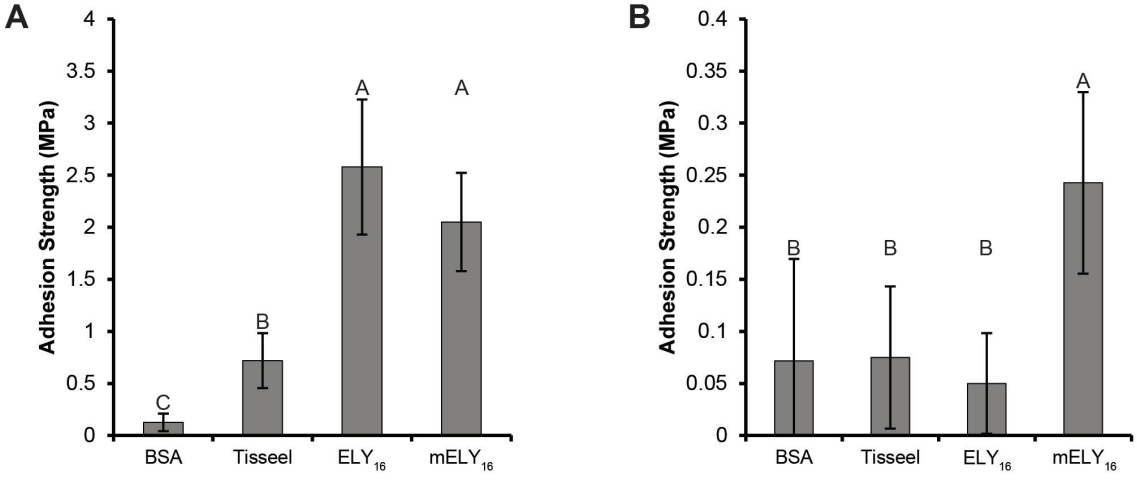

Figure 4.4. Lap shear adhesion testing of ELY_{16} and $mELY_{16}$ in (A) dry and (B) humid environments. In each condition, ELY_{16} and $mELY_{16}$ were compared with BSA as a negative control protein and the fibrin sealant Tisseel as a commercial comparison. (A) In dry conditions, both ELY_{16} and $mELY_{16}$ exhibited significantly higher adhesion strength than either control group. (B) In humid conditions, the addition of DOPA to ELY_{16} provided enhanced adhesion strength compared with ELY_{16} alone, BSA, or Tisseel. Groups with identical letters are statistically similar ($p > 0.05$) as determined by either the Games-Howell (dry cure) or Tukey's HSD (humid cure) *post hoc* test.

strength. Snapshots of underwater application are shown in Figure 4.5B-C, and videos of the underwater application are available in Supporting Information (Videos 1-3). The underwater adhesion strength of BSA could not be tested as it solubilized immediately in solution. Because Tisseel immediately crosslinks when dispensed, it could be applied underwater and tested; however, underwater application of Tisseel was difficult because it adhered to the applicator tip and dispersed slightly in solution (see Video 4 in Supporting Information). After a 24 h cure underwater in PBS at 37 °C, $mELY_{16}$ exhibited an average adhesion strength of 3 kPa, whereas neither ELY_{16} alone nor Tisseel provided any detectable adhesion strength.

4.5 Discussion

In this study, we developed an elastin-based adhesive with tunable phase transition behavior that allows for underwater application. We designed the protein as an ELP to confer valuable properties such as high yield from *E. coli*, cytocompatibility, and "smart" coacervation behavior to respond to environmental factors such as temperature, pH, and salinity. In addition, the protein design is rich in tyrosine and DOPA residues in order to mimic the wet adhesive abilities of mussels and sandcastle worms.

Two recent studies produced protein-based adhesives from other structural proteins. The first study combined MAP sequences with an amyloid fiber-forming sequence to create recombinant self-assembling wet adhesive proteins [33]. Similar to our system, the recombinant proteins were expressed in *E. coli* and post-translationally modified with tyrosinase. The second study focused on a resilin-based protein [32]. In this case, DOPA was incorporated through a chemical oxidation reaction originally designed to crosslink tyrosine residues. In each of these studies, the proteins demonstrated adhesive properties, but bulk adhesion strength was not investigated.

In the present study, we used mushroom tyrosinase to confer wet adhesion via conversion of tyrosine residues to DOPA. Several methods were used to assess the effect

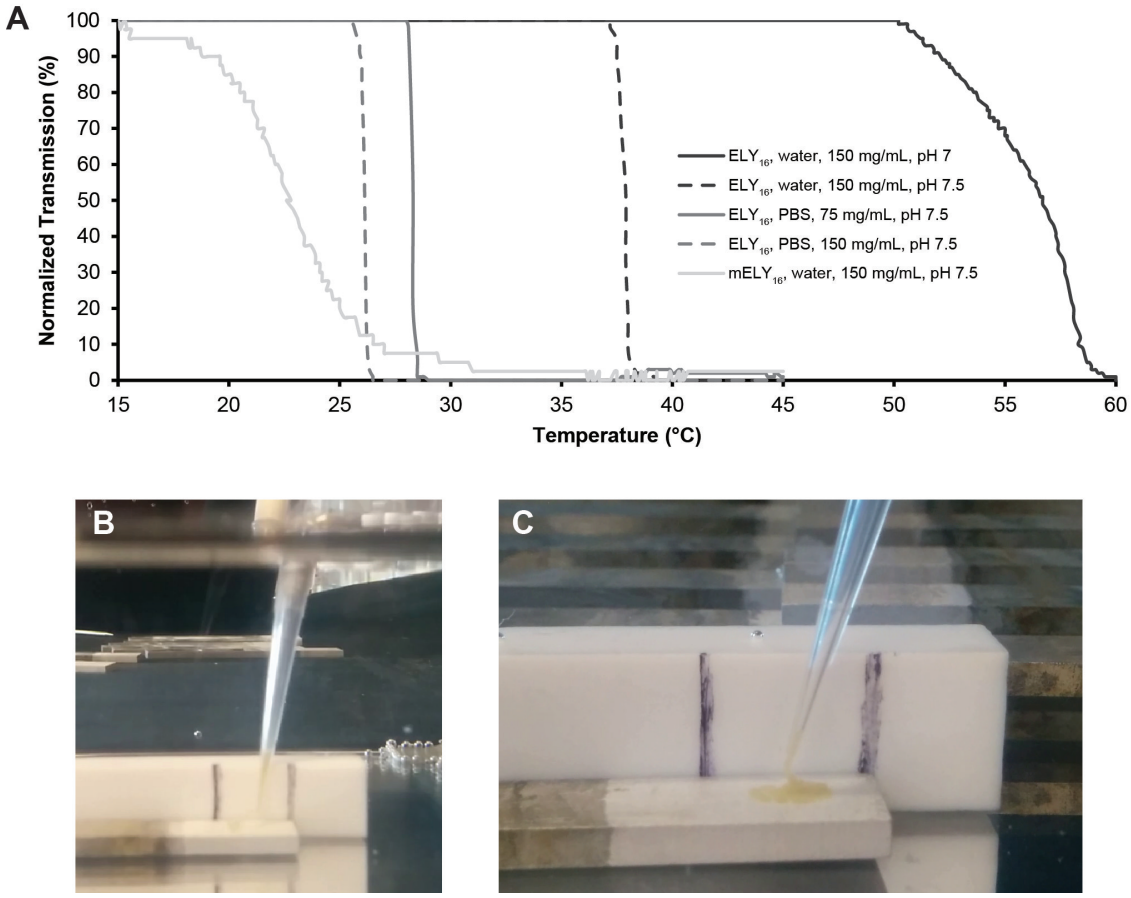

Figure 4.5. Phase transition behavior of ELY_{16} and $mELY_{16}$ allows for underwater adhesive application. (A) Turbidity testing of ELY_{16} and $mELY_{16}$ at pH 7-7.5 to determine the tunability of the LCST. The sharp decrease in light transmission corresponds to a rise in turbidity associated with the onset of coacervation. Raising the pH, adding salt, or increasing the protein concentration resulted in lower LCST values. $mELY_{16}$ also demonstrated a much lower LCST value compared with ELY_{16} alone. (B-C) Snapshots of videos taken of underwater application of $mELY_{16}$ coacervate. Full videos available in Supporting Information.

of tyrosinase modification on ELY_{16}, including difference spectrophotometry, amino acid analysis, SDS-PAGE, and MALDI-TOF. There was a discrepancy in the conversion values measured spectroscopically (54%) and analytically (>85%). However, the spectroscopic method measures chelation of borate by DOPA, a result which could be confounded by oxidation of DOPA or phenolic side products like TOPA [177]. Furthermore, we did not include borate in the tyrosinase reaction mixture to prevent the formation of TOPA [179], and SDS-PAGE and MALDI-TOF indicate that the molecular weight of $mELY_{16}$ was higher than would be expected for conversion of all tyrosine residues in ELY_{16} to DOPA. These results support the idea that $mELY_{16}$ contained a mixture of tyrosine, DOPA, and TOPA.

The use of mushroom tyrosinase in previous studies has had varying results. The study by Zhong et al. reported conversion values ranging from 52-65% as measured by difference spectrophotometry and amino acid analysis [33]. On the other hand, various papers by the Cha group reported conversion values varying from <5% to 40% [27, 116, 132, 160, 181] as measured by MALDI-TOF, difference spectrophotometry, and/or an iron-phenanthroline-based colorimetric assay [182]. MALDI-TOF was often used as a secondary form of measurement to a spectroscopic method; when both results were reported, there was an approximate difference of 5-10% between the assays. Overall, the conversion values reported in these studies are significantly lower than those measured for $mELY_{16}$. It is known, however, that tyrosinase is greatly affected by steric hindrance and shows increased activity on free tyrosine and short peptides compared to folded proteins [16,179,183]. Unlike the proteins utilized in previous studies, however, each tyrosine residue in ELY_{16} is flanked by glycine residues, substantially reducing the probability of tyrosinase being sterically hindered.

The next aspect of our adhesive protein that we assessed was cytocompatibility. Both ELY_{16} and $mELY_{16}$ are highly cytocompatible, as demonstrated by high viability and spread morphology of fibroblasts grown on each protein. Similar to our protein, cytocompatibility studies performed with the mussel-mimetic fp-151 protein demonstrated no toxicity to mammalian cells [27]. The addition of an RGD sequence

to the protein further improved its cytocompatibility and cell attachment characteristics [132]; because our protein is also designed to be modular, this type of domain addition could be easily performed in our system to improve cell attachment to ELY_{16} and $mELY_{16}$. Cytocompatibility has also been assessed in several DOPA-rich synthetic polymers. Although mild toxicity has been seen with citrate-based adhesives [108] and one catechol-modified PEG adhesive [133], other catechol-modified PEG adhesives have been shown to be highly biocompatible [134, 184].

Next, we assessed the bulk adhesion strength of our proteins to determine their potential as glues. We compared the adhesion strength of ELY_{16} and $mELY_{16}$ with that of BSA, a protein control, and Tisseel, an FDA-approved fibrin sealant as a commercial comparison. In dry conditions, both ELY_{16} and $mELY_{16}$ demonstrated significant (>2 MPa) adhesion strength. In addition, the adhesion strengths of our proteins were significantly greater than BSA and even Tisseel, thus demonstrating their potential as bulk adhesive materials relative to commercial standards.

Bulk adhesion studies have been performed with other mussel-mimetic adhesive materials. For example, initial bulk adhesion studies with fp-151 showed lap shear adhesion strengths of up to 1 MPa [116]. As with ELY_{16} and $mELY_{16}$, both the modified (tyrosinase-converted) and unmodified fp-151 proteins demonstrated similar adhesion strengths, indicating that the presence of DOPA did not affect adhesion in dry conditions. Later optimization of bulk adhesion was performed with fp-151 and other mussel-mimetic proteins and resulted in dry shear adhesion strengths of $\sim$2.5 MPa [160], a value similar to those achieved with ELY_{16} and $mELY_{16}$. Interestingly, the formation of a complex coacervate with hyaluronic acid and either fp-151 or fp-131 improved the dry adhesion strength to $\sim$4 MPa [174]. However, none of these proteins, either alone or as a coacervate, were tested in moist or underwater conditions.

In humid conditions, $mELY_{16}$ achieved an adhesion strength of 0.24 MPa, a value significantly higher than the strengths of BSA, ELY_{16}, or Tisseel ($\leq$0.07 MPa). Similar strengths were achieved with citrate-based adhesives when bonding porcine tissue in humid conditions [108]. The citrate adhesives bonded with strengths ranging

from 0.03 - 0.12 MPa, outperforming a fibrin-based adhesive which bonded with a strength of 0.02 MPa. Unlike our material, however, the citrate-based adhesives elicited a mild to moderate cytotoxic response that was directly correlated to both the soluble fraction of the adhesive and the concentration of the sodium periodate crosslinker [108]. Several catechol-modified PEG-based polymers were also tested in moist conditions. In one study, a catechol-modified PEG adhesive was applied to wet bovine pericardium and cured overnight while immersed in PBS; its final adhesion strength reached $\leq$8 kPa, whereas a commercial PEG-based sealant (CoSeal) possessed nearly zero adhesion strength in the same conditions [133]. However, this catechol-modified adhesive showed a small initial cytotoxic response, as well. Other catechol-modified PEG adhesives have reached strengths from 30-50 kPa when tested on porcine skin in a similar setup [185–187], although these have been shown to be highly biocompatible [134, 184].

None of these materials, however, was set up to adhere while completely underwater. Because of their ability to coacervate, our proteins possessed the ability to be applied while completely underwater. Although neither ELY_{16} nor Tisseel demonstrated any detectable adhesion strength when tested underwater, $mELY_{16}$ held an average bond strength of 3 kPa. Few other materials have been tested under such challenging adhesion conditions. First, a polystyrene-based polymer rich in catechol and cation residues attempted this feat and reached an adhesion strength of $\leq$400 kPa [121]. The polymer was dissolved in a mixture of chloroform and methanol, which allows it to maintain phase separation underwater but restricts its use to non-biomedical applications due to the toxicity of the organic solvents.

A different strategy for underwater adhesion was achieved by mimicking the sandcastle worm, which produces a set of proteins that form a complex coacervate upon being released into seawater [50,57]. The Stewart research group developed a synthetic adhesive composed of catechol- and charge-rich molecules that forms a complex coacervate when mixed at specific ratios and pH values [60, 61]. When applied and tested underwater, initial formulations of this adhesive reached strengths $\leq$100 kPa [60].

This version of the adhesive was also utilized for craniofacial reconstruction [188]; the toxic response with this adhesive was similar to that from other common methods of reconstruction, and in addition, the adhesive was degradable and osteoconductive. Later formulations of the adhesive added a secondary network of PEG-diacrylate (PEGDA), which resulted in increased underwater adhesion strength to an impressive 1.2 MPa [61].

Although the adhesion strength of $mELY_{16}$ is lower than reported values for other underwater adhesive systems, further optimization of various conditions (e.g., via adjustment of pH, concentration, DOPA content, crosslinker, etc.) could identify a formulation with enhanced mechanical properties. Furthermore, the LCST at which ELPs like ELY_{16} form a coacervate is sensitive to guest residue hydrophobicity, concentration, molecular weight, pH, and salt [76, 189–192]. This sensitivity makes our adhesive design "smart" – that is, the design can be modulated to form a coacervate under conditions that suit a specific situation. Additionally, ELPs form coacervates without the addition of any secondary components [66], so precise mixing and measurement are not necessary for successful application, unlike the system mimicking the sandcastle worm [60, 61]. With the combination of these properties, we believe that our material design shows exciting promise as a cytocompatible underwater adhesive material.

4.6 Conclusions

We have designed and produced a mussel-mimetic elastin-based adhesive protein that can be purified in high yields. It exhibits cytocompatibility and strong adsorptive properties that could be utilized for application as a coating. In dry conditions, both ELY_{16} and $mELY_{16}$ produce significant (>2 MPa) bulk adhesive strength, and in humid conditions, the presence of DOPA provides a substantial enhancement in adhesion strength. Furthermore, the ELP sequence permits the coacervation temperature to be tuned to suit a specific situation, and the coacervate form allows for underwater adhesive application. In all conditions, $mELY_{16}$ demonstrates an adhe-

sion strength significantly greater than that of a commercially available fibrin sealant. Finally, because of its recombinant design, our adhesive can be easily modified to suit a variety of applications. Future studies will optimize the adhesive performance of $mELY_{16}$ and explore its potential as a tissue adhesive.

4.7 Acknowledgments

This work was supported by the Purdue School of Chemical Engineering and the College of Engineering, the National Science Foundation (Awards DMR-1309787, CHE-0952928, and a Graduate Fellowship to M.J.B.), a 3M Nontenured Faculty Award, a Purdue Research Foundation Summer Faculty Grant, a Steven C. Beering Fellowship to M.J.B., and the Office of Naval Research (Awards N00014-13-1-0327 and N00014-13-1-0245). We thank Baxter Biosurgery for the generous donation of Tisseel, and Dr. Alyssa Panitch for her donation of the NIH/3T3 fibroblasts. We also thank Melissa L. Sweat for her help with videography, Sydney Hollingshead for her help with turbidity measurements, Dr. Connie Bonham (Campus-Wide Mass Spectrometry Center, Purdue University) for her assistance with MALDI-TOF, and Dr. John Schulze (Molecular Structure Facility, University of California, Davis) for his assistance with amino acid analysis.

4.8 Supporting Information

Videos depicting underwater application of ELY_{16} coacervate and Tisseel for adhesion testing are also available with Electronic Supporting Information.

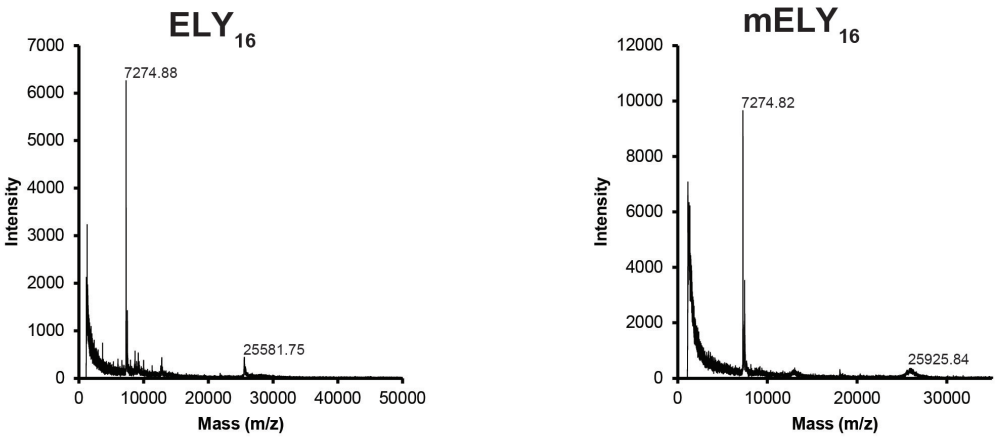

Figure 4.6. MALDI-TOF spectra of ELY_{16} and $mELY_{16}$. Peaks near 7274 are bacterial contaminant proteins that often persist through purification procedures.

Table 4.1.
Amino acid analysis of ELY_{16} and $mELY_{16}$.

Amino Acid	**Expected mol %**	**ELY_{16} Observed mol %**	**$mELY_{16}$ Observed mol %**
ASX	2.19	2.42	2.08
THR	0.73	0.87	0.96
SER	0.36	0.52	0.40
GLX	1.09	1.55	0.78
PRO	17.88	17.15	16.42
GLY	36.86	36.13	37.09
ALA	0.73	1.5	0.77
VAL	23.72	22.69	25.53
ILE	0.00	0.18	0.00
LEU	1.09	1.20	1.11
PHE	0.00	0.12	0.23
HIS	2.55	2.26	2.57
LYS	6.20	6.94	6.48
ARG	0.73	0.81	0.71
TYR	5.84	5.66	0.68
DOPA	N/A	0.00	4.19

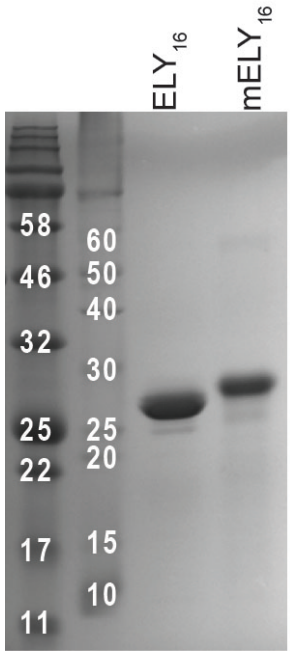

Figure 4.7. SDS-PAGE gel showing that conversion of ELY_{16} to $mELY_{16}$ significantly increases its molecular weight.

5. CONCLUSIONS

5.1 Summary

This work describes the development and characterization of novel adhesive materials inspired by natural proteins. First, a synthetic mussel-mimetic polymer, poly[(3,4-dihydroxystyrene)-*co*-styrene], was evaluated for cytocompatibility. Previous work with the polymer demonstrated that it possessed significant adhesion strength equivalent or superior to several commercial glues, but it was unclear whether the polymer would be appropriate for biomedical applications. To investigate polymer cytocompatibility, we cultured mouse fibroblasts with polymer extracts or directly in contact with the polymer. The polymer exhibited high cytocompatibility; cells cultured with polymer possessed equivalent viabilities, rates of proliferation, and morphologies when compared to a positive control group.

Next, we investigated the factors affecting the adhesion strength of elastin-like polypeptides (ELPs) to determine the potential for these proteins to act as glues. The effects of extrinsic (pH, concentration, crosslinker, humidity, cure time and temperature) and intrinsic (amino acid composition, structure, length) factors were assessed using a system of recombinant ELPs. Of the extrinsic factors tested, only humidity and cure time and temperature affected adhesion strength. Generally, adhesion strength increased up to an maximum level as moisture content decreased. Of the intrinsic factors, increased length and decreased structure improved adhesion strength, whereas changes of $\sim$10% in amino acid composition had no effect. When compared to commercially available protein-based adhesives, our ELPs exhibited equivalent or superior adhesion strength.

Finally, we designed and performed initial testing on a bioinspired underwater adhesive material. An ELP was designed to contain mussel-mimetic guest residues to

confer wet adhesion strength. Following enzymatic modification, the protein displayed cytocompatibility and increased adsorption to glass. In a dry environment, both the modified and unmodified ELP possessed significant (>2 MPa) adhesion strength, and in a humid environment, the modified ELP possessed improved water resistance relative to adhesive controls. Finally, the ELP exhibited tunable phase transition behavior that allowed it to form a coacervate in physiological conditions. Because of its properties, the modified protein coacervate could be applied and tested underwater and provided an adhesion strength superior to that of an FDA-approved tissue sealant.

5.2 Future Directions

This dissertation lays a foundation for exciting future research in biomimetic adhesives. We first showed that a mussel-mimetic polymer was highly cytocompatible with a mouse fibroblast cell line. Future studies could examine the *in vivo* biocompatibility of the polymer and test the effectiveness of the polymer for surgical wound closure in animal models.

Next, we showed that ELPs possess inherent adhesion strength that varies with moisture content, length, and protein structure. Previous studies have shown that natural glues such as that from the frog *Notaden bennetti* and or the velvet worm possess amino acid compositions similar not only to elastin, but also to other structural proteins such as resilin, abductin, and silk [2, 5, 62, 140]. Potential future work could examine the differences in adhesion strength among these types of structural proteins to probe the effects of protein hydrophobicity and specific secondary structure. Because resilin, silk, and abductin can be produced recombinantly [4, 193, 194], protein molecular weight and composition could be controlled across all proteins in the study.

Finally, we designed and characterized a bioinspired elastomeric underwater adhesive. Future work with this protein would characterize adhesion strength relative to DOPA content to determine if an optimum DOPA content exists. Future studies could also investigate the interaction between coacervation and adhesion, since

previous work has shown that coacervation has the potential to enhance adhesive properties [57,174]. Once optimized conditions are found, adhesion on biological substrates could be investigated *in vitro* (e.g., with porcine skin) and *in vivo*. Another aspect of this material that could be investigated is that of mechanical properties. Soft hydrogels could be formed through chemical and physical crosslinking of the DOPA groups (e.g., through oxidation or chelation of transition metals) [185, 195–197], and mechanical properties could be further modulated by crosslinking or testing in conditions below or above the protein inverse transition temperature [79, 198]. Once characterized, these hydrogels could be targeted for applications such as soft tissue adhesives or tissue engineering scaffolds. Finally, modular protein engineering could be utilized to modulate cellular interactions with the adhesive via the insertion of bioactive sequences (e.g., RGD cell adhesive domain or stem cell differentiation motifs) [199].

REFERENCES

REFERENCES

[1] R J Stewart, T C Ransom, and V Hlady. Natural underwater adhesives. *J. Polym. Sci. Part B, Polym. Phys.*, 49:757–771, 2011.

[2] L D Graham, V Glattauer, D Li, M J Tyler, and J A M Ramshaw. The adhesive skin exudate of *Notaden bennetti* frogs (Anura: Limnodynastidae) has similarities to the prey capture glue of *Euperipatoides* sp. velvet worms (Onychophora: Peripatopsidae). *Comp. Biochem. Physiol. Part B Biochem. Mol. Biol.*, 165:250–259, 2013.

[3] L Debelle and A M Tamburro. Elastin: Molecular description and function. *Int. J. Biochem. Cell Biol.*, 31:261–272, 1999.

[4] R S-C Su, Y Kim, and J C Liu. Resilin: Protein-based elastomeric biomaterials. *Acta Biomater.*, 10:1601–1611, 2014.

[5] D Li, M G Huson, and L D Graham. Proteinaceous adhesive secretions from insects, and in particular the egg attachment glue of *Opodiphthera* sp. moths. *Arch. Insect Biochem. Physiol.*, 69:85–105, 2008.

[6] H G Silverman and F F Roberto. Understanding marine mussel adhesion. *Mar. Biotechnol.*, 9:661–681, 2007.

[7] R Kumar, V Choudhary, S Mishra, I K Varma, and B Mattiason. Adhesives and plastics based on soy protein products. *Ind. Crops Prod.*, 16:155–172, 2002.

[8] N Li. *Isolation, characterization, and adhesion performance of sorghum, canola, and camelina proteins*. PhD thesis, Kansas State University, 2013.

[9] H J Cha, D S Hwang, and S Lim. Development of bioadhesives from marine mussels. *J. Biotechnol.*, 3:631–638, 2008.

[10] J H Waite. Adhesion à la Moule. *Integr. Comp. Biol.*, 42:1172–1180, 2002.

[11] J J Wilker. Marine bioinorganic materials: Mussels pumping iron. *Curr. Opin. Chem. Biol.*, 14:276–283, 2010.

[12] M E Yu and T J Deming. Synthetic polypeptide mimics of marine adhesives. *Macromolecules*, 31:4739–4745, 1998.

[13] H Yamamoto, S Kuno, A Nagai, A Nishida, S Yamauchi, and K Ikeda. Insolubilizing and adhesives studies of water-soluble synthetic model proteins. *Int. J. Biol. Macromol.*, 12:305–310, 1990.

[14] J H Waite. Precursors of quinone tanning: dopa-containing proteins. *Methods Enzymol.*, 258, 1995.

[15] D C Hansen, S G Corcoran, and J H Waite. Enzymatic tempering of a mussel adhesive protein film. *Langmuir*, 14:1139–1147, 1998.

[16] K Marumo and J H Waite. Optimization of hydroxylation of tyrosine and tyrosine-containing peptides by mushroom tyrosinase. *Biochem. Biophys. Acta*, 872:98–103, 1986.

[17] S W Taylor, G W Luther, and J H Waite. Polarographic and spectrophotometric investigation of iron(III) complexation to 3,4-dihydroxyphenylalanine-containing peptides and proteins from *Mytilus edulis*. *Inorg. Chem.*, 33:5819–5824, 1994.

[18] M J Sever, J T Weisser, J Monahan, S Srinivasan, and J J Wilker. Metal-mediated cross-linking in the generation of a marine-mussel adhesive. *Angew. Chemie-International Ed.*, 43:448–450, 2004.

[19] M C van der Leeden. Are conformational changes, induced by osmotic pressure variations, the underlying mechanism of controlling the adhesive activity of mussel adhesive proteins? *Langmuir*, 21:11373–9, 2005.

[20] L Ninan, R L Stroshine, J J Wilker, and R Shi. Adhesive strength and curing rate of marine mussel protein extracts on porcine small intestinal submucosa. *Acta Biomater.*, 3:687–694, 2007.

[21] D J Crisp, G Walker, G A Young, and A B Yule. Adhesion and substrate choice in mussels and barnacles. *J. Colloid Interface Sci.*, 104:40–50, 1985.

[22] H Lee, N F Scherer, and P B Messersmith. Single-molecule mechanics of mussel adhesion. *Proc. Natl. Acad. Sci. U. S. A.*, 103:12999–13003, 2006.

[23] J Sedó, J Saiz-Poseu, F Busqué, and D Ruiz-Molina. Catechol-based biomimetic functional materials. *Adv. Mater.*, 25:653–701, 2013.

[24] E Faure, C Falentin-Daudré, C Jérôme, J Lyskawa, D Fournier, P Woisel, and C Detrembleur. Catechols as versatile platforms in polymer chemistry. *Prog. Polym. Sci.*, 38:236–270, 2013.

[25] R L Strausberg and R P Link. Protein-based medical adhesives. *Trends Biotechnol.*, 8:53–57, 1990.

[26] D S Hwang, H J Yoo, J H Jun, W K Moon, and H J Cha. Expression of functional recombinant mussel adhesive protein Mgfp-5 in Escherichia coli. *Appl. Environ. Microbiol.*, 70:3352–3359, 2004.

[27] D S Hwang, Y Gim, H J Yoo, and H J Cha. Practical recombinant hybrid mussel bioadhesive fp-151. *Biomaterials*, 28:3560–3568, 2007.

[28] D S Hwang, Y Gim, and H J Cha. Expression of functional recombinant mussel adhesive protein type 3A in Escherichia coli. *Biotechnol. Prog.*, 21:965–970, 2005.

[29] J D Platko, M Deeg, V Thompson, Z Al-Hinai, H Glick, K Pontius, P Colussi, C Taron, and D L Kaplan. Heterologous expression of *Mytilus californianus* foot protein three (Mcfp-3) in *Kluyveromyces lactis*. *Protein Expr. Purif.*, 57:57–62, 2008.

[30] A J Salerno and I Goldberg. Cloning, expression, and characterization of a synthetic analog to the bioadhesive precursor protein of the sea mussel Mytilus edulis. *Appl. Microbiol. Biotechnol.*, 39:221–226, 1993.

[31] M Kitamura, K Kawakami, N Nakamura, K Tsumoto, H Uchiyama, Y Ueda, I Kumagai, and T Nakaya. Expression of a model peptide of a marine mussel adhesive protein in *Escherichia coli* and characterization of its structural and functional properties. *Polym. Sci. A Polym. Chem.*, 37:729–736, 1999.

[32] G Qin, A Rivkin, S Lapidot, X Hu, I Preis, S B Arinus, O Dgany, O Shoseyov, and D L Kaplan. Recombinant exon-encoded resilins for elastomeric biomaterials. *Biomaterials*, 32:9231–9243, 2011.

[33] C Zhong, T Gurry, A A Cheng, J Downey, Z Deng, C M Stultz, and T K Lu. Strong underwater adhesives made by self-assembling multi-protein nanofibres. *Nat. Nanotechnol.*, 9:858–866, 2014.

[34] O Johnson. U.S. patent 1460757: Adhesive, 1923.

[35] A Pizzi. Recent developments in eco-efficient bio-based adhesives for wood bonding: opportunities and issues. *J. Adhes. Sci. Technol.*, 20:829–846, 2006.

[36] J E Kinsella. Functional properties of soy proteins. *J. Am. Oil Chem. Soc.*, 56:242–258, 1979.

[37] L Sair. U.S. patent 2881076: Proteinaceous soy composition and method of preparing, 1959.

[38] A L Lambuth. Soybean glues. In I Skeist, editor, *Handbook of Adhesives*, pages 172–180. Van Nostrand, New York, 2nd edition, 1977.

[39] C D Mackay. Good adhesive bonding starts with surface preparation. *Adhesives Age*, 41:30–32, 1998.

[40] N S Hettiarachchy, U Kalapathy, and D J Myers. Alkali-modified soy protein with improved adhesive and hydrophobic properties. *J. Am. Oil Chem. Soc.*, 72:1461–1464, 1995.

[41] W Huang and X Sun. Adhesive properties of soy proteins modified by urea and guanidine hydrochloride. *J. Am. Oil Chem. Soc.*, 77:101–104, 2000.

[42] W Huang and X S Sun. Adhesive properties of soy proteins modified by sodium dodecyl sulfate and sodium dodecylbenzene sulfonate. *J. Am. Oil Chem. Soc.*, 77:705–708, 2000.

[43] S Petruccelli and M C Anon. Partial reduction of soy protein isolate disulfide bonds. *J. Agric. Food Chem.*, 43:2001–2006, 1995.

[44] U Kalapathy, N S Hettiarachchy, D Myers, and K C Rhee. Alkali-modified soy proteins: Effect of salts and disulfide bond cleavage on adhesion and viscosity. *J. Am. Oil Chem. Soc.*, 73:1063–1066, 1996.

[45] I Kowarsky. U.S. patent 2722484: Methods for hardening proteins and hardening solutions, 1955.

[46] U Kalapathy, N S Hettiarachchy, D Myers, and M A Hanna. Modification of soy proteins and their adhesive properties on woods. *J. Am. Oil Chem. Soc.*, 72:507–510, 1995.

[47] Y Liu and K Li. Chemical modification of soy protein for wood adhesives. *Macromol. Rapid Commun.*, 23:739–742, 2002.

[48] Y Liu and K C Li. Modification of soy protein for wood adhesives using mussel protein as a model: The influence of a mercapto group. *Macromol. Rapid Commun.*, 25:1835–1838, 2004.

[49] P M Favi, S Yi, S C Lenaghan, L Xia, and M Zhang. Inspiration from the natural world: From bio-adhesives to bio-inspired adhesives. *J. Adhes. Sci. Technol.*, 28:290–319, 2014.

[50] L P Bré, Y Zheng, A P Pêgo, and W Wang. Taking tissue adhesives to the future: From traditional synthetic to new biomimetic approaches. *Biomater. Sci.*, 1:239–253, 2013.

[51] K Kamino. Barnacle underwater attachment. In A M Smith and J A Callow, editors, *Biological Adhesives*, pages 145–166. Springer-Verlag, Berlin Heidelberg, 2006.

[52] D E Barlow, G H Dickinson, B Orihuela, J L Kulp, D Rittschof, and K J Wahl. Characterization of the adhesive plaque of the barnacle *Balanus amphitrite*: Amyloid-like nanofibrils are a major component. *Langmuir*, 26:6549–6556, 2010.

[53] K Kamino. Underwater adhesive of marine organisms as the vital link between biological science and material science. *Mar. Biotechnol.*, 10:111–121, 2008.

[54] L Khandeparker and A C Anil. Underwater adhesion: The barnacle way. *Int. J. Adhes. Adhes.*, 27:165–172, 2007.

[55] K Kamino, K Inoue, T Maruyama, N Takamatsu, S Harayama, and Y Shizuri. Barnacle cement proteins: Importance of disulfide bonds in their insolubility. *J. Biol. Chem.*, 275:27360–27365, 2000.

[56] R J Stewart. Protein-based underwater adhesives and the prospects for their biotechnological production. *Appl. Microbiol. Biotechnol.*, 89:27–33, 2011.

[57] R J Stewart, C S Wang, and H Shao. Complex coacervates as a foundation for synthetic underwater adhesives. *Adv. Colloid Interface Sci.*, 167:85–93, 2011.

[58] B J Endrizzi and R J Stewart. Glueomics: An expression survey of the adhesive gland of the sandcastle worm. *J. Adhes.*, 85:546–559, 2009.

[59] R J Stewart, J C Weaver, D E Morse, and J H Waite. The tube cement of *Phragmatopoma californica*: A solid foam. *J. Exp. Biol.*, 207:4727–4734, 2004.

[60] H Shao, K N Bachus, and R J Stewart. A water-borne adhesive modeled after the sandcastle glue of *P. californica*. *Macromol. Biosci.*, 9:464–471, 2009.

[61] S Kaur, G M Weerasekare, and R J Stewart. Multiphase adhesive coacervates inspired by the sandcastle worm. *ACS Appl. Mater. Interfaces*, 3:941–944, 2011.

[62] L D Graham, V Glattauer, M G Huson, J M Maxwell, R B Knott, J W White, P R Vaughan, Y Peng, M J Tyler, J A Werkmeister, and J A Ramshaw. Characterization of a protein-based adhesive elastomer secreted by the Australian frog *Notaden bennetti*. *Biomacromolecules*, 6:3300–3312, 2005.

[63] J Gosline, M Lillie, E Carrington, P Guerette, C Ortlepp, and K Savage. Elastic proteins: Biological roles and mechanical properties. *Philos. Trans. R. Soc. London Ser. B, Biol. Sci.*, 357:121–132, 2002.

[64] B B Aaron and J M Gosline. Elastin as a random-network elastomer: A mechanical and optical analysis of single elastin fibers. *Biopolymers*, 20:1247–1260, 1981.

[65] B Li, D O Alonso, B J Bennion, and V Daggett. Hydrophobic hydration is an important source of elasticity in elastin-based biopolymers. *J. Am. Chem. Soc.*, 123:11991–11998, 2001.

[66] D W Urry and T M Parker. Mechanics of elastin: Molecular mechanism of biological elasticity and its relationship to contraction. *J. Muscle Res. Cell Motil.*, 23:543–559, 2002.

[67] B Li and V Daggett. Molecular basis for the extensibility of elastin. *J. Muscle Res. Cell Motil.*, 23:561–573, 2002.

[68] B Vrhovski, S Jensen, and A S Weiss. Coacervation characteristics of recombinant human tropoelastin. *Eur. J. Biochem.*, 250:92–98, 1997.

[69] B Li, D O Alonso, and V Daggett. The molecular basis for the inverse temperature transition of elastin. *J. Mol. Biol.*, 305:581–592, 2001.

[70] C M Venkatachalam and D W Urry. Development of a linear helical conformation from its cyclic correlate. Beta-spiral model of the elastin poly(pentapeptide) $(VPGVG)_n$. *Macromolecules*, 14:1225–1229, 1981.

[71] H Broch, M Moulabbi, D Vasilescu, and A M Tamburro. Conformational and electrostatic properties of V-G-G-V-G, a typical sequence of the glycine-rich regions of elastin: An ab initio quantum molecular study. *Int. J. Pept. Protein Res.*, 47:394–404, 1996.

[72] V Villani and A M Tamburro. Conformational chaos of an elastin-related peptide in aqueous solution. *Ann. N. Y. Acad. Sci.*, 879:284–287, 1999.

[73] J C Rodríguez-Cabello, S Prieto, F J Arias, J Reguera, and A Ribeiro. Nanobiotechnological approach to engineered biomaterial design: The example of elastin-like polymers. *Nanomedicine*, 1:267–280, 2006.

[74] S A Maskarinec and D A Tirrell. Protein engineering approaches to biomaterials design. *Curr. Opin. Biotechnol.*, 16:422–426, 2005.

[75] W R Gray, L B Sandberg, and J A Foster. Molecular model for elastin structure and function. *Nature*, 246:461–466, 1973.

[76] D E Meyer and A Chilkoti. Quantification of the effects of chain length and concentration on the thermal behavior of elastin-like polypeptides. *Biomacromolecules*, 5:846–851, 2004.

[77] D W Urry, T M Parker, C Luan, D C Gowda, K U Prasad, M C Reid, and A Safavy. Temperature of polypeptide inverse temperature transition depends on mean residue hydrophobicity. *J. Am. Chem. Soc.*, 113:4346–4348, 1991.

[78] D W Urry and T M Parker. Biocompatibility of the bioelastic materials poly(GVGVP) and its gamma-irradiation cross-linked matrix: Summary of generic biological test results. *J. Bioact. Compat. Polym.*, 6:263–282, 1991.

[79] K Di Zio and D A Tirrell. Mechanical properties of artificial protein matrices engineered for control of cell and tissue behavior. *Macromolecules*, 36:1553–1558, 2003.

[80] D T McPherson, J Xu, and D W Urry. Product purification by reversible phase transition following *Escherichia coli* expression of genes encoding up to 251 repeats of the elastomeric pentapeptide GVGVP. *Gene*, 57:51–57, 1996.

[81] T G Weiser, S E Regenbogen, K D Thompson, A B Haynes, S R Lipsitz, W R Berry, and A A Gawande. An estimation of the global volume of surgery: A modelling strategy based on available data. *Lancet*, 372:139–144, 2008.

[82] P E Cruse and R Foord. A five-year prospective study of 23,649 surgical wounds. *Arch. Surg.*, 107:206–210, 1973.

[83] A J Singer, M Kinariwala, R Lirov, and H C Thode. Patterns of use of topical skin adhesives in the emergency department. *Acad. Emerg. Med.*, 17:670–672, 2010.

[84] A J Ritchie and L G Rocke. Staples versus sutures in the closure of scalp wounds: a prospective, double-blind, randomized trial. *Injury*, 20:217–218, 1989.

[85] J Quinn, J Maw, K Ramotar, G Wenckebach, and G Wells. Octylcyanoacrylate tissue adhesive versus suture wound repair in a contaminated wound model. *Surgery*, 122:69–72, 1997.

[86] P K Amid. Causes, prevention, and surgical treatment of postherniorrhaphy neuropathic inguinodynia: Triple neurectomy with proximal end implantation. *Hernia*, 8:343–349, 2004.

[87] S Zhang and R Ruiz Sr. US Patent 8652510 B2: Sterilized liquid compositions of cyanoacrylate monomer mixtures, 2014.

[88] J V Quinn. *Tissue adhesives in clinical medicine*. People's Medical Publishing House, 2005.

[89] N Chafke, B Gasser, V Lindner, N Rouyer, R Rooke, J G Kretz, P Nicolini, and B Eisenmann. Albumin as a sealant for a polyester vascular prosthesis: its impact on the healing sequence in humans. *J. Cardiovasc. Surg. (Torino).*, 37:431–440, 1996.

[90] J C Wheat and J S Wolf. Advances in bioadhesives, tissue sealants, and hemostatic agents. *Urol. Clin. North Am.*, 36:265–275, 2009.

[91] Y Nakayama and T Matsuda. Photocurable surgical tissue adhesive glues composed of photoreactive gelatin and poly(ethylene glycol) diacrylate. *J. Biomed. Mater. Res. Part A*, 48:511–521, 1999.

[92] E J Beckman, M Buckley, S Agarwal, and J Zhang. U.S. patent 7264823 B2: Medical adhesive and methods of tissue adhesion, 2007.

[93] J H de Groot, R de Vrijer, B S Wildeboer, C S Spaans, and A J Pennings. New biomedical polyurethane ureas with high tear strengths. *Polym. Bull.*, 38:211–218, 1997.

[94] F M Benoit. Degradation of polyurethane foams used in the Même breast implant. *J. Biomed. Mater. Res.*, 27:1341–1348, 1993.

[95] A T Trott. Cyanoacrylate tissue adhesives: an advance in wound care. *J. Am. Med. Assoc.*, 277:1559–1560, 1997.

[96] T B Reece, T S Maxey, and I L Kron. A prospectus on tissue adhesives. *Am. J. Surg.*, 182:40S–44S, 2001.

[97] D K Ousterhout, G V Gladieux, and F Leonard. Cutaneous absorption of N-alkyl alpha-cyanoacrylate. *J. Biomed. Mater. Res.*, 2:157–163, 1968.

[98] M Brodie, L Vollenweider, J L Murphy, F Xu, A Lyman, W D Lew, and B P Lee. Biomechanical properties of Achilles tendon repair augmented with a bioadhesive-coated scaffold. *Biomed. Mater.*, 6, 2011.

[99] L Ninan, J Monahan, R L Stroshine, J J Wilker, and R Y Shi. Adhesive strength of marine mussel extracts on porcine skin. *Biomaterials*, 24:4091–4099, 2003.

[100] J M Albes, C Krettek, B Hausen, R Rohde, A Haverich, and H G Borst. Biophysical properties of the gelatin-resorcin-formaldehyde/glutaraldehyde adhesive. *Ann. Thorac. Surg.*, 56:910–915, 1993.

[101] M Radosevich, H I Goubran, and T Burnouf. Fibrin sealant: Scientific rationale, production methods, properties, and current clinical use. *Vox Sang.*, 72:133–143, 1997.

[102] C Joch. The safety of fibrin sealants. *Cardiovasc. Surg.*, 11:23–28, 2003.

[103] W D Spotnitz and S Burks. Hemostats, sealants, and adhesives: Components of the surgical toolbox. *Transfusion*, 52:2243–2255, 2008.

[104] PMA P130023: Summary of Safety and Effectiveness Data (TissuGlu, Cohera Medical). Technical report, United States Food and Drug Administration, 2014.

[105] M Mehdizadeh and J Yang. Design strategies and applications of tissue bioadhesives. *Macromol. Biosci.*, 13:271–288, 2013.

[106] B D Ratner, A S Hoffman, F J Schoen, and J E Lemons, editors. *Biomaterials Science: An Introduction to Materials in Medicine*. Elsevier, Boston, 3rd edition, 2013.

[107] M Donkerwolcke, F Burny, and D Muster. Tissues and bone adhesives - historical aspects. *Biomaterials*, 19:1461–1466, 1998.

[108] M Mehdizadeh, H Weng, D Gyawali, L Tang, and J Yang. Injectable citrate-based mussel-inspired tissue bioadhesives with high wet strength for sutureless wound closure. *Biomaterials*, 33:7972–7983, 2012.

[109] A N Azadani, P B Matthews, L Ge, Y Shen, C-S Jhun, T S Guy, and E E Tseng. Mechanical properties of surgical glues used in aortic root replacement. *Ann. Thorac. Surg.*, 87:1154–1160, 2009.

[110] P A Leggat, D R Smith, and U Kedjarune. Surgical applications of cyanoacrylate adhesives: A review of toxicity. *ANZ J. Surg.*, 77:209–213, 2007.

[111] H Lee, B P Lee, and P B Messersmith. A reversible wet/dry adhesive inspired by mussels and geckos. *Nature*, 448:338–342, 2007.

[112] A Mahdavi, L Ferreira, C Sundback, J W Nichol, E P Chan, D J D Carter, C J Bettinger, S Patanavanich, L Chignozha, E Ben-Joseph, A Galakatos, H Pryor, I Pomerantseva, P T Masiakos, W Faquin, A Zumbuehl, S Hong, J Borenstein, J Vacanti, R Langer, and J M Karp. A biodegradable and biocompatible gecko-inspired tissue adhesive. *Proc. Natl. Acad. Sci. U. S. A.*, 105:2307–2312, 2008.

[113] J J Wilker. Biomaterials: Redox and adhesion on the rocks. *Nat. Chem. Biol.*, 7:579–80, 2011.

[114] T J Deming. Mussel byssus and biomolecular materials. *Curr. Opin. Chem. Biol.*, 3:100–105, 1999.

[115] L M Rzepecki and J H Waite. DOPA proteins: Versatile varnishes and adhesives from marine fauna. In *Bioorganic Marine Chemistry*, volume 4, pages 119–148. Springer-Verlag, Berlin, 1991.

[116] H J Cha, D S Hwang, S Lim, J D White, C R Matos-Pérez, and J J Wilker. Bulk adhesive strength of recombinant hybrid mussel adhesive protein. *Biofouling*, 25:99–107, 2009.

[117] G Westwood, T N Horton, and J J Wilker. Simplified polymer mimics of cross-linking adhesive proteins. *Macromolecules*, 40:3960–3964, 2007.

[118] C R Matos-Pérez, J D White, and J J Wilker. Polymer composition and substrate influences on the adhesive bonding of a biomimetic, cross-linking polymer. *J. Am. Chem. Soc.*, 134:9498–9505, 2012.

[119] C L Jenkins, H J Meredith, and J J Wilker. Molecular weight effects upon the adhesive bonding of a mussel mimetic polymer. *ACS Appl. Mater. Interfaces*, 5:5091–5096, 2013.

[120] H J Meredith, C L Jenkins, and J J Wilker. Enhancing the adhesion of a biomimetic polymer yields performance rivaling commercial glues. *Adv. Funct. Mater.*, 24:3259–3267, 2014.

[121] J D White and J J Wilker. Underwater bonding with charged polymer mimics of marine mussel adhesive proteins. *Macromolecules*, 44:5085–5088, 2011.

[122] E Santaniello, A Manzocchi, and C Farachi. Tetrabutylammonium periodate; A selective and versatile oxidant for organic substrates. *Synthesis (Stuttg).*, pages 563–565, 1980.

[123] M E Fray, P Prowans, J E Puskas, and V Altstadt. Biocompatibility and fatigue properties of polystyrene-polyisobutylene-polystyrene , an emerging thermoplastic elastomeric biomaterial. *Biomacromolecules*, 7:844–850, 2006.

[124] Plastics Foodservice Packaging Group: PFPG FDA Task Force. *The safety of styrene-based polymers for food-contact use: Update 2013*. American Chemistry Council, Washington, D.C., 2013.

[125] 21CFR1.177.1640: Polystyrene and rubber-modified polystyrene. In *Code of Federal Regulations*. US National Archives and Records Administration, 2009.

[126] A King, B Strand, A-M Rokstad, B Kulseng, A Andersson, G Skjåk-Bræk, and S Sandler. Improvement of the biocompatibility of alginate/poly-L-lysine/alginate microcapsules by the use of epimerized alginate as a coating. *J. Biomed. Mater. Res. Part A*, 64A:533–539, 2003.

[127] H G Gratzner. Monoclonal antibody to 5-bromo- and 5-iododeoxyuridine: A new reagent for detection of DNA replication. *Science*, 218:474–475, 1982.

[128] D Muir, S Varon, and M Manthorpe. An enzyme-linked immunosorbent assay for bromodeoxyuridine incorporation using fixed microcultures. *Anal. Biochem.*, 185:377–382, 1990.

[129] C R Arbeitman, M F del Grosso, I Ibañez, G G Bermúdez, H Durán, V C Chappa, R Mazzei, and M Behar. Irradiation of polystyrene and polypropylene to study NIH 3T3 fibroblasts adhesion. *Nucl. Instruments Methods Phys. Res. B*, 268:3059–3062, 2010.

[130] Y Ai, Y Wei, J Nie, and D Yang. Study on the synthesis and properties of mussel mimetic poly(ethylene glycol) bioadhesive. *J. Photochem. Photobiol. B.*, 120:183–190, 2013.

[131] S H Ku, J S Lee, and C B Park. Spatial control of cell adhesion and patterning through mussel-inspired surface modification by polydopamine. *Langmuir*, 26:15104–15108, 2010.

[132] D S Hwang, S B Sim, and H J Cha. Cell adhesion biomaterial based on mussel adhesive protein fused with RGD peptide. *Biomaterials*, 28:4039–4046, 2007.

[133] Y Liu, H Meng, S Konst, R Sarmiento, R Rajachar, and B P Lee. Injectable dopamine-modified poly(ethylene glycol) nanocomposite hydrogel with enhanced adhesive property and bioactivity. *ACS Appl. Mater. Interfaces*, 6:16982–16992, 2014.

[134] C E Brubaker, H Kissler, L J Wang, D B Kaufman, and P B Messersmith. Biological performance of mussel-inspired adhesive in extrahepatic islet transplantation. *Biomaterials*, 31:420–427, 2010.

[135] G Qi. *Modified soy protein based adhesives and their physicochemical properties*. PhD thesis, Kansas State University, 2011.

[136] J N Shera. *Soy protein isolate molecular contributions to bulk adhesive properties*. PhD thesis, The University of Southern Mississippi, 2007.

[137] M E Yu, J Y Hwang, and T J Deming. Role of L-3,4-dihydroxyphenylalanine in mussel adhesive proteins. *J. Am. Chem. Soc.*, 121:5825–5826, 1999.

[138] K Numata and P J Baker. Synthesis of adhesive peptides similar to those found in blue mussel (*Mytilus edulis*) using papain and tyrosinase. *Biomacromolecules*, 15:3206–3212, 2014.

[139] P A Suci and G G Geesey. Comparison of adsorption behavior of two *Mytilus edulis* foot proteins on three surfaces. *Colloids Surfaces B Biointerfaces*, 22:159–168, 2001.

[140] A Pena-Francesch, B Akgun, A Miserez, W Zhu, H Gao, and M C Demirel. Pressure sensitive adhesion of an elastomeric protein complex extracted from squid ring teeth. *Adv. Funct. Mater.*, 24:6227–6233, 2014.

[141] S C Heilshorn, J C Liu, and D A Tirrell. Cell-binding domain context affects cell behavior on engineered proteins. *Biomacromolecules*, 6:318–323, 2005.

[142] J R McDaniel, D C Radford, and A Chilkoti. A unified model for *de novo* design of elastin-like polypeptides with tunable inverse transition temperatures. *Biomacromolecules*, 14:2866–2872, 2013.

[143] Q Wang, X Xia, W Huang, Y Lin, Q Xu, and D L Kaplan. High throughput screening of dynamic silk-elastin-like protein biomaterials. *Adv. Funct. Mater.*, 24(27):4303–4310, 2014.

[144] J Kyte and R F Doolittle. A simple method for displaying the hydropathic character of a protein. *J. Mol. Biol.*, 157:105–132, 1982.

[145] J N Renner, Y Kim, K M Cherry, and J C Liu. Modular cloning and protein expression of long, repetitive resilin-based proteins. *Protein Expr. Purif.*, 82:90–96, 2012.

[146] F M Ausubel, R Brent, R E Kingston, D D Moore, J G Seidman, J A Smith, and K Struhl, editors. *Current Protocols in Molecular Biology*. John Wiley & Sons, New York, 2003.

[147] J S Bonifacino, M Dasso, J B Harford, J Lippincott-Schwatz, and K M Yamada, editors. *Current Protocols in Cell Biology*. John Wiley & Sons, New York, 2002.

[148] M D Abràmoff, P J Magalhães, and S J Ram. Image processing with ImageJ. *Biophotonics Int.*, 11:36–41, 2004.

[149] *Standard D1002: Apparent shear strength of single-lap-joint adhesively bonded metal specimens by tension loading (metal-to-metal)*. ASTM International, West Conshohocken, PA, 2010.

[150] *Standard D2651: Preparation of metal surfaces for adhesive bonding*. ASTM International, West Conshohocken, PA, 2008.

[151] D W Urry. Physical chemistry of biological free energy transduction as demonstrated by elastic protein-based polymers. *J. Phys. Chem. B*, 101:11007–11028, 1997.

[152] D E Meyer and A Chilkoti. Genetically encoded synthesis of protein-based polymers with precisely specified molecular weight and sequence by recursive directional ligation: Examples from the elastin-like polypeptide system. *Biomacromolecules*, 3(2):357–367, 2002.

[153] D W Urry, R G Shaw, and K U Prasad. Polypentapeptide of elastin: Temperature dependence of ellipticity and correlation with elastomeric force. *Biochem. Biophys. Res. Commun.*, 130:50–57, 1985.

[154] E M Petrie. *Handbook of adhesives and sealants*. McGraw Hill, New York, 2007.

[155] D S Hwang, H Zeng, Q Lu, J Israelachvili, and J H Waite. Adhesion mechanism in a DOPA-deficient foot protein from green mussels. *Soft Matter*, 8:5640–5648, 2012.

[156] H Zeng. Protein adsorption on solid surfaces. In *Polymer Adhesion, Frict, and Lubrication*, pages 230–241. John Wiley & Sons, 2013.

[157] T Pirzer, M Geisler, T Scheibel, and T Hugel. Single molecule force measurements delineate salt, pH and surface effects on biopolymer adhesion. *Phys. Biol.*, 6, 2009.

[158] Z Zhong, X S Sun, X Fang, and J A Ratto. Adhesion properties of soy protein with fiber cardboard. *J. Am. Oil Chem. Soc.*, 78:37–41, 2001.

[159] L M Hight and J J Wilker. Synergistic effects of metals and oxidants in the curing of marine mussel adhesive. *J. Mater. Sci.*, 42:8934–8942, 2007.

[160] B Yang, D G Kang, J H Seo, Y S Choi, and H J Cha. A comparative study on the bulk adhesive strength of the recombinant mussel adhesive protein fp-3. *Biofouling*, 29:483–90, 2013.

[161] Y Liu and K Li. Development and characterization of adhesives from soy protein for bonding wood. *Int. J. Adhes. Adhes.*, 27:59–67, 2007.

[162] N Li, Y Wang, M Tilley, S R Bean, X Wu, X S Sun, and D Wang. Adhesive performance of sorghum protein extracted from sorghum DDGS and flour. *J. Polym. Environ.*, 19:755–765, 2011.

[163] D S Hwang and J H Waite. Three intrinsically unstructured mussel adhesive proteins, mfp-1, mfp-2, and mfp-3: Analysis by circular dichroism. *Protein Sci.*, 21:1689–1695, 2012.

[164] Z Zhang and Y Hua. Urea-modified soy globulin proteins (7S and 11S): Effect of wettability and secondary structure on adhesion. *J. Am. Oil Chem. Soc.*, 84:853–857, 2007.

[165] G Y Choi, W Zurawsky, and A Ulman. Molecular weight effects in adhesion. *Langmuir*, 15:8447–8450, 1999.

[166] A Galliano, S Bistac, and J Schultz. Adhesion and friction of PDMS networks: Molecular weight effects. *J. Colloid Interface Sci.*, 265:372–379, 2003.

[167] M E R Shanahan and F Michel. Physical adhesion of rubber to glass: Cross-link density effects near equilibrium. *Int. J. Adhes. Adhes.*, 11:170–176, 1991.

[168] B T Poh and A T Yong. Dependence of peel adhesion on molecular weight of epoxidized natural rubber. *J. Adhes.*, 85:435–446, 2009.

[169] I Khan and B T Poh. Material properties and influence of molecular weight and testing rate on adhesion properties of epoxidized natural rubber-based adhesives. *J. Polym. Environ.*, 20:132–141, 2012.

[170] N J Elizondo, P J A Sobral, and F C Menegalli. Development of films based on blends of *Amaranthus cruentus* flour and poly(vinyl alcohol). *Carbohydr. Polym.*, 75:592–598, 2009.

[171] S S Ali, X Tang, S Alavi, and J Faubion. Structure and physical properties of starch/poly vinyl alcohol/sodium montmorillonite nanocomposite films. *J. Agric. Food Chem.*, 59:12384–12395, 2011.

[172] M Orlinsky, R M Goldberg, L Chan, A Puertos, and H L Slajer. Cost analysis of stapling versus suturing for skin closure. *Am. J. Emerg. Med.*, 13:77–81, 1995.

[173] *Tisseel Prescribing Information*. Baxter Healthcare Corporation, Westlake Village, CA, 2014.

[174] S Lim, Y S Choi, D G Kang, Y H Song, and H J Cha. The adhesive properties of coacervated recombinant hybrid mussel adhesive proteins. *Biomaterials*, 31:3715–3722, 2010.

[175] J N Renner, K M Cherry, R S-C Su, and J C Liu. Characterization of resilin-based materials for tissue engineering applications. *Biomacromolecules*, 13:3678–3685, 2012.

[176] Y Kim, J N Renner, and J C Liu. Incorporating the BMP-2 peptide in genetically-engineered biomaterials accelerates osteogenic differentiation. *Biomater. Sci.*, 2:1110–1119, 2014.

[177] J Herbert Waite. Determination of (catecholato)borate complexes using difference spectrophotometry. *Anal. Chem.*, 56:1935–1939, 1984.

[178] L A Burzio and J H Waite. Cross-linking in adhesive quinoproteins: Studies with model decapeptides. *Biochemistry*, 39:11147–11153, 2000.

[179] S W Taylor. Chemoenzymatic synthesis of peptidyl 3,4-dihydroxyphenylalanine for structure-activity relationships in marine invertebrate polypeptides. *Anal. Biochem.*, 302:70–74, 2002.

[180] L A Burzio and J H Waite. The other Topa: formation of 3,4,5-trihydroxyphenylalanine in peptides. *Anal. Biochem.*, 306:108–114, 2002.

[181] D S Hwang, Y Gim, D G Kang, Y K Kim, and H J Cha. Recombinant mussel adhesive protein Mgfp-5 as cell adhesion biomaterial. *J. Biotechnol.*, 127:727–735, 2007.

[182] P B Issopoulos. High-sensitivity spectrophotometric determination of trace amounts of levodopa, carbidopa and alpha-methyldopa. *Fresenius J. Anal. Chem.*, 336:124–128, 1990.

[183] J-G Jee, S-J Park, and H-J Kim. Tyrosinase-induced cross-linking of tyrosine-containing peptides investigated by matrix-assisted laser desorption/ionization time-of-flight mass spectrometry. *Rapid Commun. Mass Spectrom.*, 14:1563–1567, 2000.

[184] G Bilic, C E Brubaker, P B Messersmith, A S Mallik, T M Quinn, C Haller, E Done, L Gucciardo, S M Zeisberger, R Zimmermann, J Deprest, and A H Zisch. Injectable candidate sealants for fetal membrane repair: Bonding and toxicity *in vitro*. *Am. J. Obstet. Gynecol.*, 202:85.e1–85.e9, 2010.

[185] S A Burke, M Ritter-Jones, B P Lee, and P B Messersmith. Thermal gelation and tissue adhesion of biomimetic hydrogels. *Biomed. Mater.*, 2:203–210, 2007.

[186] C E Brubaker and P B Messersmith. Enzymatically degradable mussel-inspired adhesive hydrogel. *Biomacromolecules*, 12:4326–4334, 2011.

[187] D G Barrett, G G Bushnell, and P B Messersmith. Mechanically robust, negative-swelling, mussel-inspired tissue adhesives. *Adv. Healthc. Mater.*, 2:745–755, 2013.

[188] B D Winslow, H Shao, R J Stewart, and P A Tresco. Biocompatibility of adhesive complex coacervates modeled after the Sandcastle glue of *P. californica* for craniofacial reconstruction. *Biomaterials*, 31:9373–9381, 2010.

[189] M Miao, C M Bellingham, R J Stahl, E E Sitarz, C J Lane, and F W Keeley. Sequence and structure determinants for the self-aggregation of recombinant polypeptides modeled after human elastin. *J. Biol. Chem.*, 278:48553–48562, 2003.

[190] C M Bellingham, K A Woodhouse, P Robson, S J Rothstein, and F W Keeley. Self-aggregation characteristics of recombinantly expressed human elastin polypeptides. *Biochim. Biophys. Acta*, 1550:6–19, 2001.

[191] M Miao, J T Cirulis, S Lee, and F W Keeley. Structural determinants of cross-linking and hydrophobic domains for self-assembly of elastin-like polypeptides. *Biochemistry*, 44:14367–14375, 2005.

[192] A Girotti, J Reguera, F J Arias, M Alonso, A M Testera, and J C Rodríguez-Cabello. Influence of the molecular weight on the inverse temperature transition of a model genetically engineered elastin-like pH-responsive polymer. *Macromolecules*, 37:3396–3400, 2004.

[193] G H Altman, F Diaz, C Jakuba, T Calabro, R L Horan, J Chen, H Lu, J Richmond, and D L Kaplan. Silk-based biomaterials. *Biomaterials*, 24:401–416, 2003.

[194] R S Su, J N Renner, and J C Liu. Synthesis and characterization of recombinant abductin-based proteins. *Biomacromolecules*, 14:4301–4308, 2013.

[195] B P Lee, J L Dalsin, and P B Messersmith. Synthesis and gelation of DOPA-modified poly(ethylene glycol) hydrogels. *Biomacromolecules*, 3:1038–1047, 2002.

[196] M Krogsgaard, M A Behrens, J S Pedersen, and H Birkedal. Self-healing mussel-inspired multi-pH-responsive hydrogels. *Biomacromolecules*, 14:297–301, 2013.

[197] B J Kim, D X Oh, S Kim, J H Seo, D S Hwang, A Masic, D K Han, and H J Cha. Mussel-mimetic protein-based adhesive hydrogel. *Biomacromolecules*, 15:1579–1585, 2014.

[198] P J Nowatzki and D A Tirrell. Physical properties of artificial extracellular matrix protein films prepared by isocyanate crosslinking. *Biomaterials*, 25:1261–1267, 2004.

[199] J C Rodríguez-Cabello, J Reguera, A Girotti, M Alonso, and A Testera. Developing functionality in elastin-like polymers by increasing their molecular complexity: The power of the genetic engineering approach. *Prog. Polym. Sci.*, 30:1119–1145, 2005.

[200] Y Kim. *Modulating cell differentiation with protein-engineered microenvironments*. PhD thesis, Purdue University, 2014.

APPENDICES

A. CLONING SCHEMES AND PROTEIN CODING SEQUENCES

A.1 General Description of Methods and Sequences

Cloning schemes for all proteins created are shown, as well as relevant DNA and protein coding sequences.

DNA oligonucleotides were purchased from Sigma-Aldrich. All cloning was modeled *in silico* with Geneious Pro software prior to in-lab construction. Constructs were cloned in the 10-β bacterial host (New England Biolabs). The pAL and pJB plasmids are derivatives of pUC19 designed by Andrew Lundfelt and M. Jane Brennan to have a custom polylinker region. The pET28aRW plasmid is a derivative of pET28a designed by Ralf Weberskirch to contain a T7 tag, a 7xHis tag, and an enterokinase cleavage site.

Cloning was completed with great help from Renay Sheng-Chuan Su, Teresa Lin, Peter Meléndez, Haefa Mansour, and Victoria Messerschmidt.

Figures A.1, A.2, and A.3 show the molecular cloning schemes for $(EL18\text{-}9Y)_2$, $(EL6Y\alpha)_8$, and RZY_{20}, respectively. Elastomeric domains are shown in blue, and the 9Y pre-adhesive domain is shown in red.

Figure A.4 contains the full DNA sequence (single stranded) of pET28aRW-$(EL6Y4)_8$, including the corresponding amino acid sequences (blue) and relevant restriction sites (red) as shown in the cloning scheme in Figure A.2. pET28aRW-$(EL6YK3)_8$, -$(EL6Y3)_8$, -$(EL6Y2)_8$, -RZY_{20}, and -$(EL18\text{-}9Y)_2$ are constructed exactly the same way as pET28aRW-$(EL6Y4)_8$, so only the coding regions for these proteins are shown (see Figures A.5 - A.9).

A.2 A Note on Nomenclature

Many of the proteins designed and characterized for this dissertation underwent several name changes. For example, in the original ELP designs, $(EL18\text{-}9Y)_2$ was originally called $(EL3\text{-}9Y)_2$, as the elastin domain contained 3 cassettes of 6 VPGXG pentapeptides. All other original ELP designs followed a similar naming convention to $(EL3\text{-}9Y)_2$.

The newer ELP protein designs have also undergone several name changes. When originally designed in Geneious, $(EL6Y4)_n$ was referred to as "Design 1", $(EL6Y2)_n$ as "Design 3", and $(EL6YK3)_n$ as "Design 5". "Design 2" (also referred to as $(EL6Y3)_n$) contained guest residues in the order YKYFEY and was successfully cloned into pJB. However, further cloning was not pursued because it was predicted to suffer from similar insolubility at neutral pH as $(EL6Y4)_8$. A fourth design ("Design 4", guest residues YRKYRG) was fully cloned *in silico* but was never pursued *in vitro* because it was decided that Design 3 contained preferential guest residues (i.e., K) with an identical tyrosine content.

Within each design in Geneious, the various concatemers are referred to by the number of total elastin pentapeptides (e.g., pET-EL48 instead of pET28aRW-$(EL6Y\alpha)_8$). Also, pJB was originally referred to in the Geneious files as pAL2 as it is a modification of the original pAL vector developed by Andrew Lundfelt.

In general, the newer ELPs were named to reflect the tyrosine content ("Y4", "Y3", "Y2", etc.) compared to the number of elastin repeats as their original purpose was to have their tyrosines converted to DOPA. For the purposes of clarity in Chapter 3, the naming convention for all of the newer ELPs was again changed. Instead of being named $(EL6Y\alpha)_n$, where n refers to the number of cassettes, proteins were referred to in the style created by the Chilkoti group [76, 152]: ELP[$A_iB_jC_k$-n] where A, B, and C refer to guest residues (i.e., X in the VPGXG pentapeptide) with frequency indicated by subscripts i, j, and k. The total number of elastin pen-

tapeptides is indicated by *n*. Therefore, $(EL6Y4)_8$ became ELP[KEY_4-48], $(EL6Y2)_8$ became ELP[$K_2Y_2V_2$-48], and $(EL6YK3)_8$ became ELP[K_3Y_3-48].

For the purposes of clarity and brevity, the name of $(EL6Y2)_8$ was again modified for use in Chapter 4. The protein was renamed "ELY_{16}" to reflect its elastin-based sequence (EL) and the number of tyrosine (Y) residues (16). When converted with tyrosinase enzyme, the protein was referred to as "mELY_{16}" where "m" refers to its "modified" nature.

A.3 Cloning Schemes

A.4 DNA and Amino Acid Sequences

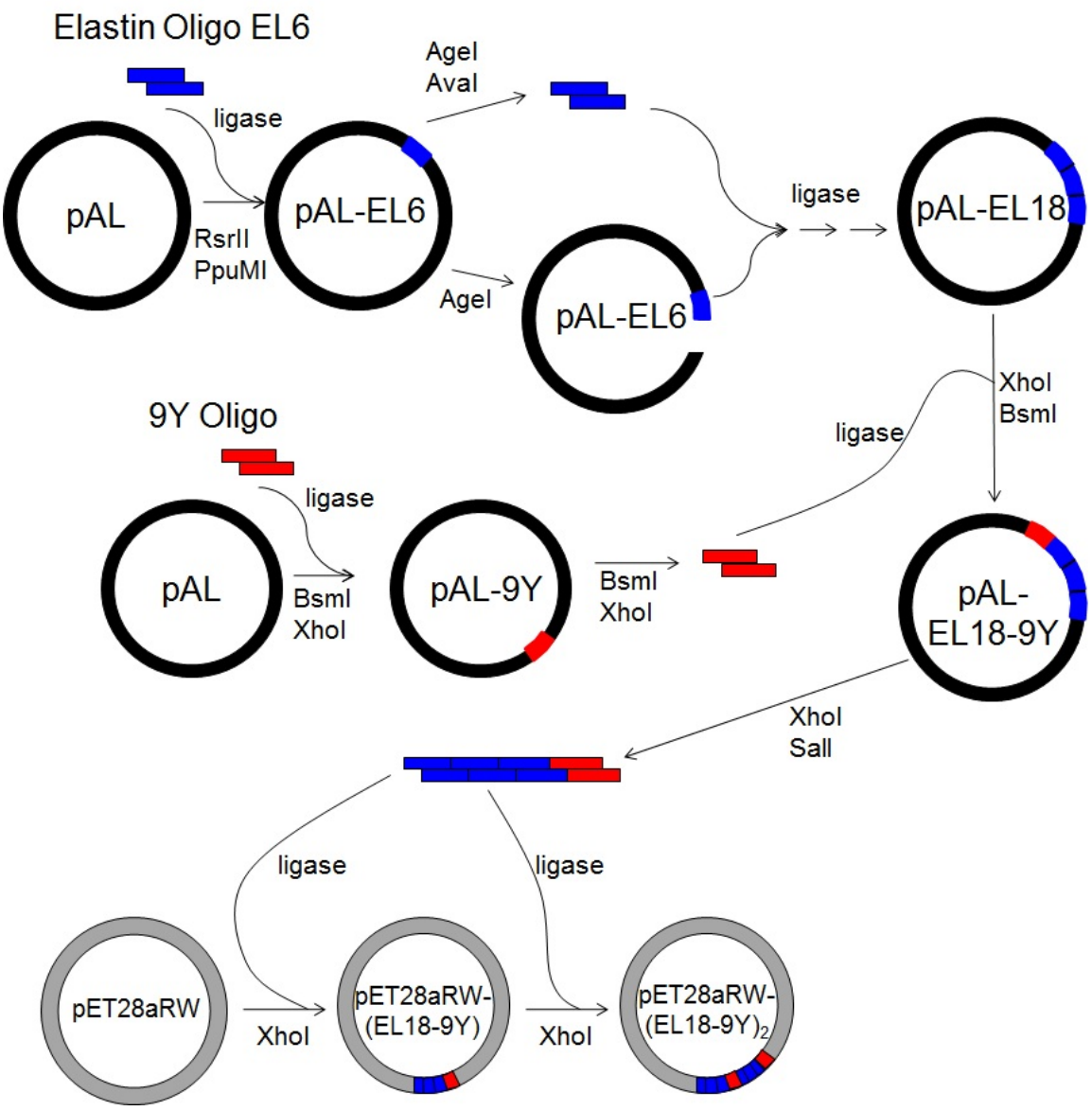

Figure A.1. Cloning scheme to construct pET28aRW-$(EL18\text{-}9Y)_2$.

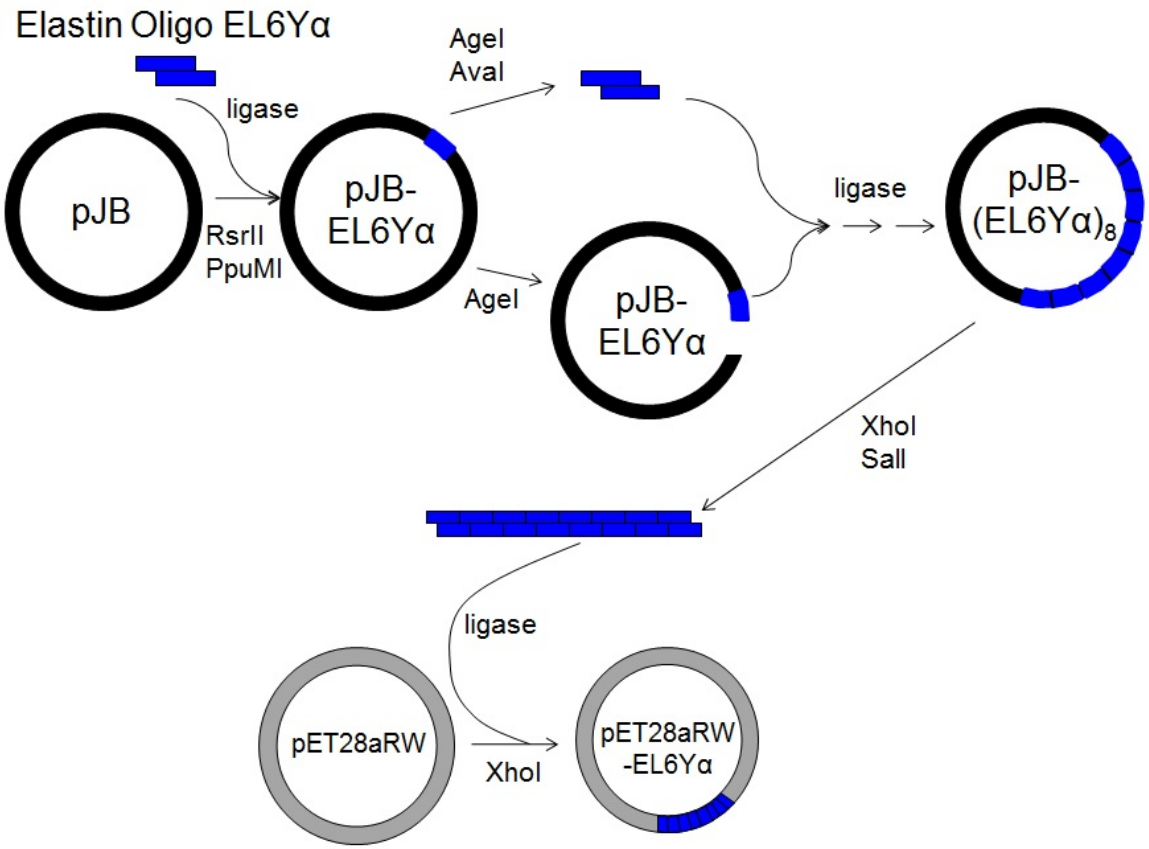

Figure A.2. Cloning scheme to construct pET28aRW-$(EL6Y4)_8$, pET28aRW-$(EL6Y3)_8$, and pET28aRW-$(EL6Y2)_8$.

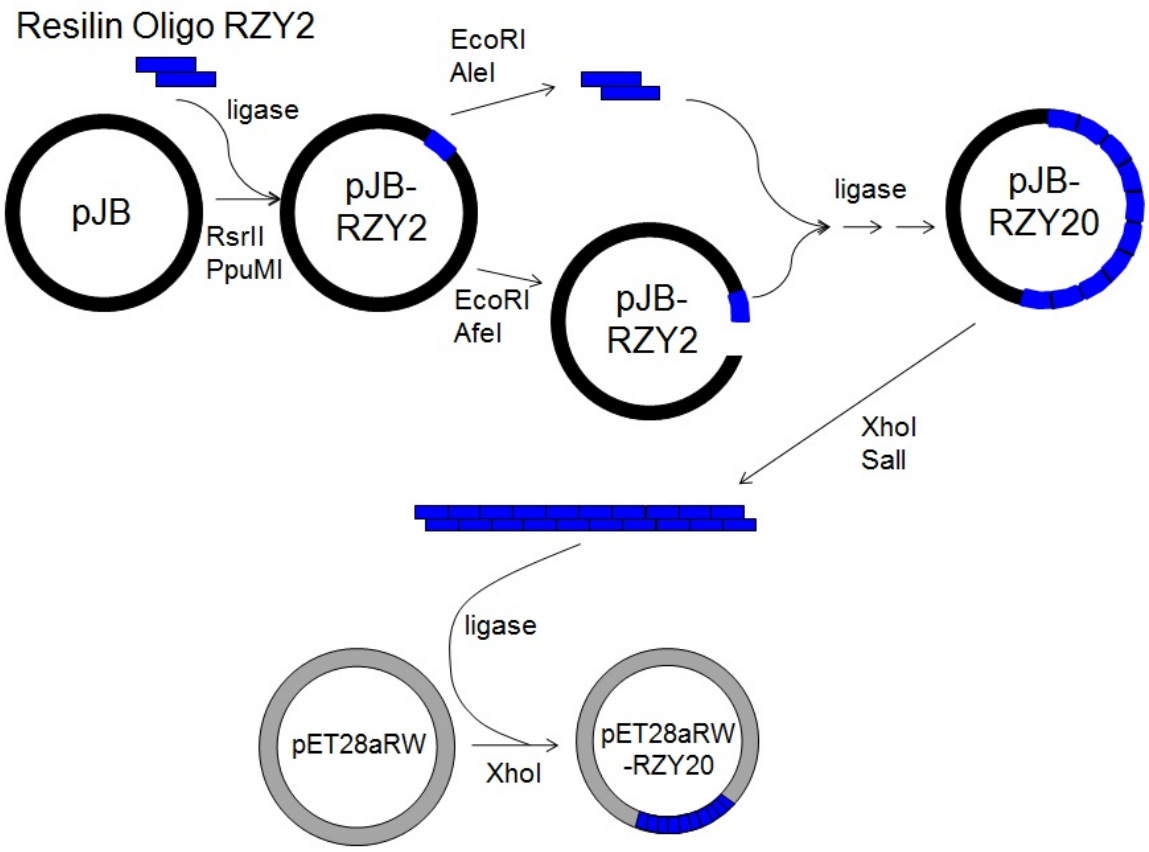

Figure A.3. Cloning scheme to construct pET28aRW-RZY_{20}.

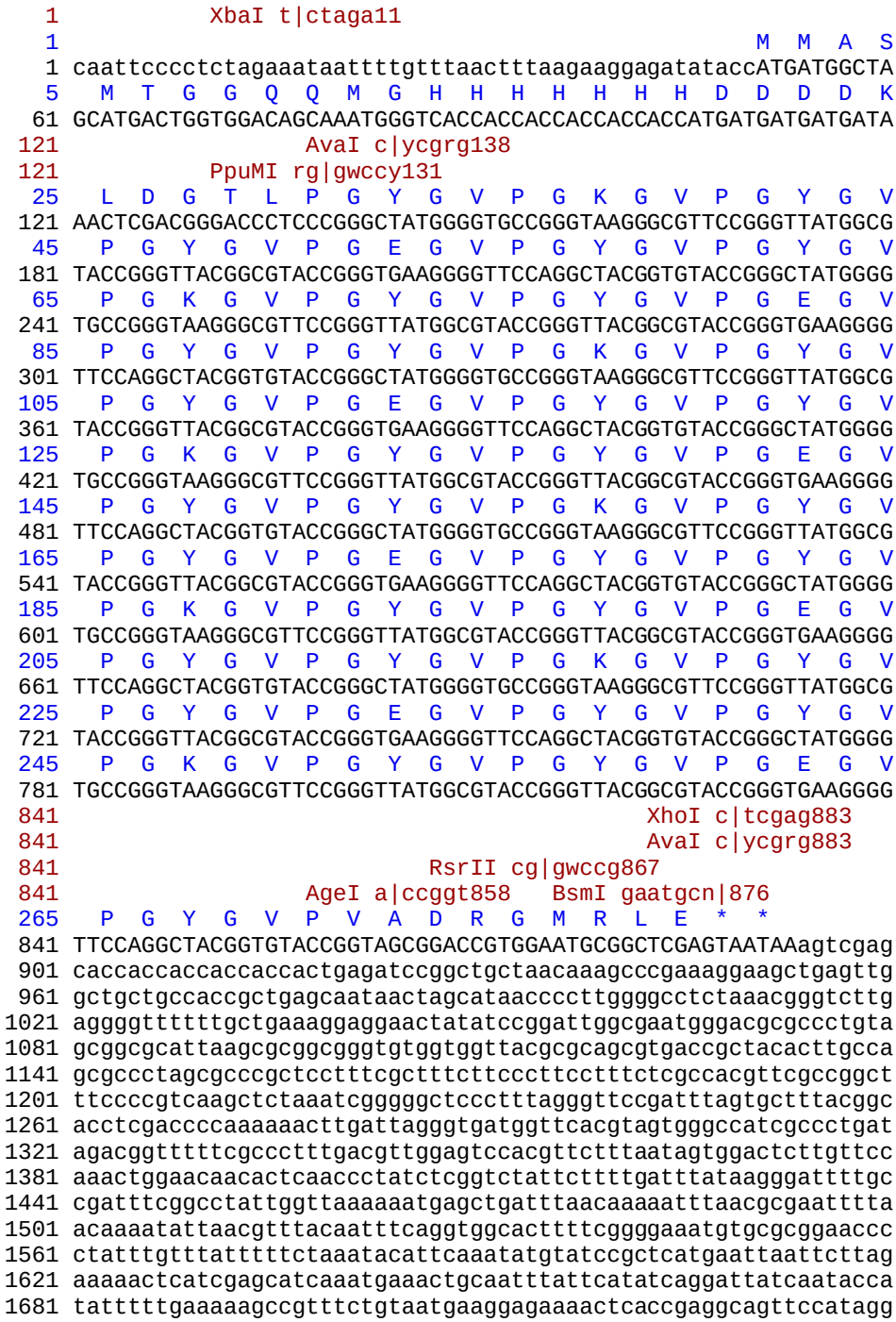

Figure A.4. Complete plasmid DNA sequence for pET28aRW-$(EL6Y4)_8$ (molecular weight = 26.580 kDa). Pertinent restriction sites are labeled in red, and coding regions are labeled in blue.

```
1741 atggcaagatcctggtatcggtctgcgattccgactcgtccaacatcaatacaacctatt
1801 aatttcccctcgtcaaaaataaggttatcaagtgagaaatcaccatgagtgacgactgaa
1861 tccggtgagaatggcaaaagtttatgcatttctttccagacttgttcaacaggccagcca
1921 ttacgctcgtcatcaaaatcactcgcatcaaccaaaccgttattcattcgtgattgcgcc
1981 tgagcgagacgaaatacgcgatcgctgttaaaaggacaattacaaacaggaatcgaatgc
2041 aaccggcgcaggaacactgccagcgcatcaacaatattttcacctgaatcaggatattct
2101 tctaatacctggaatgctgttttcccggggatcgcagtggtgagtaaccatgcatcatca
2161 ggagtacggataaaatgcttgatggtcggaagaggcataaattccgtcagccagtttagt
2221 ctgaccatctcatctgtaacatcattggcaacgctacctttgccatgtttcagaaacaac
2281 tctggcgcatcgggcttcccatacaatcgatagattgtcgcacctgattgcccgacatta
2341 tcgcgagcccatttatacccatataaatcagcatccatgttggaatttaatcgcggccta
2401 gagcaagacgtttcccgttgaatatggctcataacacccttgtattactgtttatgtaa
2461 gcagacagttttattgttcatgaccaaaatcccttaacgtgagttttcgttccactgagc
2521 gtcagaccccgtagaaaagatcaaaggatcttcttgagatccttttttctgcgcgtaat
2581 ctgctgcttgcaaacaaaaaaaccaccgctaccagcggtggtttgtttgccggatcaaga
2641 gctaccaactctttttccgaaggtaactggcttcagcagagcgcagataccaaatactgt
2701 ccttctagtgtagccgtagttaggccaccacttcaagaactctgtagcaccgcctacata
2761 cctcgctctgctaatcctgttaccagtggctgctgccagtggcgataagtcgtgtcttac
2821 cgggttggactcaagacgatagttaccggataaggcgcagcggtcgggctgaacgggggg
2881 ttcgtgcacacagcccagcttggagcgaacgacctacaccgaactgagatacctacagcg
2941 tgagctatgagaaagcgccacgcttcccgaagggagaaaggcggacaggtatccggtaag
3001 cggcagggtcggaacaggagagcgcacgagggagcttccagggggaaacgcctggtatct
3061 ttatagtcctgtcgggtttcgccacctctgacttgagcgtcgatttttgtgatgctcgtc
3121 aggggggcggagcctatggaaaaacgccagcaacgcggccttttacggttcctggcctt
3181 ttgctggccttttgctcacatgttctttcctgcgttatcccctgattctgtggataaccg
3241 tattaccgcctttgagtgagctgataccgctcgccgcagccgaacgaccgagcgcagcga
3301 gtcagtgagcgaggaagcggaagagcgcctgatgcggtattttctccttacgcatctgtg
3361 cggtatttcacaccgcatatatggtgcactctcagtacaatctgctctgatgccgcatag
3421 ttaagccagtatacactccgctatcgctacgtgactgggtcatggctgcgccccgacacc
3481 cgccaacacccgctgacgcgccctgacgggcttgtctgctcccggcatccgcttacagac
3541 aagctgtgaccgtctccgggagctgcatgtgtcagaggttttcaccgtcatcaccgaaac
3601 gcgcgaggcagctgcggtaaagctcatcagcgtggtcgtgaagcgattcacagatgtctg
3661 cctgttcatccgcgtccagctcgttgagtttctccagaagcgttaatgtctggcttctga
3721 taaagcgggccatgttaagggcggttttttcctgtttggtcactgatgcctccgtgtaag
3781 ggggatttctgttcatgggggtaatgataccgatgaaacgagagaggatgctcacgatac
3841 gggttactgatgatgaacatgcccggttactggaacgttgtgagggtaaacaactggcgg
3901 tatggatgcggcgggaccagagaaaaatcactcagggtcaatgccagcgcttcgttaata
3961 cagatgtaggtgttccacagggtagccagcagcatcctgcgatgcagatccggaacataa
4021 tggtgcagggcgctgacttccgcgtttccagactttacgaaacacggaaaccgaagacca
4081 ttcatgttgttgctcaggtcgcagacgttttgcagcagcagtcgcttcacgttcgctcgc
4141 gtatcggtgattcattctgctaaccagtaaggcaaccccgccagcctagccgggtcctca
4201 acgacaggagcacgatcatgcgcacccgtggggccgccatgccggcgataatggcctgct
4261 tctcgccgaaacgtttggtggcgggaccagtgacgaaggcttgagcgagggcgtgcaaga
4321 ttccgaataccgcaagcgacaggccgatcatcgtcgcgctccagcgaaagcggtcctcgc
4381 cgaaaatgacccagagcgctgccggcacctgtcctacgagttgcatgataaagaagacag
4441 tcataagtgcggcgacgatagtcatgccccgcgcccaccggaaggagctgactgggttga
4501 aggctctcaagggcatcggtcgagatcccggtgcctaatgagtgagctaacttacattaa
4561 ttgcgttgcgctcactgcccgctttccagtcgggaaacctgtcgtgccagctgcattaat
4621 gaatcggccaacgcgcggggagaggcggtttgcgtattgggcgccagggtggtttttctt
4681 ttcaccagtgagacgggcaacagctgattgcccttcaccgcctggccctgagagagttgc
4741 agcaagcggtccacgctggtttgccccagcaggcgaaaatcctgtttgatggtggttaac
```

Figure A.4 (continued)

```
4801 ggcgggatataacatgagctgtcttcggtatcgtcgtatcccactaccgagatatccgca
4861 ccaacgcgcagcccggactcggtaatggcgcgcattgcgcccagcgccatctgatcgttg
4921 gcaaccagcatcgcagtgggaacgatgccctcattcagcatttgcatggtttgttgaaaa
4981 ccggacatggcactccagtcgccttcccgttccgctatcggctgaatttgattgcgagtg
5041 agatatttatgccagccagccagacgcagacgcgccgagacagaacttaatgggcccgct
5101 aacagcgcgatttgctggtgacccaatgcgaccagatgctccacgcccagtcgcgtaccg
5161 tcttcatgggagaaaataatactgttgatgggtgtctggtcagagacatcaagaaataac
5221 gccggaacattagtgcaggcagcttccacagcaatggcatcctggtcatccagcggatag
5281 ttaatgatcagcccactgacgcgttgcgcgagaagattgtgcaccgccgctttacaggct
5341 tcgacgccgcttcgttctaccatcgacaccaccacgctggcacccagttgatcggcgcga
5401 gatttaatcgccgcgacaatttgcgacggcgcgtgcagggccagactggaggtggcaacg
5461 ccaatcagcaacgactgtttgcccgccagttgttgtgccacgcggttgggaatgtaattc
5521 agctccgccatcgccgcttccactttttcccgcgttttcgcagaaacgtggctggcctgg
5581 ttcaccacgcgggaaacggtctgataagagacaccggcatactctgcgacatcgtataac
5641 gttactggtttcacattcaccaccctgaattgactctcttccgggcgctatcatgccata
5701 ccgcgaaaggttttgcgccattcgatggtgtccgggatctcgacgctctcccttatgcga
5761 ctcctgcattaggaagcagcccagtagtaggttgaggccgttgagcaccgccgccgcaag
5821 gaatggtgcatgcaaggagatggcgcccaacagtcccccggccacggggcctgccaccat
5881 acccacgccgaaacaagcgctcatgagcccgaagtggcgagcccgatcttccccatcggt
5941 gatgtcggcgatataggcgccagcaaccgcacctgtggcgccggtgatgccggccacgat
6001 gcgtccggcgtagaggatcgagatctcgatcccgcgaaattaatacgactcactataggg
6061 gaattgtgagcggataa
```

Figure A.4 (continued)

```
  1         PpuMI rg|gwccy9
  1  SalI c|tcgac2 AvaI c|ycgrg16
  1 V  D  G  T  L  P  G  Y  G  V  P  G  K  G  V  P  G  V  G  V
  1 GTCGACGGGACCCTCCCGGGCTATGGGGTGCCGGGTAAAGGCGTTCCGGGTGTGGGCGTA
 21 P  G  Y  G  V  P  G  K  G  V  P  G  V  G  V  P  G  Y  G  V
 61 CCGGGTTACGGCGTACCGGGTAAAGGGGTTCCAGGCGTGGGTGTACCGGGCTATGGGGTG
 41 P  G  K  G  V  P  G  V  G  V  P  G  Y  G  V  P  G  K  G  V
121 CCGGGTAAAGGCGTTCCGGGTGTGGGCGTACCGGGTTACGGCGTACCGGGTAAAGGGGTT
 61 P  G  V  G  V  P  G  Y  G  V  P  G  K  G  V  P  G  V  G  V
181 CCAGGCGTGGGTGTACCGGGCTATGGGGTGCCGGGTAAAGGCGTTCCGGGTGTGGGCGTA
 81 P  G  Y  G  V  P  G  K  G  V  P  G  V  G  V  P  G  Y  G  V
241 CCGGGTTACGGCGTACCGGGTAAAGGGGTTCCAGGCGTGGGTGTACCGGGCTATGGGGTG
101 P  G  K  G  V  P  G  V  G  V  P  G  Y  G  V  P  G  K  G  V
301 CCGGGTAAAGGCGTTCCGGGTGTGGGCGTACCGGGTTACGGCGTACCGGGTAAAGGGGTT
121 P  G  V  G  V  P  G  Y  G  V  P  G  K  G  V  P  G  V  G  V
361 CCAGGCGTGGGTGTACCGGGCTATGGGGTGCCGGGTAAAGGCGTTCCGGGTGTGGGCGTA
141 P  G  Y  G  V  P  G  K  G  V  P  G  V  G  V  P  G  Y  G  V
421 CCGGGTTACGGCGTACCGGGTAAAGGGGTTCCAGGCGTGGGTGTACCGGGCTATGGGGTG
161 P  G  K  G  V  P  G  V  G  V  P  G  Y  G  V  P  G  K  G  V
481 CCGGGTAAAGGCGTTCCGGGTGTGGGCGTACCGGGTTACGGCGTACCGGGTAAAGGGGTT
181 P  G  V  G  V  P  G  Y  G  V  P  G  K  G  V  P  G  V  G  V
541 CCAGGCGTGGGTGTACCGGGCTATGGGGTGCCGGGTAAAGGCGTTCCGGGTGTGGGCGTA
201 P  G  Y  G  V  P  G  K  G  V  P  G  V  G  V  P  G  Y  G  V
601 CCGGGTTACGGCGTACCGGGTAAAGGGGTTCCAGGCGTGGGTGTACCGGGCTATGGGGTG
221 P  G  K  G  V  P  G  V  G  V  P  G  Y  G  V  P  G  K  G  V
661 CCGGGTAAAGGCGTTCCGGGTGTGGGCGTACCGGGTTACGGCGTACCGGGTAAAGGGGTT
721                                          XhoI c|tcgag761
721                                          AvaI c|ycgrg761
721                        RsrII cg|gwccg745
721                AgeI a|ccggt736   BsmI gaatgcn|754
241 P  G  V  G  V  P  V  A  D  R  G  M  R  L  E
721 CCAGGCGTGGGTGTACCGGTAGCGGACCGTGGAATGCGGCTCGAG
```

Figure A.5. Coding region for $(EL6Y2)_8$ (molecular weight = 25.548 kDa). Final sequence made via insertion at the XhoI site in pET28aRW.

```
  1         PpuMI rg|gwccy9
  1  SalI g|tcgac2 AvaI c|ycgrg16
  1 V  D  G  T  L  P  G  Y  G  V  P  G  K  G  V  P  G  Y  G  V
  1 GTCGACGGGACCCTCCCGGGCTATGGGGTGCCGGGTAAGGGCGTTCCGGGTTACGGCGTA
 21 P  G  K  G  V  P  G  Y  G  V  P  G  K  G  V  P  G  Y  G  V
 61 CCGGGTAAAGGCGTACCGGGTTACGGGGTTCCAGGCAAGGGTGTACCGGGCTATGGGGTG
 41 P  G  K  G  V  P  G  Y  G  V  P  G  K  G  V  P  G  Y  G  V
121 CCGGGTAAGGGCGTTCCGGGTTACGGCGTACCGGGTAAAGGCGTACCGGGTTACGGGGTT
 61 P  G  K  G  V  P  G  Y  G  V  P  G  K  G  V  P  G  Y  G  V
181 CCAGGCAAGGGTGTACCGGGCTATGGGGTGCCGGGTAAGGGCGTTCCGGGTTACGGCGTA
 81 P  G  K  G  V  P  G  Y  G  V  P  G  K  G  V  P  G  Y  G  V
241 CCGGGTAAAGGCGTACCGGGTTACGGGGTTCCAGGCAAGGGTGTACCGGGCTATGGGGTG
101 P  G  K  G  V  P  G  Y  G  V  P  G  K  G  V  P  G  Y  G  V
301 CCGGGTAAGGGCGTTCCGGGTTACGGCGTACCGGGTAAAGGCGTACCGGGTTACGGGGTT
121 P  G  K  G  V  P  G  Y  G  V  P  G  K  G  V  P  G  Y  G  V
361 CCAGGCAAGGGTGTACCGGGCTATGGGGTGCCGGGTAAGGGCGTTCCGGGTTACGGCGTA
141 P  G  K  G  V  P  G  Y  G  V  P  G  K  G  V  P  G  Y  G  V
421 CCGGGTAAAGGCGTACCGGGTTACGGGGTTCCAGGCAAGGGTGTACCGGGCTATGGGGTG
161 P  G  K  G  V  P  G  Y  G  V  P  G  K  G  V  P  G  Y  G  V
481 CCGGGTAAGGGCGTTCCGGGTTACGGCGTACCGGGTAAAGGCGTACCGGGTTACGGGGTT
181 P  G  K  G  V  P  G  Y  G  V  P  G  K  G  V  P  G  Y  G  V
541 CCAGGCAAGGGTGTACCGGGCTATGGGGTGCCGGGTAAGGGCGTTCCGGGTTACGGCGTA
201 P  G  K  G  V  P  G  Y  G  V  P  G  K  G  V  P  G  Y  G  V
601 CCGGGTAAAGGCGTACCGGGTTACGGGGTTCCAGGCAAGGGTGTACCGGGCTATGGGGTG
221 P  G  K  G  V  P  G  Y  G  V  P  G  K  G  V  P  G  Y  G  V
661 CCGGGTAAGGGCGTTCCGGGTTACGGCGTACCGGGTAAAGGCGTACCGGGTTACGGGGTT
721                                        XhoI c|tcgag761
721                                        AvaI c|ycgrg761
721                          RsrII cg|gwccg745
721                 AgeI a|ccggt736        BsmI gaatgcn759
241 P  G  K  G  V  P  V  A  D  R  G  M  R  L  E
721 CCAGGCAAGGGTGTACCGGTAGCGGACCGTGGAATGCGGCTCGAG
```

Figure A.6. Coding region for $(EL6YK3)_8$ (molecular weight = 26.292 kDa). Final sequence made via insertion at the XhoI site in pET28aRW.

```
  1         PpuMI rg|gwccy9
  1  SalI c|tcgac2 AvaI c|ycgrg16
  1 V  D  G  T  L  P  G  Y  G  V  P  G  K  G  V  P  G  Y  G  V
  1 GTCGACGGGACCCTCCCGGGCTATGGGGTGCCGGGTAAAGGCGTTCCGGGTTACGGCGTA
 21 P  G  F  G  V  P  G  E  G  V  P  G  Y  G  V  P  G  Y  G  V
 61 CCGGGTTTCGGCGTACCGGGTGAAGGGGTTCCAGGCTACGGTGTACCGGGCTATGGGGTG
 41 P  G  K  G  V  P  G  Y  G  V  P  G  F  G  V  P  G  E  G  V
121 CCGGGTAAAGGCGTTCCGGGTTACGGCGTACCGGGTTTCGGCGTACCGGGTGAAGGGGTT
 61 P  G  Y  G  V  P  G  Y  G  V  P  G  K  G  V  P  G  Y  G  V
181 CCAGGCTACGGTGTACCGGGCTATGGGGTGCCGGGTAAAGGCGTTCCGGGTTACGGCGTA
 81 P  G  F  G  V  P  G  E  G  V  P  G  Y  G  V  P  G  Y  G  V
241 CCGGGTTTCGGCGTACCGGGTGAAGGGGTTCCAGGCTACGGTGTACCGGGCTATGGGGTG
101 P  G  K  G  V  P  G  Y  G  V  P  G  F  G  V  P  G  E  G  V
301 CCGGGTAAAGGCGTTCCGGGTTACGGCGTACCGGGTTTCGGCGTACCGGGTGAAGGGGTT
121 P  G  Y  G  V  P  G  Y  G  V  P  G  K  G  V  P  G  Y  G  V
361 CCAGGCTACGGTGTACCGGGCTATGGGGTGCCGGGTAAAGGCGTTCCGGGTTACGGCGTA
141 P  G  F  G  V  P  G  E  G  V  P  G  Y  G  V  P  G  Y  G  V
421 CCGGGTTTCGGCGTACCGGGTGAAGGGGTTCCAGGCTACGGTGTACCGGGCTATGGGGTG
161 P  G  K  G  V  P  G  Y  G  V  P  G  F  G  V  P  G  E  G  V
481 CCGGGTAAAGGCGTTCCGGGTTACGGCGTACCGGGTTTCGGCGTACCGGGTGAAGGGGTT
181 P  G  Y  G  V  P  G  Y  G  V  P  G  K  G  V  P  G  Y  G  V
541 CCAGGCTACGGTGTACCGGGCTATGGGGTGCCGGGTAAAGGCGTTCCGGGTTACGGCGTA
201 P  G  F  G  V  P  G  E  G  V  P  G  Y  G  V  P  G  Y  G  V
601 CCGGGTTTCGGCGTACCGGGTGAAGGGGTTCCAGGCTACGGTGTACCGGGCTATGGGGTG
221 P  G  K  G  V  P  G  Y  G  V  P  G  F  G  V  P  G  E  G  V
661 CCGGGTAAAGGCGTTCCGGGTTACGGCGTACCGGGTTTCGGCGTACCGGGTGAAGGGGTT
721                                          XhoI c|tcgag761
721                                          AvaI c|ycgrg761
721                       RsrII cg|gwccg745
721               AgeI a|ccggt736   BsmI gaatgcn|754
241 P  G  Y  G  V  P  V  A  D  R  G  M  R  L  E
721 CCAGGCTACGGTGTACCGGTAGCGGACCGTGGAATGCGGCTCGAG
```

Figure A.7. Coding region for $(EL6Y3)_8$ (molecular weight = 26.452 kDa). Final sequence made via insertion at the XhoI site in pET28aRW.

```
  1         PpuMI rg|gwccy9
  1  SalI c|tcgac2  AfeI agc|gct17
  1 V  D  G  T  L  S  A  Q  T  P  S  S  K  Q  Y  G  A  P  A  Q
  1 GTCGACGGGACCCTCAGCGCTCAGACCCCTTCTTCCAAGCAGTATGGCGCTCCGGCGCAG
 21 T  P  S  S  Q  Y  G  A  P  A  Q  T  P  S  S  K  Q  Y  G  A
 61 ACACCGAGCAGCCAGTACGGTGCACCGGCTCAGACCCCTTCTTCCAAGCAGTATGGCGCT
 41 P  A  Q  T  P  S  S  Q  Y  G  A  P  A  Q  T  P  S  S  K  Q
121 CCGGCGCAGACACCGAGCAGCCAGTACGGTGCACCGGCTCAGACCCCTTCTTCCAAGCAG
 61 Y  G  A  P  A  Q  T  P  S  S  Q  Y  G  A  P  A  Q  T  P  S
181 TATGGCGCTCCGGCGCAGACACCGAGCAGCCAGTACGGTGCACCGGCTCAGACCCCTTCT
 81 S  K  Q  Y  G  A  P  A  Q  T  P  S  S  Q  Y  G  A  P  A  Q
241 TCCAAGCAGTATGGCGCTCCGGCGCAGACACCGAGCAGCCAGTACGGTGCACCGGCTCAG
101 T  P  S  S  K  Q  Y  G  A  P  A  Q  T  P  S  S  Q  Y  G  A
301 ACCCCTTCTTCCAAGCAGTATGGCGCTCCGGCGCAGACACCGAGCAGCCAGTACGGTGCA
121 P  A  Q  T  P  S  S  K  Q  Y  G  A  P  A  Q  T  P  S  S  Q
361 CCGGCTCAGACCCCTTCTTCCAAGCAGTATGGCGCTCCGGCGCAGACACCGAGCAGCCAG
141 Y  G  A  P  A  Q  T  P  S  S  K  Q  Y  G  A  P  A  Q  T  P
421 TACGGTGCACCGGCTCAGACCCCTTCTTCCAAGCAGTATGGCGCTCCGGCGCAGACACCG
161 S  S  Q  Y  G  A  P  A  Q  T  P  S  S  K  Q  Y  G  A  P  A
481 AGCAGCCAGTACGGTGCACCGGCTCAGACCCCTTCTTCCAAGCAGTATGGCGCTCCGGCG
181 Q  T  P  S  S  Q  Y  G  A  P  A  Q  T  P  S  S  K  Q  Y  G
541 CAGACACCGAGCAGCCAGTACGGTGCACCGGCTCAGACCCCTTCTTCCAAGCAGTATGGC
201 A  P  A  Q  T  P  S  S  Q  Y  G  A  P  A  Q  T  P  S  S  K
601 GCTCCGGCGCAGACACCGAGCAGCCAGTACGGTGCACCGGCTCAGACCCCTTCTTCCAAG
661                                                    RsrII cg|gwccg718
661                                                  AleI cacnn|nngtg709
221 Q  Y  G  A  P  A  Q  T  P  S  S  Q  Y  G  A  P  K  W  A  D
661 CAGTATGGCGCTCCGGCGCAGACACCGAGCAGCCAGTACGGTGCACCGAAGTGGGCGGAC
721             XhoI c|tcgag734
721             AvaI c|ycgrg734
721       BsmI gaatgcn|727
241 R  G  M  R  L  E
721 CGTGGAATGCGGCTCGAG
```

Figure A.8. Coding region for RZY_{20} (molecular weight = 27.653 kDa). Final sequence made via insertion at the XhoI site in pET28aRW.

```
  1              PpuMI rg|gwccy15
  1        NdeI ca|tatg8
  1  SalI c|tcgac2       AvaI c|ycgrg22
  1 V  D  H  M  R  T  L  P  G  V  G  V  P  G  I  G  V  P  G  F
  1 GTCGACCATATGAGGACCCTCCCGGGCGTGGGGGTGCCGGGTATCGGCGTTCCGGGTTTT
 21 G  V  P  G  K  G  V  P  G  I  G  V  P  G  V  G  V  P  G  V
 61 GGCGTACCGGGTAAGGGCGTACCGGGTATTGGGGTTCCAGGCGTTGGTGTACCGGGCGTG
 41 G  V  P  G  I  G  V  P  G  F  G  V  P  G  K  G  V  P  G  I
121 GGGGTGCCGGGTATCGGCGTTCCGGGTTTTGGCGTACCGGGTAAGGGCGTACCGGGTATT
 61 G  V  P  G  V  G  V  P  G  V  G  V  P  G  I  G  V  P  G  F
181 GGGGTTCCAGGCGTTGGTGTACCGGGCGTGGGGGTGCCGGGTATCGGCGTTCCGGGTTTT
241                                                  AgeI a|ccggt292
 81 G  V  P  G  K  G  V  P  G  I  G  V  P  G  V  G  V  P  V  A
241 GGCGTACCGGGTAAGGGCGTACCGGGTATTGGGGTTCCAGGCGTTGGTGTACCGGTAGCG
301               BsmI gaatgcn|316
301 RsrII cg|gwccg301
101 D  R  H  G  G  M  R  K  Y  A  Y  G  Y  A  S  G  Y  A  S  Y
301 GACCGCCATGGAGGAATGCGGAAATATGCGTATGGTTACGCGTCCGGTTATGCTTCCTAC
361                                                  XhoI c|tcgag413
361                                                  AvaI c|ycgrg413
121 G  K  A  Y  G  S  K  E  Y  S  Y  G  S  A  Y  G  E  L  E
361 GGCAAGGCTTATGGCTCAAAAGAATACTCCTACGGCTCCGCATACGGCGAACTCGAG
```

Figure A.9. Coding region for EL18-9Y (molecular weight of two-cassette protein = 28.770 kDa). Final sequence made by inserting twice at the XhoI site in pET28aRW.

B. ADDITIONAL PROTOCOLS

B.1 Tyrosinase Immobilization

References

- Marín-Zamora ME *et al.* Cinnamic ester of D-sorbitol for immobilization of mushroom tyrosinase. *J Chem Tech and Biotech*, 2005. **80**:1356-1364.
- Marín-Zamora ME *et al.* Direct immobilization of tyrosinase enzyme from natural mushrooms (*Agaricus bisporus*) on D-sorbitol cinnamic ester. *J Biotech*, 2006. **126**:295-303.

Preparation of totally cinnamoylated derivative of D-sorbitol (SOTCN)

1. Add 3.6 g D-sorbitol to 100 mL pyridine and heat at 60C for 1 hour while stirring (should turn a light yellow)
2. Cool to room temperature and add 25 g cinnamoyl chloride
3. Stir at room temperature for 4 hours (will heat up as mixes). Meanwhile, begin stirring 200-300 mL of water at 4 °C.
4. After 4 hours, add the cinnamoyl solution to the cold, stirring water (this dissolves the unreacted reagents into solution).
5. Filter cinnamoyl/water solution with bottle top filter until "water spots" are no longer visible. The sticky precipitate is the desired product.
    a. DO NOT use filter paper - the sticky product will shred the paper.
    b. Put the precipitate on the filter last so that it doesn't clog.
    c. Liquid flow-through should be put in an appropriate waste container.
6. Wash SOTCN twice with chloroform and hexanes:

   a. Dissolve sticky precipitate in the minimum volume of chloroform.
   b. Pour solution into vigorously stirring hexanes (SOTCN precipitates).
   c. Filter as before until as dry as possible.
   d. Repeat steps a - c.
7. Dry in vacuum desiccator (with P_2O_5 as drying agent) overnight (gets bubbly!)

Coating of beads in SOTCN and immobilization of tyrosinase

1. Degrease beads by immersing in a small amount of trichloroethylene for 30 min.
   a. 20 mL is enough volume to immerse 40 mL beads
   b. VERY TOXIC! - be careful!
2. Wash beads numerous times with acetone and then water until clean.
3. Dissolve dried SOTCN in chloroform at a concentration of 0.5 g per 20 mL.
   a. Store extra SOTCN at 4 °C wrapped in foil in desiccator under N_2 or Ar.
4. Submerse beads in SOTCN/chloroform solution.
5. Use a vacuum to evaporate chloroform until dry (overnight).
6. Polymerize SOTCN with a Mercury lamp (UV light) for 30 minutes.
7. Place beads in a 15 mL tube and submerse in 0.1 M potassium phosphate buffer (pH 4.5) with 0.2 mg/mL Tyrosinase.
8. Incubate at 4 °C for 3 hours.
9. Wash with MilliQ water several times and store at 4 °C.

B.2 Tyrosinase Reaction

References

- Taylor S. Chemoenzymatic synthesis of peptidyl 3,4-dihydroxyphenylalanine for structure-activity relationships in marine invertebrate polypeptides. *Anal Biochem*, 2002. **302**:70-74.
- Marumo K and Waite JH. Optimization of hydroxylation of tyrosine and tyrosine-containing peptides by mushroom tyrosinase. *Biochim et Biophys Acta*, 1986. **872**:98-103.

Acetate Reaction Buffer (500 mL)

0.1 M acetate buffer, 20-200 mM ascorbic acid, 0-100 mm boric acid (optional)

- For 500 mL of stock 0.1 M acetate buffer (pH 4.5), mix:

  2.72 g sodium acetate

  1.01 mL acetic acid

  MilliQ water to final volume of 500 mL
- Add ascorbic acid fresh for each reaction (200 mM = 35.2 mg/mL)
- If desired, add boric acid (20 mM = 1.24 mg/mL)
- Adjust pH as desired

Tyrosinase Reaction

1. Mix reaction buffer and protein as desired (recommended final concentration: 2 mg/mL)
2. Right before incubation, add tyrosinase enzyme
   a. For soluble enzyme, add 50-150 units per mL of reaction
   b. For immobilized enzyme, add 0.05-0.2 g wet beads per mL of reaction
3. Incubate at 37 °C, 150-250 rpm for at least 2 h

4. Quench reaction by adding 20 μL 6 N HCl per mL of reaction
5. Dialyze extensively against 5% acetic acid at 4 °C

    a. Change buffer at least 10 times

    b. This is to eliminate all traces of ascorbic acid which causes a false positive in DOPA measurement assays

B.3 IRPH Assay for Measurement of DOPA

References

- Issopoulos PB. High-sensitivity spectrophotometric determination of trace amounts of Levodopa, Carbidopa and α-Methyldopa. *Fresenius J Anal Chem*, 1990. **336**:124-128.

Iron(III)-*o*-phenanthroline (IRPH) Mixture (50 mL)

- Mix:

    0.1 g *o*-phenanthroline monohydrate

    1 mL 1 N HCl

    0.08 g ammonium ferric sulfate dodecahydrate

- Fill with MilliQ to 50 mL
- Stable for at least 1 month if stored in cool, dark place (refrigerator)

Measure DOPA concentration

Note: Since assay is kinetic in nature, a new standard curve is required each time

1. Pre-read 96-well plate
2. Add to wells:

    10 μL sample or standard solution (0 - 1 mM DOPA)

200 μL MilliQ water

50 μL IRPH solution

Note: A half-volume assay will also work, but make sure to use the same volume for all wells

3. Incubate at room temperature for 75 minutes
4. Measure in plate reader at 510 nm

NOTE: Anomalous behavior was noted when using this assay with highly-converted protein (i.e., $mELY_{16}$ from Chapter 4). During assay incubation, the rate of color development for the samples was different from the rate of color development for the standard L-DOPA solutions. As a result, after 1 min of incubation, a "conversion" value of 80% was measured, but after 15 min, the "conversion" value had dropped to 38%. Calculated conversion values continued to drop as the incubation time increased. Because the assay was verified only for free L-DOPA and related compounds, it is possible that the anomalous behavior is related to the presence of 3,4,5-trihydroxyphenylalanine (TOPA) residues or the interaction of the protein backbone with the assay reagents.

B.4 Difference Spectrophotometry for Measurement of DOPA

REFERENCES

- Waite JH. Determination of (catecholato)borate complexes using difference spectrophotometry. *Anal Chem*, 1984. **56**:1935-1939.

MEASURE DOPA CONCENTRATION

1. Pre-read 96-well plate
2. For each sample or standard, measure the absorbance at 292 nm of:

100 μL 0.1 N HCl + 100 μL sample or standard

100 μL sodium borate (pH 8.5) + 100 μL sample or standard

3. After zeroing data to pre-read, subtract the HCl absorbance from the borate absorbance for each sample or standard. Height of peak at 292 nm is proportional to DOPA concentration.

B.5 Silver Staining of Adsorbed Protein in Microtiter Plates

References

- Root DD and Wang K. Kinetic silver staining of proteins. *The Protein Protocols Handbook, 2nd edition*, Humana Press, Inc., p. 1935-1939.

Reagent A (50 mL)

0.2% $AgNO_3$, 0.2% NH_4NO_3, 1% tungstosilicic acid, 0.3% formaldehyde solution

- Mix:

  0.1 g $AgNO_3$

  0.1 g NH_4NO_3

  0.5 g tungstosilicic acid

  150 μL of 37% formaldehyde solution

- Fill to 50 mL with MilliQ water
- Store in the dark at room temperature

Protocol

1. Adsorb protein solution(s) of interest to wells of plate by incubating overnight at 4 °C

   For 96-well plate, use 50 μL solution

   For 24-well plate, use 350 μL solution

2. GENTLY wash the wells with adsorbed protein several times with MilliQ water
3. Prepare standard protein solutions in MilliQ water.
4. Add standard solutions to wells of plate in same volumes as used to adsorb protein in step 1.
5. Cover plate with a Kimwipe and allow to dry out (may take several days)
6. Mix equal volumes of reagents A and B (5% (w/v) Na_2CO_3) immediately before use. Quickly (within 10 min) add a fixed volume of the mixture to all wells with protein (samples and standards).

   For 96-well plate, add 100 μL

   For 24-well plate, add 500 μL
7. Let incubate at room temperature for at least 18 h, or until reaches equilibrium
8. Read the absorbance of the wells at 405 nm using plate reader.

   Standard curve should be linear up to 2500 ng/mL

B.6 Protein Adsorption

References

- Protocol is based on procedure developed by Yeji Kim for her dissertation [200].

Protocol

1. Adsorb protein solution(s) to materials of interest by incubating overnight at 4 °C. Materials should be in disk form and placed in a 96 or 24 well plate. Potential materials include:

   Glass (acid- or base-washed coverslips)

   Poly(vinyl chloride) (PVC) or poly(tetrafluoroethylene) (PTFE)disks

   Order thin sheets of materials. Wash with soap and water before use.

   Punch out disks with leather punch. Disks should fit into wells of plate.

   Aluminum: Wrap glass/PTFE disks in aluminum foil. Super glue in place.

2. GENTLY wash the disks with adsorbed protein several times with MilliQ water and transfer to a fresh plate.
3. Prepare standard protein solutions in MilliQ water.

   It is important to use the same protein for both adsorption and standard solutions, as different proteins react differently to protein concentration assays.
4. To wells in plate, add the same volume of protein standard solution or water (to wells with adsorbed protein disks).
5. Perform protein concentration assay of choice.

   BCA assay is recommended, although Bradford is good for higher expected concentrations. Silver staining can work for very low concentrations.
6. Compare reading on adsorbed protein disks to standard curve and calculate the amount of protein present on the disks.

B.7 Lap Shear Adhesion Testing

Notes: Protocol is based on ASTM Standard D1002. Aluminum adherends made from Farmer's Copper 6061-T6. Cut to size: 3.5 in long, 0.125 in thick, and 0.5 in wide. A 0.25 in diameter hole for fixing into Instron is located 0.825 in from one end. Area for overlap is on end opposite the hole, and is 1.2 cm long.

Preparing Adhesion Samples

1. Choose adherend pairs very carefully. Having consistently smooth/rough adherends of same thickness can make a big difference in the results.
2. On a large flat board (Teflon, plastic, etc), tape a metal plate of same thickness as adherends.
3. Dispense 10 - 40 μL sample evenly in the overlap region on a pair of adherends. Spread evenly over entire overlap region.

Note: Appropriate volume will not result in any leakage outside of overlap area when adherends are pressed together.

4. Add 3 - 15 μL crosslinker solution, if desired.

5. Align and press adherends together:

    a. Align long side of one adherend with Teflon measuring block (should have a 1.2 cm square drawn to help ensure consistent overlap area).

    b. Lift 2nd adherend and drop gently onto 1st adherend so that the "hole end" of 2nd adherend rests on metal plate and adherends overlap in overlap region.

    c. Press bond together. If desired, "mix" crosslinker into solution by gently lifting and pressing down on 2nd adherend.

    d. Align adherends by sandwiching between 2 white Teflon measuring blocks.

    e. GENTLY pull white blocks away without disturbing bond area.

    f. If desired, place a weight (conical tube filled with lead shot) onto overlap area during cure.

    g. For humid cure, wet paper towels with water and squeeze out excess. Gently place damp towels so that they completely cover the overlap area of adherends. Gently cover adherends with plastic wrap, taping and sealing all edges to prevent drying.

    h. For underwater curing, set up a large tub with a flat bottom as you would normally set up a testing board. Add water or PBS until have bath ~1-2" deep, and pre-warm bath for several hours if curing above room temperature. Set up each adherend in the center of the tub as usual, being very careful not to disrupt the adhesive solution when placing the top adherend (i.e., place it very gently and evenly). Press down on overlap and VERY CAREFULLY move to one side of the tub. Setting up in the center of the tub gives you more room to manipulate the adherends. Continue until all adherends are set up. Gently and slowly move the entire tub into incubator for cure. Test as usual.

6. Let all samples cure at desired temperature for desired time.

Testing Adhesion Samples on Instron 5544

1. Attach 2 kN load cell and lap shear apparatus, if necessary.
2. Turn on Instron 20-30 min before testing to warm up.
3. Turn on and sign into computer

   Username: Wilkeradmin

   Password is posted on computer
4. Double-click on Merlin icon on desktop
5. Select "Monahan-1" method
6. Once method loads, click on button in upper-right that looks like a cylinder with an arrow pointing down on the bottom.
7. Click on Limits. Change values to -1.8E+003 and 1.8E+003.
8. Put metal rod through holes in top of lap shear apparatus.

   Note: Be sure to use the same rods in the same location each time
9. Click "Calibrate" and then click "OK".
10. Once is finished calibrating, check the box "Enabled" in Min/Max Limit
11. Click "Done".
12. Click button on right that looks like 3 staggered hourglasses
13. Click on "Specimen". Change the sample name, then click on the results window, and then click on the specimen window again.
14. Measure sample overlap region with calipers. *Note: Can measure after testing instead*
15. Place sample in testing apparatus:

    Pinch sample in overlap area and press one end into the rubber stopper at the bottom of the apparatus.

Put metal rod through apparatus and adherend together to hold sample in place.

Check that sample is sitting vertically in all directions.

Jog down on the Instron (arrows on controller pad) and slide in 2nd metal rod through top of apparatus and top adherend.

Important: Make sure no strain is being put on sample before running test! Use fine tuning (plastic spinning knob on controller pad) to put a small gap above and below rod in top sample hole.

16. Press triangular "play" button (in software or on controller) to start test.
17. Press square "stop" button (in software or on controller) once sample breaks to stop test.
18. Record max load (ignore other numbers).
19. Calculate adhesion strength: (Strength (MPa)) = (Load (N))/(area of overlap (mm^2))
20. When finished, save data: File - Data - End and Save. Save to DATA folder.
21. Transfer data from DATA folder (shortcut on Desktop) to folder of choice.
22. Exit Merlin software and shut down computer and Instron.
23. Take pictures of broken overlap regions, if desired.

B.8 Adherend Cleaning

Protocol is modified from ASTM standard D2651-01.

1. Prepare adherends by soaking in acetone and scraping off any visible solids from overlap area. If acetone is insufficient to remove sample, soak in trichloroethylene (toxic!).
2. Set up base wash in medium crystallizing dish:

6.75 g sodium metasilicate

3.38 g sodium hydroxide

1.13 g sodium dodecyl benzene sulfonate

300 mL DI water

Stir and heat to 75 °C

3. Set up acid wash in medium crystallizing dish:

   33.75 g ferric sulfate

   14 mL sulfuric acid

   278 mL DI water

   Stir and heat to 60 °C

4. Set up adherends on metal rods with a spacer (0.5" nut) between each adherend and place in base bath as follows:

   First row: 5 adherends

   Second row: 9 adherends

   Third row: 10 adherends

   Fourth row: 11 adherends

   Fifth row: 10 adherends

   Sixth row: 9 adherends

   Seventh row: 5 adherends

5. Soak in base bath for 10-15 min.

   Note: Bath level should be high enough to submerge adherend overlap area. If level gets low due to evaporation, add more DI water.

6. Rinse adherends with water into appropriate waste container. Wipe with paper towel.

7. Move adherends to acid bath and soak for 10-15 minutes.

8. Rinse adherends with water into appropriate waste container. Wipe with paper towel.

9. Soak adherends in methanol for 1-2 min.
10. Soak adherends in boiling water for 1 min.

    Note: This step is not part of the ASTM standard, but it prevents a side reaction between the adherend surface and periodate.
11. Let adherends dry for at least one day, or put in oven (55-60 °C) for a few minutes to speed drying process.

B.9 Nickel Column Purification

From QIAGEN QIAexpressionist and in-lab experimentation

Buffers for Native Conditions

50 mM NaH_2PO_4, 300 mM NaCl, varied imidazole, pH 8.0

Mix and fill to 1 L with MilliQ water:

- 6.9 g NaH_2PO_4-H_2O
- 17.54 g NaCl
- Imidazole (MW 68.08 g/mol):

  Lysis buffer: 10 mM

  Wash buffer: 20 mM

  Elution buffer: 250 mM
- Adjust pH to 8.0 with NaOH/HCl

Buffers for Denaturing Conditions

100 mM NaH_2PO_4, 10 mM Tris, 8 M urea, varied pH

Mix and fill to 1 L with MilliQ water:

- 13.8 g NaH_2PO_4-H_2O

- 1.2 g Tris(base)
- 480.5 g Urea
- Adjust pH with NaOH/HCl:

  Buffer B (Lysis): pH 8.0

  Buffer C (Wash): pH 6.3 (*optional: add 10-20 mM imidazole*)

  Buffer D (Elution of monomers): pH 5.9

  Buffer E (Elution of aggregates): pH 4.5

  Buffer "D/E" (General elution): pH 5.5

Purification

Note: Use each column for ONE protein. If solution is not dripping at reasonable rate, can use a small amount of air pressure to speed things up. However, do NOT let agarose dry out, and do not push liquid through faster than 2 cm/min, as this will not allow binding to occur properly.

1. Add Ni-NTA slurry to column (0.5 mL bed per mL of slurry). Let liquid drip out.
2. Equilibrate column with at least 4 bed volumes lysis buffer.
3. Add up to 8 mL cleared lysate per mL bed volume to column. Forcibly mix Ni-NTA bed and cleared lysate.
4. Close up column and incubate on rotary shaker at 37 °C, 200 rpm for 1-2 h.
5. Let solution drip out of column. Take a sample for SDS-PAGE analysis ("Flow Through").
6. Wash with 2 bed volumes of wash buffer. Collect wash samples or fractions for SDS-PAGE analysis.
7. Elute protein with at least 5 total bed volumes of elution buffer. Collect samples/fractions for analysis by SDS-PAGE.

8. Clean column by rinsing with 0.5 M NaOH for 30 minutes.

   Note: If agarose turns a brownish-gray color, column needs to be regenerated.

9. Store column at 4 °C in 30% ethanol to prevent microbial growth.

B.10 Nickel Column Regeneration

From QIAGEN QIAexpressionist

Regeneration Buffer (50 mL)

6 M GuHCl, 0.2 M acetic acid

- 28.65 g GuHCl
- 0.57 mL acetic acid
- Fill to 50 mL with MilliQ water

Procedure

Wash column with following solutions:

1. 2 bed volumes Regeneration Buffer
2. 5 bed volumes MilliQ water
3. 3 bed volumes 2% SDS
4. 1 bed volume 25% ethanol
5. 1 bed volume 50% ethanol
6. 1 bed volume 75% ethanol
7. 5 bed volumes 100% ethanol
8. 1 bed volume 75% ethanol
9. 1 bed volume 50% ethanol

10. 1 bed volume 25% ethanol
11. 1 bed volume MilliQ water
12. 5 bed volumes 100 mM EDTA, pH 8.0 (1.46 g EDTA per 50 mL)
13. 6-7 bed volumes MilliQ water
14. 2 bed volumes 100 mM $NiSO_4$ (1.31 g $NiSO_4$-$6H_2O$ per 50 mL)
15. 2 bed volumes MilliQ water
16. 2 bed volumes Regeneration Buffer

Equilibrate column with 2 bed volumes of either lysis buffer (for immediate use) or 30% ethanol (for storage at 4 °C).

B.11 BrdU Cell Proliferation Assay

Note: Protocol has been optimized for NIH/3T3 fibroblasts cultured on glass coverslips in a 24-well plate. Volumes and incubation times (especially for the BrdU label) may need to be modified for other setups. All reagents from Calbiochem except for secondary antibody (AlexaFluor 488 goat anti-mouse IgG from Molecular Probes).

1. Culture cells as desired.
2. On day of assay, add 200 μL BrdU label solution (1 μL label per 2 mL medium) to each well.
3. Fix cells with 500 μL ice-cold filtered 70% ethanol for 5 min.
4. Wash twice with 2 mL filtered PBS, incubating each wash for 5 min.
5. Denature DNA with 500 μL 2 N HCl for 30 min.
6. Wash twice with 2 mL PBS, incubating each wash for 5 min.
7. Block with 500 μL blocking solution (1% BSA, 0.1% Triton X-100 in PBS) for 1 h.
8. Flip coverslips facedown onto parafilm with 70 μL droplet of anti-BrdU solution (antibody diluted 1:100 in diluent solution) and incubate for 1 h.

Also do a "No primary antibody" control by incubating a positive control coverslip in blocking solution instead of antibody solution.

9. Transfer coverslips back to well plate and wash 3 times as before in PBS.
10. Incubate coverslips in 70 μL secondary antibody solution (diluted 1:1000 in PBS with 1% BSA) as before for 1 h.

    Also do a "No secondary antibody" control by incubating a different positive control coverslip in 1% BSA solution without antibody.
11. Transfer coverslips back to plate and wash 3 times with PBS as before.
12. Incubate coverslips as before with 50 μL DRAQ5 nuclear stain solution (stain diluted 1:500 in PBS) for 30 min.
13. Wash coverslips by dipping into two separate 50 mL aliquots of filtered PBS, then dab with a Kimwipe.
14. Mount coverslips facedown on glass slide with 50% glycerol in PBS (or antifade agent). Soak up excess solution with Kimwipe.
15. Seal coverslips with clear nail polish and let dry for at least 10 min.
16. Store at 4 °C until ready to image.
17. Image on confocal microscope with 488 nm and 632 nm lasers.

C. ADDITIONAL DATA

C.1 $(EL18\text{-}9Y)_2$ Project

Significant work was performed with the protein $(EL18\text{-}9Y)_2$ (see Fig. C.1). However, its design of a tyrosine-rich 9Y domain resulted in high insolubility, making it difficult with which to work. Notably, it would not remain soluble in any form of salt solution and could only be solubilized in either 5% acetic acid or 8 M urea. Because of its intractability in salt, coacervation (by the addition of salt) could not be achieved, so purification was performed using denaturing nickel affinity chromatography. Finally, tyrosinase conversion could not be effectively performed on the protein because it would not remain soluble in the reaction buffer under any conditions in which the enzyme would function, even with the use of immobilization to stabilize the enzyme. Due to a lack of DOPA conversion and general insolubility, the project was eventually abandoned. However, the following data were collected on the protein's expression, purification, cytotoxicity, adsorption, bulk adhesion, characterization with MALDI-TOF and amino acid analysis. An optimization study of the immobilized tyrosinase reaction was also performed using BSA as a model protein to assess the effects of reaction conditions on conversion.

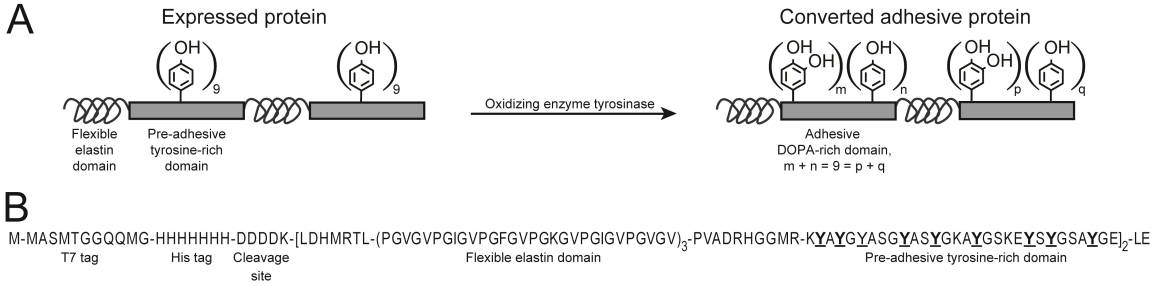

Figure C.1. (A) Schematic of adhesive protein $(EL18\text{-}9Y)_2$. The expressed protein consists of flexible elastin domains and pre-adhesive tyrosine-rich domains. After oxidation with the enzyme tyrosinase, the pre-adhesive domain is converted to an adhesive domain containing a mixture of tyrosine and DOPA residues. (B) Complete amino acid sequence of expressed protein $(EL18\text{-}9Y)_2$. The protein consists of a T7 tag for detection, a 7xHis tag for purification, an enterokinase cleavage site, and then two cassettes each containing a flexible elastin domain and a pre-adhesive tyrosine-rich domain. Pre-adhesive tyrosine residues are underlined.

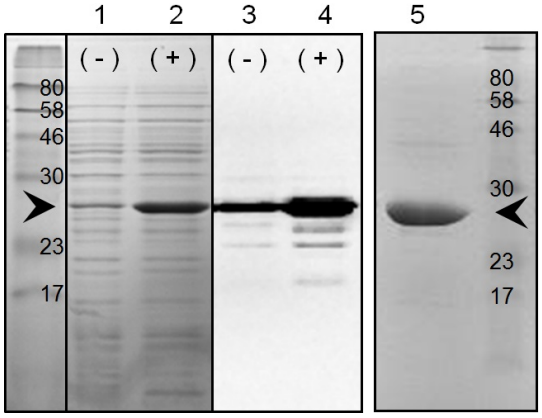

Figure C.2. Expression (lanes 1-4) and purification (lane 5) of $(EL18\text{-}9Y)_2$, as assessed by SDS-PAGE and Western blot. Purity of the protein sample in lane 5 is greater than 95%, as assessed by densitometry analysis. The (-) and (+) symbols indicate before and after induction of protein expression with IPTG. The arrowheads in the standard protein ladders indicate protein expected molecular weight (28.77 kDa).

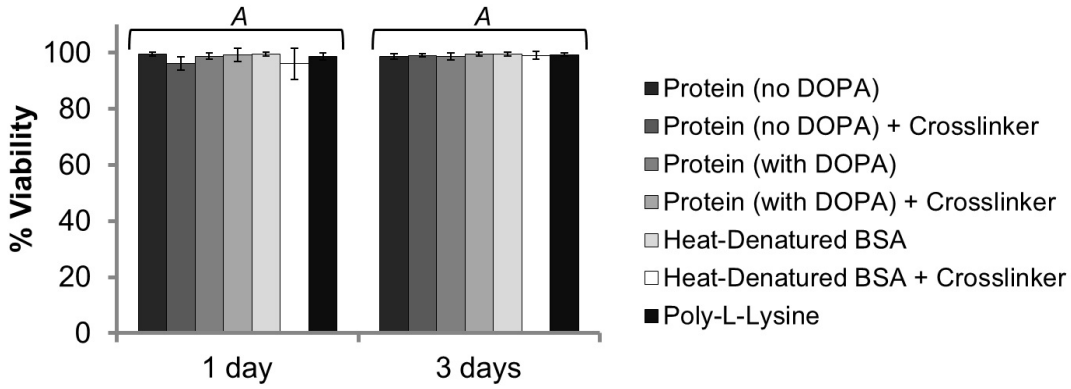

Figure C.3. $(EL18\text{-}9Y)_2$ displays no cytotoxicity as compared to a positive control. Protein solutions were adsorbed to acid-washed glass coverslips overnight at 4 °C and then washed gently with water. For soluions with crosslinker, concentrated sodium periodate solution was added simultaneously with protein solution at a ratio of 3 DOPA for each periodate ion. DOPA conversion calculated to be 4% from IRPH assay. NIH/3T3 mouse fibroblasts were cultured on the adsorbed protein or poly-L-lysine positive control for 1 or 3 days, then assayed with LIVE/DEAD staining. At least 40 cells per coverslip were counted with NIS Elements software, and viability was calculated by the ratio of living cells to the total number of cells.

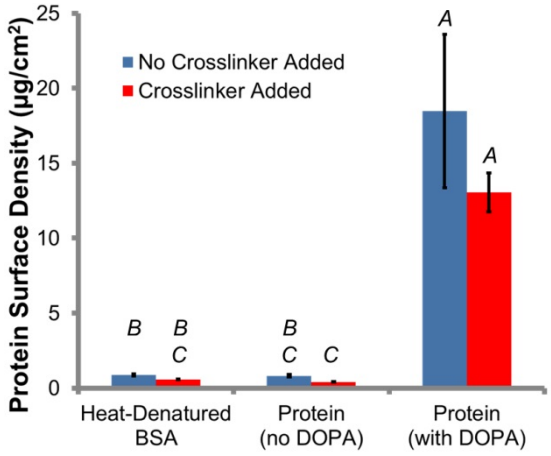

Figure C.4. Adsorption of $(EL18\text{-}9Y)_2$ to glass coverslips. Converted protein adsorbs significantly more than unconverted protein or a non-adhesive control, BSA. The increase in adsorption could be due to the aggregation of protein that results from the tyrosinase conversion procedure. To measure adsorption, protein solution was first adsorbed to acid-washed glass coverslips in a 24-well plate overnight at 4°C. Sodium periodate crosslinker was added simultaneously to relevant coverslips at a ratio of 3 DOPA:1 periodate ion (DOPA conversion calculated to be 4% from IRPH assay.) Following adsorption, excess protein solution was aspirated, and the coverslips were washed gently several times with water and then transferred to a fresh 24-well plate. Protein content was measured using a bicinchoninic acid (BCA) assay and compared to protein standards in solution. Letters indicate Tukey groupings ($p<0.05$).

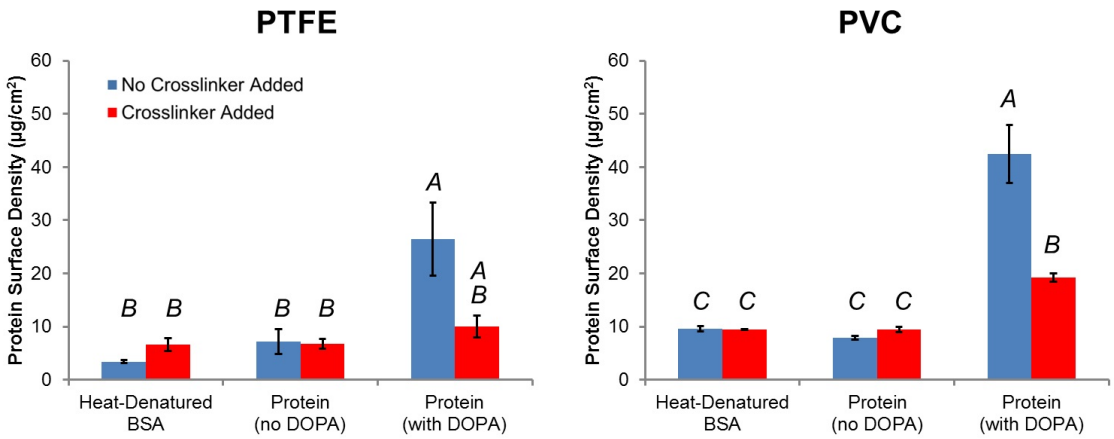

Figure C.5. Adsorption of $(EL18\text{-}9Y)_2$ to poly(tetrafluoroethylene) and poly(vinyl chloride) disks. Converted protein adsorbs significantly more than unconverted protein or a nonadhesive control, BSA. The increase in adsorption could be due to the aggregation of protein that results from the tyrosinase conversion procedure. To measure adsorption, protein solution was first adsorbed to small washed disks in a 96-well plate overnight at 4°C. Sodium periodate crosslinker was added simultaneously to relevant coverslips at a ratio of 3 DOPA:1 periodate ion (DOPA conversion calculated to be 4% from IRPH assay.) Following adsorption, excess protein solution was aspirated, and the coverslips were washed gently several times with water and then transferred to a fresh 96-well plate. Protein content was measured using a bicinchoninic acid (BCA) assay and compared to protein standards in solution. Letters indicate Tukey groupings ($p<0.05$).

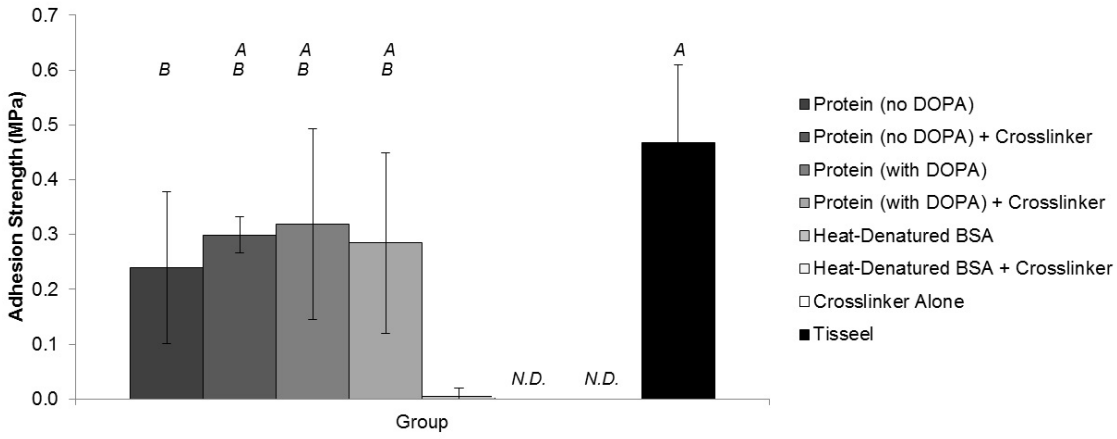

Figure C.6. Bulk adhesive strength of $(EL18\text{-}9Y)_2$ is similar to fibrin-based surgical adhesive Tisseel and significantly greater than nonadhesive control BSA or crosslinker alone. Protein solutions (20 μL of BSA and $(EL18\text{-}9Y)_2$ at 300 mg/mL, 100 μL of Tisseel to match total protein content) were applied to aluminum adherends for lap shear testing. Adherends were cured for 6 h at 37°C with 55 g weights placed on the overlap region to ensure good contact. Letters indicate Tukey groupings ($p<0.05$).

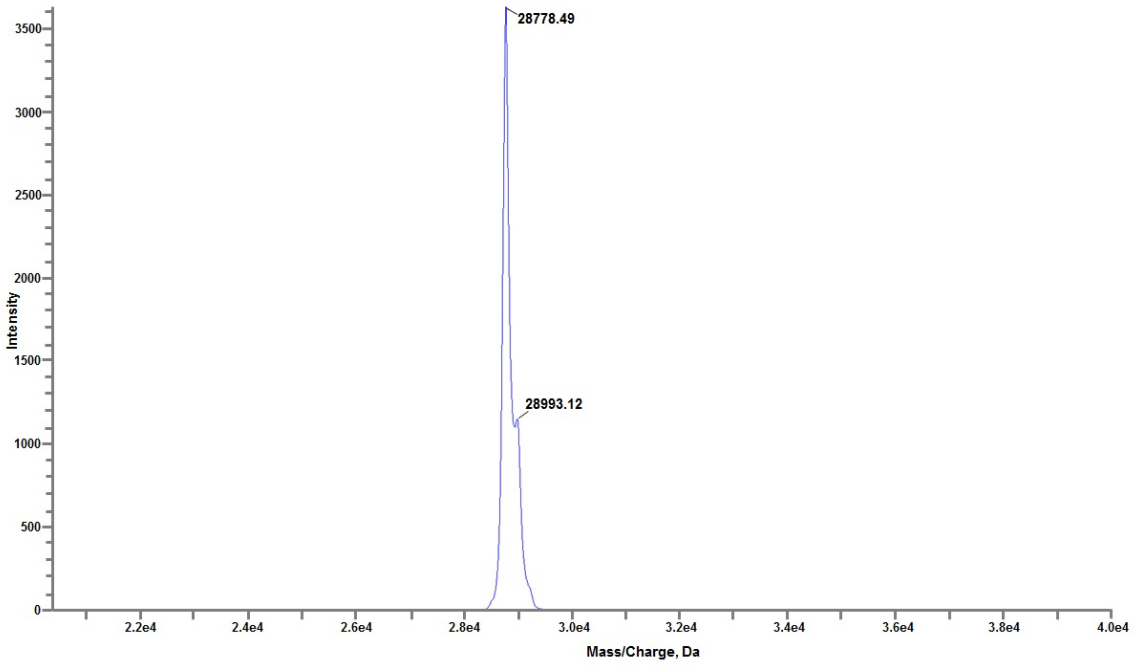

Figure C.7. Matrix-assisted laser desorption/ionization-time of flight (MALDI-TOF) mass spectrometry of $(EL18\text{-}9Y)_2$ showing that purified product is expected molecular weight (28.77 kDa).

Table C.1.
Amino acid analysis of $(EL18\text{-}9Y)_2$ showing the protein has expected amino acid composition.

Amino Acid	**Observed mol%**	**Expected mol%**
ASX	3.04	2.67
SER	3.72	3.67
GLX	2.73	2.33
GLY	28.03	30.33
HIS	4.06	3.67
ARG	2.41	2.00
THR	1.22	1.00
ALA	4.40	4.33
PRO	12.39	12.67
TYR	6.12	6.00
VAL	16.47	16.67
MET	2.84	2.67
LYS	4.58	4.33
ILE	3.79	4.00
LEU	2.10	1.67
PHE	2.10	2.00

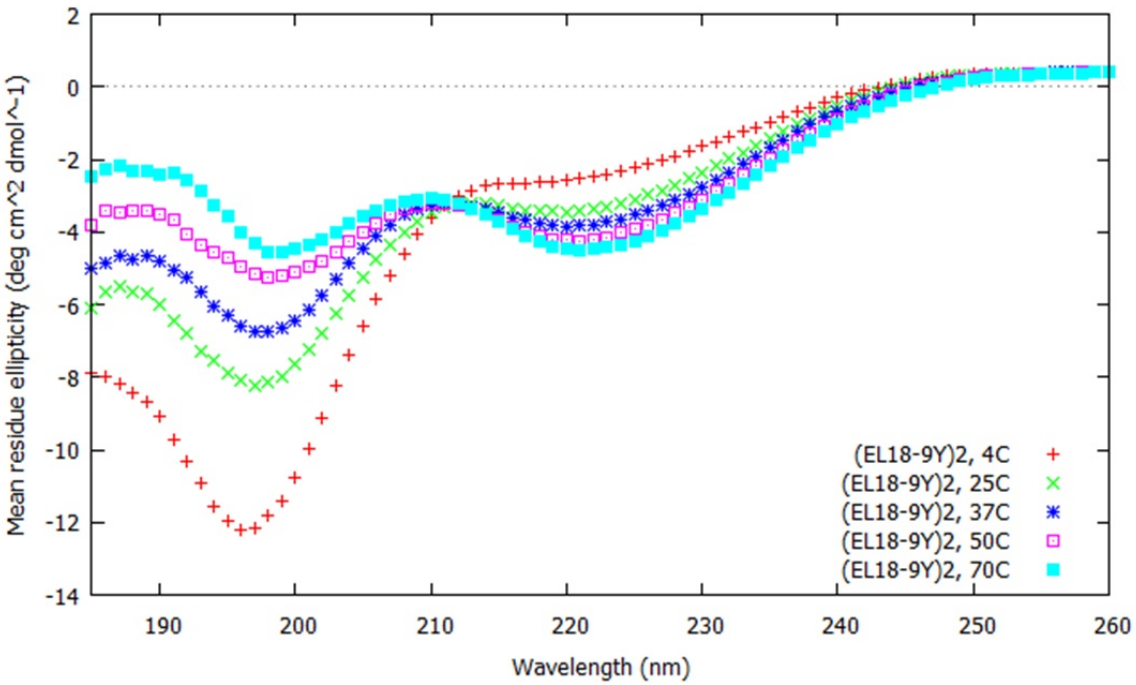

Figure C.8. Circular dichroism spectroscopy of $(EL18\text{-}9Y)_2$ from 4°C to 70°C, showing structural changes expected of an elastin-based protein. Negative peaks near 197 nm are indicative of a disordered structure, while the negative peaks near 222 nm are indicative of beta-turn structure. As the temperature of the sample is increased, the elastin-based protein gains structure in the form of beta-turns, as has been seen previously in the work of Urry et al. [153].

Table C.2.

Tyrosinase reaction optimization with BSA and $(EL18\text{-}9Y)_2$. Immobilized tyrosinase reactions were performed in 50 mL conical tubes in order to assess the effects of oxygenation method, buffer type, ascorbic acid concentration, and pH. From these experiments, it was found that the optimal conditions for tyrosinase reactions used agitation (easier to control than bubbled air), acetate buffer, 200 mM ascorbic acid, at pH 4.5. Following the reaction, samples were dialyzed extensively against 5% acetic acid, and conversion was measured with the IRPH assay. Although over 10% conversion was measured, it was accompanied by protein oxidation, aggregation, and insolubility. Further studies performed by Jessica Román also determined that the IRPH assay was likely detecting non-specific oxidation (in addition to any potential DOPA residues), which would be likely to occur after reacting for multiple days.

Protein	**Reaction Time (d)**	**pH**	**Aeration Method**	**Ascorbic Acid (mM)**	**Buffer Type**	**Percent Conversion**
BSA	10	3	Bubbled Air	50	Phosphate	9.2
BSA	10	3	Agitation	100	Phosphate	1.9
BSA	10	4	Agitation	100	Phosphate	9.9
BSA	10	4.5	Agitation	100	Phosphate	13.6
BSA	10	7	Agitation	100	Phosphate	6.6
BSA	9	4.5	Agitation	50	Acetate	9.1
BSA	9	4.5	Agitation	50	Phosphate	3.9
BSA	9	4.5	Agitation	100	Phosphate	10.7
BSA	9	4.5	Agitation	200	Phosphate	12.2
$(EL18\text{-}9Y)_2$	10	4.4	Agitation	100	Acetate	9.6

C.2 Unused Protein Designs

Along with $(EL18\text{-}9Y)_2$, several similar protein designs were developed that varied the number of tyrosine residues in the tyrosine-rich domain as well as the length of the elastin domain in each cassette. Each design followed the schematic shown in Figure C.9.

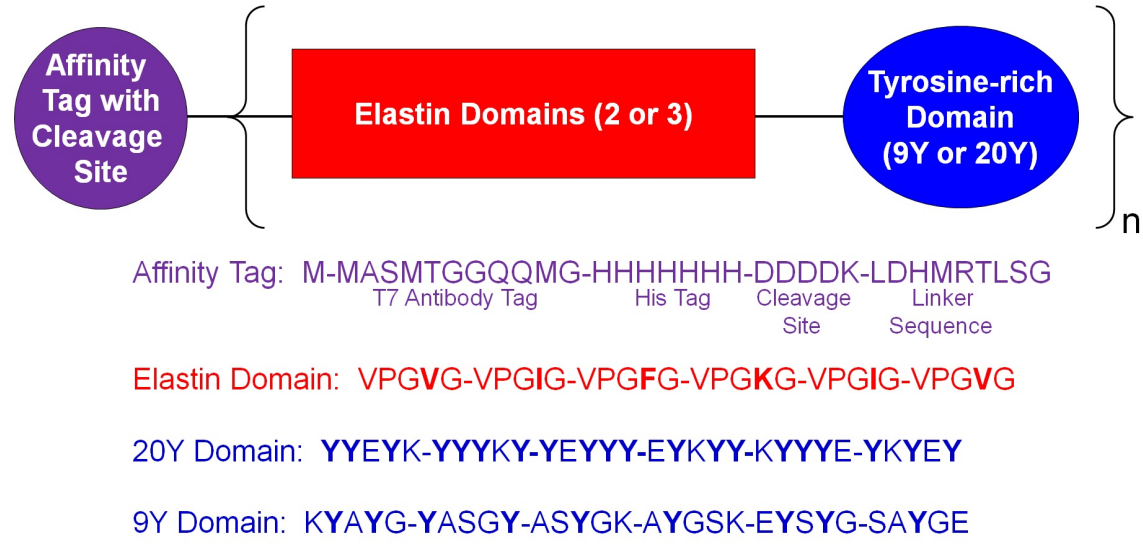

Figure C.9. Schematic showing overall design of original family of proteins. Each protein possessed an N-terminal domain containing a T7 tag, a 7xHis tag, and an enterokinase cleavage tag. This domain was followed by an elastin-based domain containing either 2 or 3 cassettes of the amino acid sequence indicated. The elastin domain was followed by a tyrosine-rich domain with either the 9Y or the 20Y sequence. The elastin domain and the tyrosine-rich domain together formed a cassette which was repeated n times.

The first protein attempted was $(EL12\text{-}20Y)_4$. After extensive troubleshooting with various expression techniques (cold expression, autoinduction, etc.), it was determined that this protein would not express due to the presence of four rare Arginine codons (one from each cassette). Western blots of expression samples showed no bands at the expected molecular weight of 50 kDa, but very faint bands were present near

27 kDa and 39 kDa, the expected weights at which two of the rare codons might cause translation to halt. To help ameliorate this issue, expression of shorter versions of this protein, $(EL12\text{-}20Y)_2$ and $(EL12\text{-}20Y)_3$, were attempted. Western blots showed that a full-length version of these proteins were expressed, but their expression bands were not discernible by eye using SDS-PAGE, indicating poor overall expression (see Figure C.10). It is believed that the low expression level is due to having so many tyrosines in the 20Y domain that the bacterial translational machinery cannot provide enough charged Tyrosine tRNAs to keep up with demand. Finally, expression of $(EL18\text{-}9Y)_2$ and $(EL18\text{-}9Y)_3$ was attempted and yielded strong over-expression (see Figures C.2 and C.11). Because the three-cassette version showed even less solubility than $(EL18\text{-}9Y)_2$, the two-cassette version was selected for further analysis and characterization as described in Section C.1.

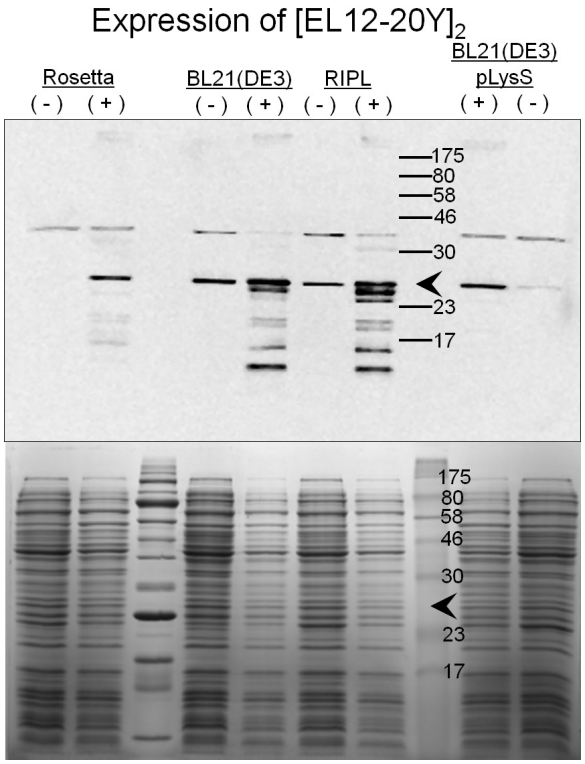

Figure C.10. Western blot and corresponding SDS-PAGE of expression samples of the protein(EL12-20Y)$_2$ in four different expression hosts. Although a full-length version of the protein expressed in all four hosts, as evidenced by a band on the Western blot at the correct molecular weight, no corresponding expression band is visible on SDS-PAGE, indicating poor overall expression. (-) indicates a sample taken before IPTG induction, (+) indicates a sample taken at harvest, and the arrowheads point to the expected molecular weight of 26.3 kDa. The bands visible near 39 kDa on the Western blot were determined to be a bacterial protein detected at background levels by the T7 antibody.

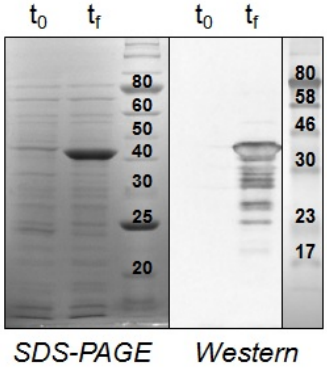

Figure C.11. SDS-PAGE gel and corresponding Western blot of expression samples of the protein(EL18-9Y)$_3$ in Rosetta2(DE3)pLysS expression host. The protein runs near its expected molecular weight of 41.65 kDa. The symbol t_0 indicates a sample taken before IPTG induction and t_f indicates a sample taken at harvest. Protein ladder molecular weights are labeled in kDa.

VITA

VITA

M. Jane Brennan

Education

Purdue University, West Lafayette, IN Aug 2010 - Aug 2015

Doctor of Philosophy, Chemical Engineering

Overall GPA 3.78/4.00

Purdue University, West Lafayette, IN Aug 2006 - May 2010

Bachelor of Science in Agricultural and Biological Engineering

Overall GPA 3.97/4.00

Honors

Academic and Research Honors

National Science Foundation Graduate Research Fellowship (2011-2014)

Purdue Teaching Academy Graduate Teaching Award (2014)

Purdue Chemical Engineering Graduate Research Symposium 2nd Place Oral Presentation (2014)

Biomaterials Day Symposium 2nd Place Podium Presentation (2013)

Purdue ChE Graduate Research Symposium Best Poster (2013)

Biomaterials Day Symposium Third Place Poster Award (2011)

School of Chemical Engineering Faculty Fellowship (2010-2011)

Purdue University Beering Fellowship (2010-2015)

Travel Awards

Purdue College of Engineering Travel Award (2014)
Purdue Graduate Student Government Travel Award (2014)
AIChE Women's Initiatives Committee Travel Award (2013)
Purdue Chemical Engineering Eastman Travel Award (2013)
Purdue Women in Engineering Program Travel Award (2013)

Publications

- **Brennan MJ**, Meredith HJ, Jenkins CL, Wilker JJ, and Liu JC. Cytocompatibility studies of a biomimetic polymer with simplified structure and high-strength adhesion. In preparation.
- **Brennan MJ**, Hollingshead SE, Wilker JJ, and Liu JC. Critical factors for the bulk adhesion of elastomeric proteins. In preparation.
- **Brennan MJ**, Wilker JJ, and Liu JC. A bioinspired elastin-based protein as a cytocompatible underwater adhesive. In preparation.
- Wang J, **Stine MJ**, and Lu C. Microfluidic cell electroporation using a mechanical valve. *Analytical Chemistry*, 2007. **79**(24): p. 9584-9587.

Selected Presentations

- **Brennan MJ**, Román JK, Mansour H, Renner JN, Lin T, Su RS-C, Wilker JJ, and Liu JC. Adhesive Elastin-Based Proteins as Soft Tissue Glues. Oral technical presentation given at the Purdue Chemical Engineering Graduate Research Symposium; August 21st, 2014; West Lafayette, IN.
- **Brennan MJ**, Román JK, Renner JN, Lin T, Su RS-C, Wilker JJ, and Liu JC. Adhesive Elastin-Based Proteins as Soft Tissue Glues. Poster presented at the Gordon Research Conference and Seminar on Bioinspired Materials; June 21st - 24th, 2014; Newry, ME.

- **Brennan MJ**, Su RS-C, Román JK, Wilker JJ, and Liu JC. Adhesive Elastin-Based Proteins as Soft Tissue Glues. Oral technical presentation given at the AIChE Annual Meeting; November 7th, 2013; San Francisco, CA.
- **Brennan MJ**, Su RS-C, Román JK, Wilker JJ, and Liu JC. Adhesive Elastin-Based Proteins as Soft Tissue Glues. Oral technical presentation given at Biomaterials Day; October 26th, 2013; Cleveland, OH.
- **Brennan MJ**, Román JK, Renner JN, Mansour H, Lin T, Su RS-C, Wilker JJ, Liu JC. Adhesive Elastin-based Proteins as Soft Tissue Surgical Glues. Poster presented at the Purdue Chemical Engineering Graduate Research Symposium; August 15th, 2013; West Lafayette, IN.
- **Brennan MJ**, Su RS-C, Wilker JJ, Liu JC. Adhesive Elastin-Based Proteins as a Soft Tissue Surgical Adhesive. Poster presented at Biomaterials Day; October 29th, 2011; West Lafayette, IN.

Selected Activities

Professional Societies

American Society for Engineering Education (ASEE)
American Institute for Chemical Engineers (AIChE)

Outreach

Adjudication for the International Genetically Engineered Machine (iGEM) Competition (2011-2015)
Purdue ChE Graduate Student Organization (GSO) (2012-2015)
Purdue ChE Graduate Women's Gatherings Co-President (2011-2012)
Introduce a Girl to Engineering Day (IGED) (2014-2015)
Exciting Discoveries for Girls in Engineering (EDGE) Camp (2011-2012)